CONCENTRATION POLARIZATION IN ULTRAFILTRATION

models and experiments

PROEFSCHRIFT

ter verkrijging van
de graad van doctor aan de Universiteit Twente,
op gezag van de rector magnificus
prof.dr.ir. J.H.A. de Smit
volgens besluit van het College van Dekanen
in het openbaar te verdedigen
op vrijdag 16 september 1988 te 16.00 uur

door

GERT BESSEL VAN DEN BERG

geboren op 7 mei 1960 te Amersfoort

Dit proefschrift is goedgekeurd door de promotor prof.dr. C.A. Smolders

Assistent promotor: dr.ir. I.G. Rácz

Referent: dr.ir. J.G. Wijmans

ISBN 90-9002372-0

Druk: Alfa, Enschede.

VOORWOORD

Aan het begin van dit proefschrift wil ik de vele mensen bedanken zonder wie het hierna beschreven onderzoek niet in zijn huidige vorm verschenen zou zijn. Een aantal daarvan wil ik daarbij speciaal noemen, in een min of meer chronologische volgorde.

'Een goed begin is het halve werk', ofwel de vliegende start die ik heb gehad bij mijn promotie-onderzoek heb ik voor een groot deel te danken aan Jan Henk Hanemaaijer en de membraangroep van de afdeling Technologie van het NIZO te Ede. Tijdens het uitvoeren van mijn doktoraalopdracht daar werd mij duidelijk dat membraantechnologie een mooi ambacht is en dat met name de membraanvervuilingsproblematiek nog een paar jaar onderzoek waard was.

De overstap naar de veel grotere onderzoekgroep 'Membraanfiltratie' van de voormalige T.H. Twente was daarna eigenlijk niet zo'n heel grote verandering: in beide groepen werd natuurlijk met membranen gewerkt én er heerste een uitstekende sfeer die zich niet alleen beperkte tot de laboratoria en werkkamers.

De hulp van de stagiaires en afstudeerders bij het uitvoeren van de vele experimenten en analyses om de diverse modellen te verifiëren was onmisbaar, achtereenvolgens verschenen daarvoor: Huub Smit, Ronnie Huwaë, Alies Gonlag, Henk Haarman, Mieke Veldhuis en Paul Roeleveld.

Tenslotte wil ik Thonie van den Boomgaard, Imre Rácz en Kees Smolders bedanken voor de begeleiding tijdens het onderzoek en het kritisch doornemen van de concept-hoofdstukken en -artikelen daarna.

CONTENTS

Chapter 1 has been published in part in Filtration and Separation, March/April 1988, p. 115-121.
Chapter 2 has been accepted for publication in J. Membrane Sci.
Chapter 3 has been submitted for publication in J. Membrane Sci.
Chapter 4 has been published in J. Membrane Sci., 31(1987)307-320.
Chapter 5 will be submitted for publication in J. Membrane Sci.

CHAPTER 1

FLUX DECLINE IN MEMBRANE PROCESSES. INTRODUCTION.

MEMBRANES AND MEMBRANE PROCESSES

Membrane filtration processes are used industrially nowadays as an alternative to conventional separation methods such as distillation, centrifugation and extraction. Membrane filtration is used frequently since in the early sixties asymmetric membranes with much better properties were developed. Before then membrane processes were hardly used in industry because of very low transport velocities (fluxes) through rather thick membranes, low selectivities and difficulties in preparing cheap membranes and equipment, as well as the low cost of energy which made the conventional separation methods cheaper. Since asymmetric reverse osmosis membranes became available membrane technology has developed enormously. This is expressed in the vast amount of research which has been invested into developing the right membrane type and module for different kinds of separation processes, developing new processes and the best possible circumstances for separation.

These efforts have resulted in the present day commercialization of processes like ultrafiltration (UF), microfiltration (MF), reverse osmosis or hyperfiltration (RO), gas separation, (kidney-)dialysis and electrodialysis (ED). The various membrane separation methods can be divided into three classes according to their separation characteristics: (i) UF and MF use the size of the solutes to separate particles by sieving action, with a pressure difference as the driving force.; the membranes used in UF can have pores from 1 to 50 nm, while for MF the pore range is from 0.05 to 10 μm. (ii) RO, gas separation and dialysis, having (partly) dense membrane structures (pores < 1 nm), make use of a difference in affinity between several feed components and the membrane, and of a difference in diffusivity through the membrane; the driving force is a pressure difference in case of RO and gas separation and a concentration difference in case of dialysis. (iii) electrodialysis uses anion- and cation selective membranes to separate charged molecules from uncharged ones, and the ions are transported as a result of an applied potential difference.

Applications of these techniques include:

- Food industry: whey processing (RO and UF), concentration of milk for cheese production (UF), clarification and/or sterilization of various fluids such as wine, vinegar and apple juice (MF) and whey desalting (ED).
- Water treatment: production of high resistivity (>18 MΩ/cm) water for the electronics industry (MF and RO) and production of clean boiler feedwater, potable water and clean waste water (RO and ED).
- Other industries: oil-water separation (UF and MF) and recovery of paint and latices from waste water effluents (UF).

The membranes used in the various membrane processes can be very different, both the material and the configuration (modules) offer several possibilities. For UF and MF the membrane can be made out of a polymeric or inorganic material. Well known polymer materials are polysulfone, cellulose-acetate, polycarbonate, polypropylene and poly-acrylonitrile. Inorganic membranes (usually MF-type) can be made from e.g. α-Al_2O_3 or silica-glass (SiO_2). A large variety of polymeric membranes are produced to optimize their permeability and separation characteristics.

Polymeric membranes can be subdivided in homogeneous, asymmetric and composite membranes (figures 1-3). Homogeneous membranes are membranes in which the porosity or density is not dependent on the distance from the surface. These membranes can be dense or porous and have straight pores or no pores at all, and the thickness is 10 μm or more.

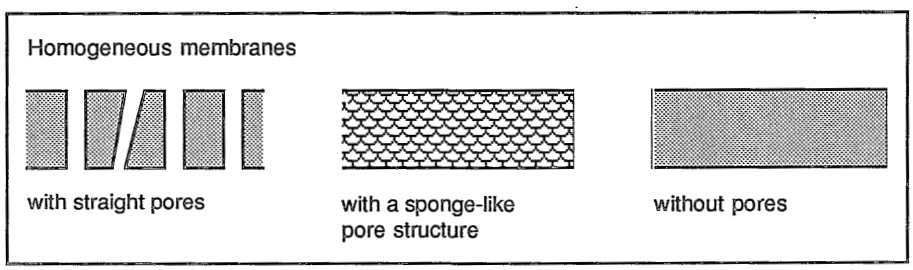

Figure 1. Schematic representation of homogeneous membranes

Asymmetric membranes, usually made by the phase-inversion method, have a thin dense skin layer (0.1 - 1 μm) with or without pores. The small thickness of the skin layer results in a low resistance for transport through the membrane.

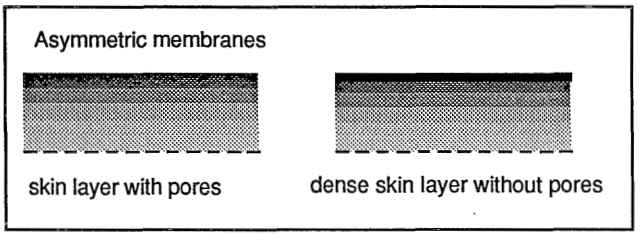

Figure 2. Schematic representation of asymmetric membranes

Finally, the composite membrane is usually made of a very permeable UF membrane with a very thin dense layer, often of a different polymer, which is chosen for its high selectivity.

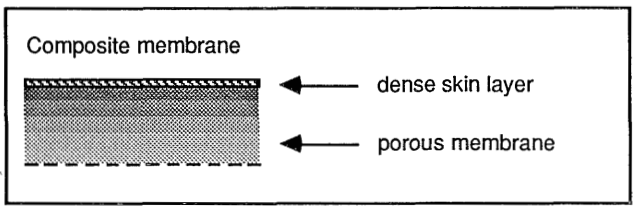

Figure 3. Schematic representation of a composite membrane

Various configurations exist to support or contain the membranes. Which configuration is to be used in practice depends both on the solution which should be filtered and the operating conditions. In general, three filtration methods can be distinguished: unstirred and stirred dead-end filtration and cross-flow filtration (figure 4). In the unstirred dead-end filtration the solution is put under pressure without any agitation in the liquid. The solute is separated from the permeating solvent (permeate) and will build up a concentrated layer of the rejected solute at the membrane interface. To prevent this large build-up of solute at the membrane surface the solution can be stirred. In the cross-flow situation the solution is pumped to flow tangentially over the membrane interface, again to prevent a solute build-up at the membrane. In practical applications the cross-flow mode is usually used.

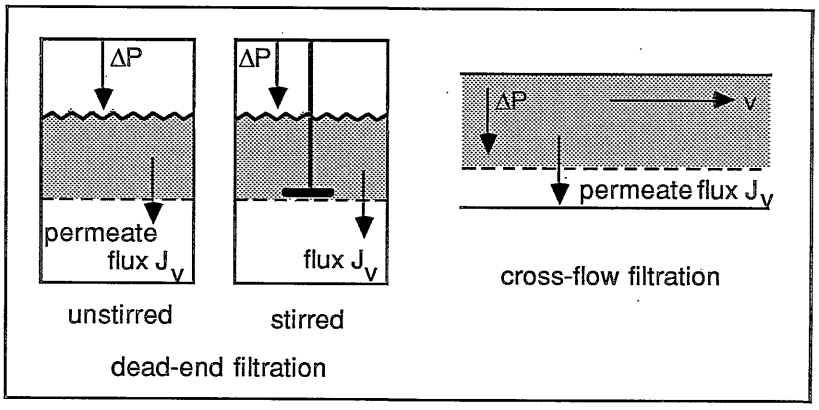

Figure 4. Schematic representation of the three filtration methods, with different operation conditions.

A membrane can be tubular or flat. The way the membrane is put into the module distinguishes the various configurations. The module with the most economical membrane area to volume ratio (packing density) contains hollow fiber membranes. Hollow fiber membranes are tubular and have outer diameters of less than 0.1 to 2 mm, resulting in a packing density of up to 30,000 m^2/m^3. The other tube-like membranes are the so called spaghetti membranes (outer diameter 1 to 5 mm) and the tubular membranes (outer diameter 5 to 25 mm). The latter kind of membrane module has a packing density of only 100 to 300 m^2/m^3 and is used for liquids which would readily foul the membrane (suspensions etc.). All tubular type of membranes are used in the cross-flow mode. Flat membranes are used in dead-end filtration equipment as well as in cross-flow filtration. In cross-flow filtration the plate-and-frame module and the spiral-wound module can be mentioned. As the names indicate, the membranes are either attached in the module in frames with plates and spacers in between or wound in a spiral with spacers in between, respectively. The packing density is about 500 m^2/m^3 for the plate-and-frame module and about 1000 m^2/m^3 for the spiral-wound module. The various cross-flow filtration modules can be used separately, sometimes with a counter-current permeate flow, or in a cascade of modules. In the latter case the different classes in filtration (MF, UF, RO etc.) can also be combined in one cascade to obtain the best possible separation.

FLUX DECLINE

One of the most important reasons why membrane processes are not more extensively used is the flux decline during filtration. The flux decline is caused by several phenomena in, on and near the membrane. These phenomena can also cause a loss in selectivity or an additional undesired selectivity. The flux decline, related to the so called pure water flux, can be a few percent of the pure water flux for relatively clean feeds in UF, up to more than 90 % decline in flux in some cases of MF. The reasons for the flux decline will be different in each case of filtration. However, in general, the flux decline is caused by a decreased driving force and/or an increased resistance.

The flux J_v can be described by:

$$\text{flux } J_v = \frac{dV}{Adt} = \frac{\text{driving force (e.g. } \Delta P, \Delta C \text{ or } \Delta T)}{\text{viscosity} * \text{total resistance}} \qquad (1)$$

The resistances which can occur during a filtration process are schematically represented in figure 5. Except for the resistance of the membrane R_m which is always present, resistances increase during filtration. Pores can become blocked by the solute (R_p), and adsorption of the solute on to the walls of the pores of the membrane results in a lower permeability (R_a).

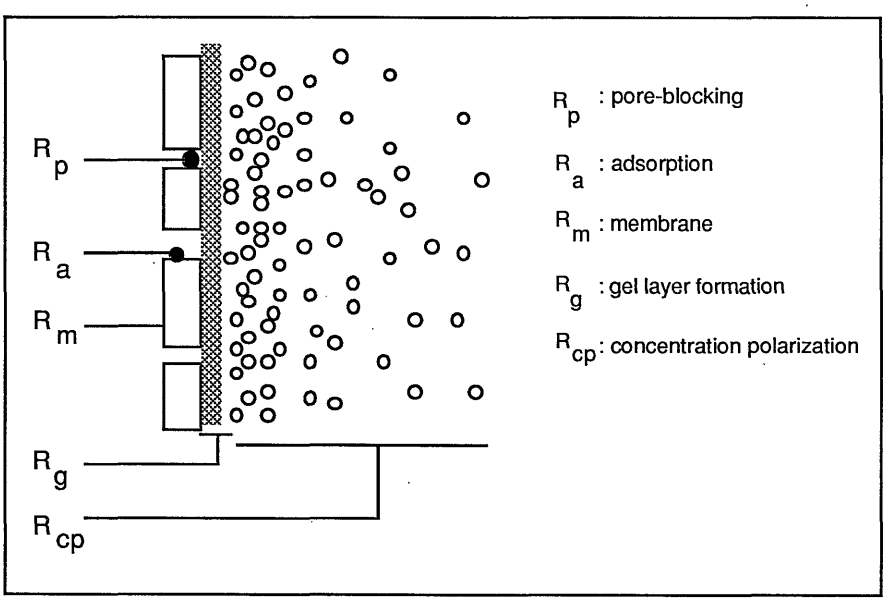

Figure 5. Possible resistances against solvent transport.

Another, very important, phenomenon is the so-called concentration polarization, which is due to solute being retained by the membrane and the solvent passing. Therefore, the solute accumulates to form a layer at the membrane interface with a relatively high concentration. The concentrated layer near the membrane is less permeable for the solvent (usually water) in comparison with an unaltered solution, which is expressed by an additional resistance R_{cp}. This phenomenon also results in a (much) higher osmotic pressure $\Delta\Pi$ at the membrane interface, even when macromolecular solutions are used, and this leads to a decrease in the driving force which becomes $\Delta P - \Delta\Pi$. Finally, the concentration at the membrane interface can reach such high values that the concentrated solution will change into a gel with a resistance R_g. Gel layer formation occurs easily with protein containing liquids.

The effects of adsorbed proteins is studied by several researchers [1-4]. In general it is found that the amount adsorbed depends on the membrane material, the solute type, the concentration and in case of proteins on the ionic strength and the pH. Adsorption will increase with increasing concentration and, in case of proteins, will increase at pH-values closer to the iso-electric point. Hydrophobic membranes (polysulfone, polypropylene, polytetrafluoroethylene) adsorb more proteins than hydrophilic membranes (cellulose-acetate, polyacrylonitrile). This can be the reason for choosing a hydrophilic membrane for a separation process involving proteins. Disadvantages of these hydrophilic membranes is often their limited chemical and temperature resistance.

Deposition of solutes on to the membrane surface will also decrease the flux. The deposition can be caused by, for example, the aggregation of proteins, even at low concentrations (lower than the gel concentration) or by precipitation of saturated salt solutions. In the first case a long-term time-dependent flux decline occurs during filtration of dilute (single) protein solutions by aggregate formation [5]. Also interaction of positive and negative proteins may lead to aggregation [6]. A salt such as calciumphosphate is known to cause a flux decline during the filtration of milk and whey when the temperature and pH are not carefully controlled. This process is called scaling and it can also occur inside the membrane.

The flux decline phenomena can be generally divided in *fouling* (irreversible and long term phenomena) and *concentration polarization* (reversible and directly occuring phenomena). Reviews of fouling and fouling control have been given by several authors [7,8] and models explaining flux decline by means of concentration polarization are considered hereafter.

CONCENTRATION POLARIZATION PHENOMENA

The build-up of solute near the membrane interface can be described in two ways: either by the cake-filtration type of description or by a description according to the film theory (figure 6).

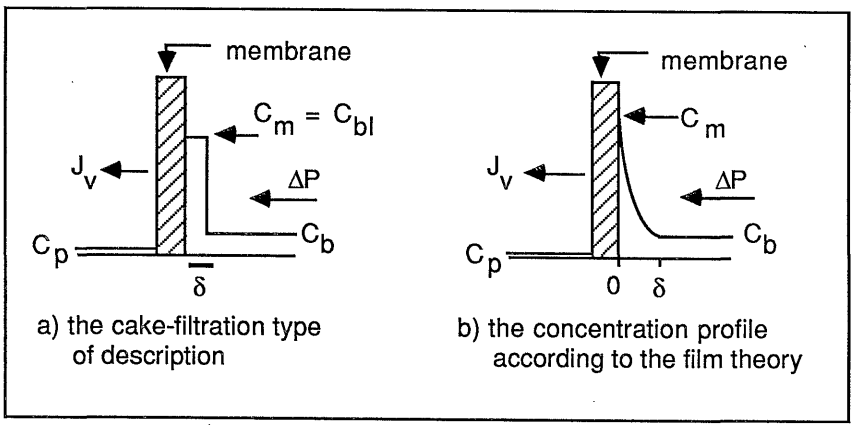

Figure 6. The concentration profiles according to the cake-filtration type of description and to the film theory.

Models according to the *cake-filtration theory* assume a constant concentration in the layer near the membrane, which sometimes depends on the applied pressure, and which increases in thickness with increasing permeate volume. For unstirred dead-end filtration conditions this concentration in the boundary layer can be calculated from the mass balance

$$C_b \cdot \Re_{obs} \cdot V_p = \delta \cdot A \cdot C_{bl} \qquad (2)$$

where C_b is the concentration in the bulk of the solution, $\Re_{obs}$ the observed retention (defined by $\Re_{obs} = [1 - (C_p / C_b)]$, V_p the total permeate volume, A the membrane area and δ the thickness of the boundary layer. We use the following equation for the flux:

$$J_v = \Delta P / \{ \eta_0 \cdot (R_m + R_{bl}) \} \qquad (3)$$

where η_0 is the viscosity of the solvent and R_{bl} is the resistance of the concentrated boundary layer.

The equation for the total resistance of the boundary layer is:

$$R_{bl} = \delta \cdot r_{bl} \tag{4}$$

where r_{bl} is the specific resistance of the boundary layer. Therefore:

$$1/J_v = 1/J_w + (\eta_0 \cdot C_b \cdot \Re_{obs} / \Delta P) \cdot (r_{bl} / C_{bl}) \cdot (V_p / A) \tag{5}$$

where J_w is the pure water flux. Integration of eq. 5, with $J_v = dV_p / Adt$, leads to:

$$t = (\eta_0 \cdot C_b \cdot \Re_{obs} / \Delta P) \cdot (r_{bl} / C_{bl}) \cdot (V_p / A)^2 \tag{6}$$

which results in the well-known relationships for unstirred dead-end filtration $V_p \sim t^{0.5}$ and $J_v \sim t^{-0.5}$.

The various methods to calculate the specific resistance of the boundary layer will be described in the paragraph on resistance models. The cake filtration type of description is also used in some methods to characterize the fouling capacity of a solution. By unstirred dead-end filtration of the solution during a fixed time a fouling index can be calculated, which is used for further research [9,10].

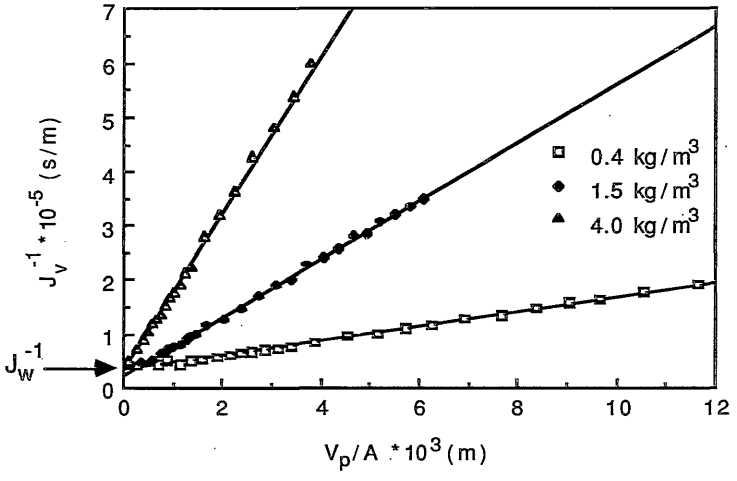

Figure 7. The reciprocal flux as a function of the permeate volume at different concentrations (unstirred dead-end UF of BSA at 1.0 10^5 Pa)

In figures 7 and 8 typical unstirred dead-end filtration plots are represented. The reciprocal flux indeed is linear to the permeate volume, and different slopes are obtained

when different concentrations or pressures are used, as predicted by eq. 5. In figure 9 the flux is given as a function of time and shows the $J_v \sim t^{-0.5}$ relationship.

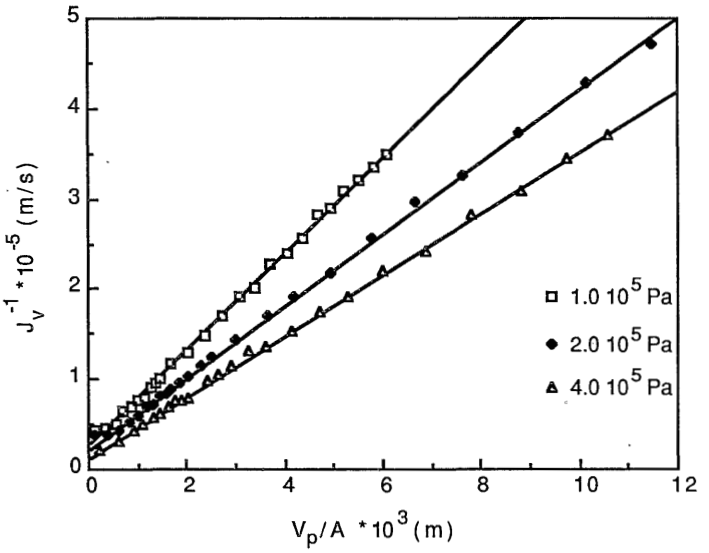

Figure 8. The reciprocal flux as a function of the permeate volume at different applied pressures (unstirred dead-end UF of BSA with C_b=1.5 kg/m^3)

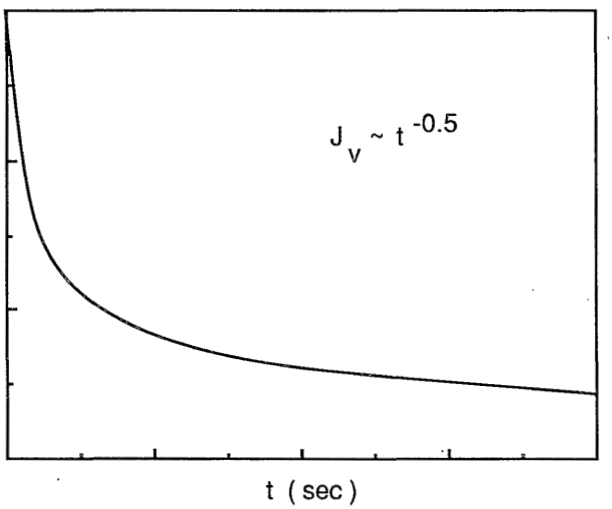

Figure 9. Typical flux behaviour during unstirred dead-end filtration

Models which describe the concentration polarization phenomenon by the *film theory* (see figure 6) usually start from a basic equation such as:

$$\partial C / \partial t + J_v.\partial C/\partial x = \partial(D.\partial C / \partial x) / \partial x \qquad (7)$$

where $J_v.\partial C/\partial x$ represents the convective transport towards the membrane, while $\partial(D.\partial C/\partial x)/\partial x$ represents the back-diffusion as a result of the concentration gradient. Thi differential equation has to be solved, analytically or numerically, knowing that for some solutes the diffusion coefficient is a function of the concentration. In some cases the diffusion coefficient has to represent the diffusion of a large number of solutes, e.g. when a liquid like milk is filtered.

When the diffusion coefficient is constant eq. 7 becomes:

$$\partial C / \partial t + J_v.\partial C/\partial x = D.\partial^2 C / \partial x^2 \qquad (8)$$

Normally the starting and boundary conditions are:

$$t = 0 \quad : C = C_b \qquad (9)$$

$$x = \delta \quad : C = C_b \qquad (10)$$

$$x = 0 \quad : J_v.C_m = D \,.\, (\partial C/\partial x)_{x=0} + (1 - \Re_{obs}) \,.\, J_v \,.\, C_b \qquad (11a)$$

$$\text{or } J_v.(C_m - C_p) = D \,.\, (\partial C/\partial x)_{x=0} \qquad (11b)$$

In a steady state situation, which is reached after some time in stirred dead-end and cross-flow filtration, eq. 8 results in the well-known film theory relationship

$$J_v = (D / \delta) \ln \{ (C_m - C_p) / (C_b - C_p) \} \qquad (12)$$

The quantity D/δ is called the mass transfer coefficient k, which is solute and equipment dependent. When the retention equals unity the concentration function for the boundary layer can be described by

$$C (\delta - x) = C_b \,.\, \exp (J_v \,.\, (\delta - x) / D) \qquad (13)$$

In figures 10 and 11 the steady-state flux is represented as a function of the applied pressure. These curves are schematic representations of typical experimental findings, when macromolecular or colloidal solutions are being ultrafiltered. The flux first increases with increasing pressure and finally becomes constant leading to a pressure-independent

filtration. In figure 10 the influence of the concentration is given, while in figure 11 the influence of the mass transfer coefficient is represented.

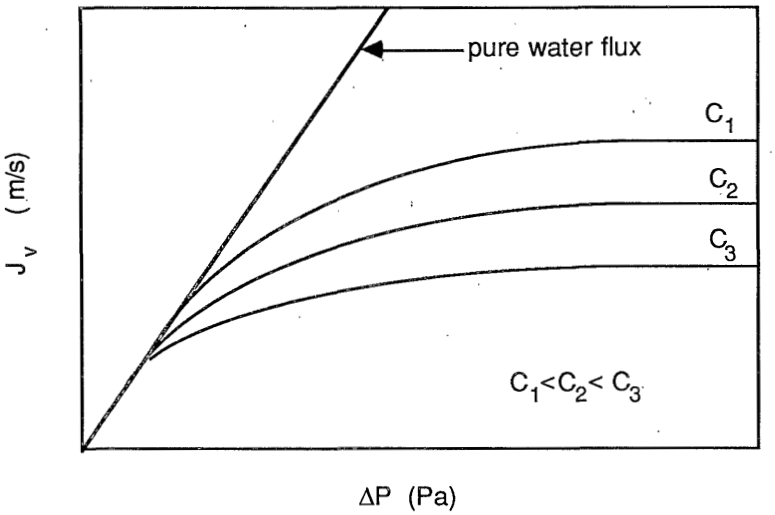

Figure 10. Steady state fluxes during cross-flow filtration of a macromolecular solute as a function of the applied pressure at three different concentrations.

Both for the cake-filtration type of description and for the dynamic description according to the film theory there are several different models in the literature to cover the effect of the concentration polarization phenomena. These models can be subdivided in: a) *resistance models*, b) *gel-polarization models* and c) *osmotic pressure models*.

There are two kinds of resistance models: filtration models (A1) and boundary layer resistance models (A2). The filtration models often use the well-known Kozeny-Carman relationship to calculate the specific resistance of a cake with a constant concentration. These models are used mostly when colloids are filtered. The boundary layer models use the relationship between the permeability of a concentrated layer for solvent molecules and the sedimentation of solute at high concentrations to calculate the specific resistance. They exist for both unstirred dead-end and cross-flow filtration.

The gel-polarization models are available for all varieties of filtration methods. Sometimes the gel concentration is difficult to determine, while the diffusivity up to the gel concentration often is assumed to be constant (e.g. equal to the diffusivity at the bulk concentration).

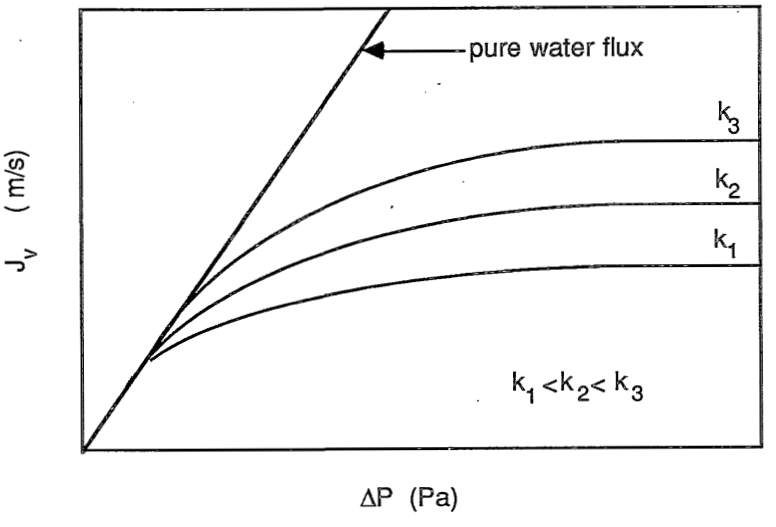

Figure 11. Steady state fluxes during cross-flow filtration of a macromolecular solute as a function of the applied pressure using three different mass transfer coefficients.

The osmotic pressure models use the decrease in the driving force by the osmotic effects to calculate the flux. Mostly the osmotic pressure Π of concentrated solutions is determined experimentally, though for simple solutions Π can also be calculated theoretically.

All the models mentioned above were derived and tested for UF. Therefore the models will be called UF-models, though there are no reasons to presume that the models are not valid for MF. For RO osmotic pressure models are usually used, sometimes in combination with a model that describes the deposition of solute particles at the membrane interface.

A. The resistance models

A1. Filtration models

The total resistance R_{bl} as needed in eq. 3 is calculated from the thickness of the boundary layer δ and the specific resistance r_{bl}. In general the total resistance will be

$$R_{bl} = {}_0\int^{\delta} r_{bl}\, dx \qquad (14)$$

which is equal to $r_{bl}.\delta$ when the cake-filtration theory is used.

The specific resistance is given by the Kozeny-Carman relationship:

$$r_{bl} = 180 \,.\, (1 - \varepsilon)^2 / [(d_s)^2.\varepsilon^3] \qquad (15)$$

where ε is the porosity of the concentrated layer and d_s is the 'diameter' of the solute particle. In case a solid deposit has been formed and its mass can be determined, the thickness δ of the concentrated layer is equal to:

$$\delta = m_s / [\rho_s \,.\, (1-\varepsilon).A] \qquad (16)$$

where m_s is the mass of the deposit or concentrated layer, ρ_s is the density of the solute and A is the membrane area. The influence of the applied pressure can be represented by

$$r_{bl} = r_{bl,0} \,.\, \Delta P^n \qquad (17)$$

where n is the compressibility factor. In the relationship

$$r_{bl} / C_{bl} = (r_{bl}/C_{bl})_0 \,.\, \Delta P^n \qquad (18)$$

n was found to be 0.5 - 0.7 for solutes like BSA and silica [11,12].

The filtration model concept has been used for all kinds of filtration: Howell and Velicangil [13] and Baker et al. [14] use it in a model for cross-flow UF, and Fane [15] and Chudacek et al. [11] use the filtration model for describing stirred and unstirred dead-end filtration of several solutes.

A2. Boundary layer resistance models (BLR models)

The basic principle of boundary layer resistance models is the correspondence of the permeability of a concentrated layer for solvent molecules near a membrane interface and the permeability of a solute in a stagnant solution, as occuring during a sedimentation experiment (figure 12).

This relationship can be described by [16]:

$$p = (\eta_0 \,.\, s\,(C)) / [C \,.\, (1 - v_1/v_0)] \qquad (19)$$

where p is the permeability of a concentrated layer of concentration C, s(C) is the sedimentation coefficient at concentration C and v_1 and v_0 are the partial specific volumes of the solute and the solvent respectively.

The specific resistance r_{bl} is equal to the reciprocal permeability p^{-1}. Combined with eq. 14 this results in the total resistance, which is needed in eq. 3 to describe the flux. The sedimentation coefficient is usually strongly dependent on the concentration, which is described by:

$$s^{-1} = (s_0)^{-1}.\ (1 + K_1.C + K_2.C^2 + K_3.C^3) \qquad (20)$$

where K_1, K_2 and K_3 are constants. At the moment three versions of the BLR model exist: one for cross-flow UF [17] and two for unstirred dead-end UF [18,19].

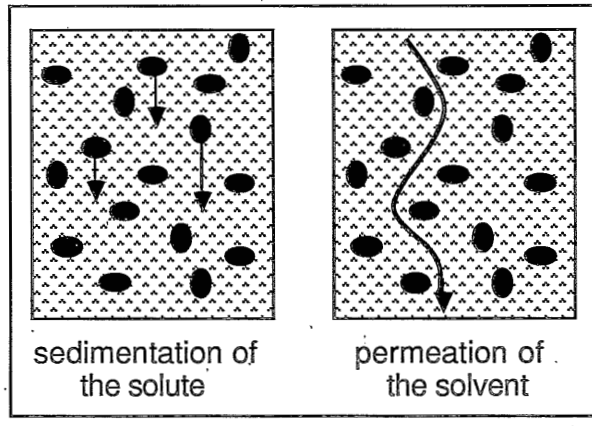

Figure 12. The resemblance of sedimentation and permeability

The cross-flow version of the BLR model uses eq. 13, 14, 19 and 20 to obtain

$$R_{bl} = \frac{D}{J_v}\,\frac{1 - v_1/v_0}{\eta_0 . s_0}\,\left[C_m - C_b + \frac{K_1}{2}.(C_m^2 - C_b^2) + \frac{K_2}{3}.(C_m^3 - C_b^3) + \frac{K_3}{4}.(C_m^4 - C_b^4) \right] \qquad (21)$$

The resistance can be calculated when the concentration at the membrane interface C_m is known. Assuming $\Re_{obs} = 1$ ($C_p = 0$) changes eq. 12 into

$$J_v = k.\ln (C_m / C_b) \qquad (22)$$

from which C_m can be calculated if k is known.

Unfortunately, the mass transfer coefficient k can not be easily calculated from process parameters. Many relationships have been proposed (by Deissler, Chilton-Colburn and others, see Gekas [20] for a review), but none can predict the exact mass transfer

coefficient a priori. Corrections can be made for the concentration dependent parameters like the increased viscosity, the changed diffusion coefficient and/or the changed density of the solution [21]. A general correction for the effect of the flux through the membrane on the mass transfer coefficient near the membrane is also known (the Stewart correction [22]). In general it can be said that these corrections make the prediction of the mass transfer coefficient very complicated. In Chapter 5 the mass transfer coefficient in cross-flow ultrafiltration will be discussed further.

The effect of an uncertainty in k on the calculated total resistance may be large, because C_m, and therefore R_{bl}, are calculated from an exponential function:

$$C_m = C_b \cdot \exp (J_v / k) \qquad (23)$$

A small error in the value of k results in a large error in C_m and an even larger error in the calculated value of the total resistance R_{bl}. Therefore Wijmans et al. [17] calculated the mass transfer coefficient and the concentration at the membrane interface by using the osmotic pressure model (section 3), after having proven that the BLR model and the osmotic pressure model are equivalent. An excellent agreement of the theoretical and experimental R_{bl}-values is the result, showing the validity of the BLR model (figure 13).

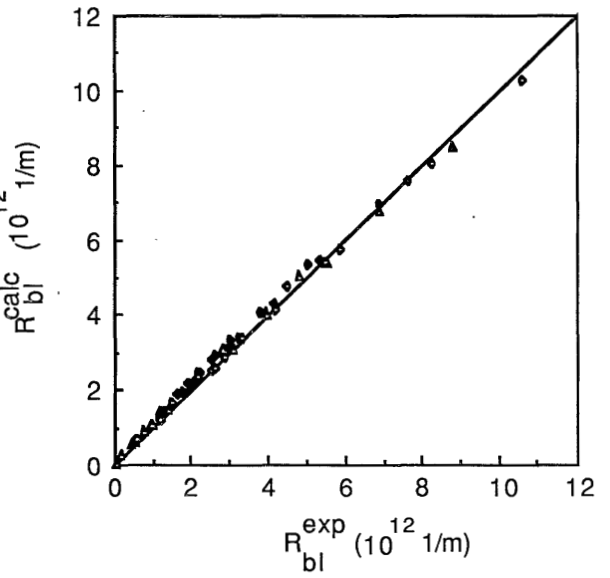

Figure 13. Comparison of the experimental and calculated resistance of the boundary layer during cross-flow UF of Dextran T70.

Nakao et al. [18] developed a BLR model for unstirred dead-end UF using the cake-filtration type of description. From the experiments several properties of the concentrated layer could be calculated, by using the experimental plot of $1 / J_v$ versus V_p / A and the derivative of eq. 5 :

$$d(1/J_v) / d(V_p / A) = (\eta_0 . C_b . \Re_{obs} / \Delta P) . (r_{bl} / C_{bl}) \quad (24)$$

Knowing the values of C_b, η_0, $\Re_{obs}$ and ΔP the value of the so called *flux decline index* r_{bl}/C_{bl} can be obtained readily from the experiments. The concentration C_{bl} can be derived from r_{bl}/C_{bl} , via eq. 19,

$$r_{bl} / C_{bl} = (1 - v_1 / v_0) / (\eta_0 . s(C_{bl})). \quad (25)$$

Unfortunately this model is not able to predict the fluxes or resistances directly, without doing some filtration experiments.

In Chapter 2 we will use the film model to describe the concentration profile near the membrane in combination with the basic BLR model equations. The flux during unstirred dead-end UF experiments can be predicted then by solving the differential equation (eq. 8) numerically.

B. Gel-polarization models

The gel-polarization models all use the film theory to describe the concentration polarization phenomena (eq. 7). A characteristic of these models is the assumption that the concentration at the membrane interface can not exceed a fixed value for C_g. An increase of the applied pressure will then result only in an increased thickness of the gel layer but not in an increase in flux. The concentration profile can be thought to be as in figure 14, with both a concentration profile and a layer of constant concentration C_g. Gel-polarization models exist for unstirred dead-end UF, for stirred dead-end UF and for cross-flow UF.

The model for unstirred dead-end UF as proposed by Trettin and Doshi [23] includes an additional boundary condition viz. $C_m = C_g$ for all t. Furthermore an assumption was made of a constant diffusion coefficient and a fixed shape of the concentration profile outside the gel-layer of the form $C = C_b + (C_g - C_b).(1 - x/\delta)^n$ (note that $\delta = \delta(t)$). The number n is larger than zero and is a function of C_g, C_b and C_p.

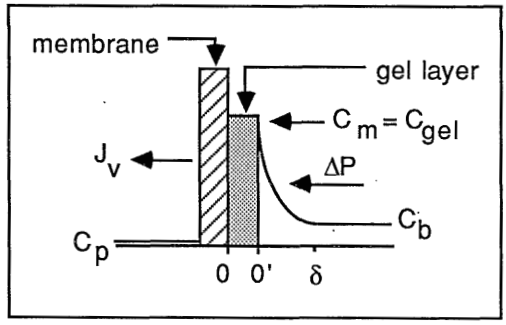

Figure 14. Representation of the concentration profile near the membrane interface according to the gel-polarization theory.

The resulting equation for the flux is:

$$J_v = \left[\frac{C_g - C_b}{C_g - C_p}\right]\left[\frac{C_g - C_p}{C_b - C_p}\right]^{0.5}\left[\frac{nD}{2(n+1)t}\right]^{0.5} \qquad (26)$$

which can be simplified, for one filtration data-set, to:

$$J_v = \text{constant} \cdot (D / t)^{0.5} \qquad (27)$$

showing the well-known $J_v \sim t^{-0.5}$ or $V_p \sim t^{0.5}$ relationship for unstirred dead-end UF.

The models for stirred dead-end UF [24] and for cross-flow UF [24,25] use the equations of the film theory completed with one assumption: $C_m = C_g$ for all t. Eq. 12 becomes:

$$J_v = (D / \delta) \ln \{ (C_g - C_p) / (C_b - C_p) \} \qquad (28)$$

and with $D / \delta = k$ and $\Re_{obs} = 1$ one obtains

$$J_v = k \cdot \ln (C_g / C_b) \qquad (29)$$

Like described in the paragraph on the BLR models, also for this model it appears to be very difficult to predict the mass transfer coefficient k from process parameters.

Many experimental results do agree with this model, e.g. $J_v \neq f(\Delta P)$, $J_v \sim - \ln(C_b)$ and J_v

= f (k). However, the model can not explain why the limiting concentration of one chosen solute at $J_v \rightarrow 0$, which is assumed to define $C = C_g$, changes when that solute is filtered in two different filtration cells [25].

C. Osmotic pressure models

In general a macromolecular solution has a very small osmotic pressure in comparison to an equal weight-percentage low molecular salt solution. However, during the filtration of the macromolecular solution a large concentration build-up can be realized. The osmotic pressure of very concentrated solutions can increase to enormous values, as shown by several measurements and/or calculations [17, 26-29] The osmotic pressure of a single solute can be calculated, up to very high concentrations, using several characteristics of the solute. The equation of van 't Hoff for ideal and dilute solutions is:

$$\Pi = R.T.C / M \qquad (30)$$

where R is the gas constant, T the absolute temperature and M the molecular weight. This equation can not be used for concentrated solutions and is extended to the equation for the osmotic pressure of non-ideal solutions:

$$\Pi = (RT / M) (C + B_2C^2 + B_3C^3 + ...) \qquad (31)$$

in which the virial coefficients B_2 and B_3 can be calculated as a function of parameters such as excluded volume, hydration and Donnan effects [27,29].

A few examples of osmotic pressures, at 400 kg/m^3:

Π (Dextrans)	$\approx$ 710 kPa [17],
Π (protein BSA at pH 5.4)	$\approx$ 130 kPa [27],
Π (protein ß-lactoglobulin at pH 6.6)	$\approx$ 260 kPa [29] and
Π (whey proteins)	$\approx$ 650 kPa [28].

Using non-equilibrium thermodynamics Kedem and Katchalsky [30] derived expressions for the solvent flux and the solute flux respectively:

$$J_v = L_p (\Delta P - \sigma \Delta \Pi) = (\Delta P - \sigma \Delta \Pi) / (\eta_0 . R_m) \qquad (32)$$

$$J_s = P(C_m - C_p) + (1 - \sigma) J_v \langle C \rangle \qquad (33)$$

where L_p is the pure water permeability, σ the reflection coefficient, $\Delta \Pi = \Pi(C_m) -$

$\Pi(C_p)$, P the membrane permeability for the solute and <C> the concentration averaged over both sides of the membrane, which is usually the logarithmic mean. Spiegler and Kedem [31] derived for the intrinsic retention $\Re$:

$$\Re = 1 - (C_p / C_m) = \sigma(1 - F) / (1 - \sigma F) \quad (34)$$

where

$$F = \exp [- (1 - \sigma) . J_v / P] \quad (35)$$

When $C_p = 0$, so $\Re_{obs} = \Re = \sigma = 1$, eq. 32 becomes:

$$J_v = (\Delta P - \Delta\Pi) / (\eta_0 . R_m) \quad (36)$$

An osmotic pressure model for unstirred dead-end filtration was described by Vilker et al. [32]. They used the film theory (i.e. eq. 7-11) in combination with eq. 32 to obtain an expression for the flux, in case of a highly rejecting membrane:

$$J_v = (D / t)^{0.5} . f (C^*, C_b) \quad (37)$$

where C* is the concentration for which $\Delta P - \sigma\Delta\Pi = 0$. For one set of conditions the function of C* and C_b is constant, which turns eq. 37 into:

$$J_v = \text{constant} . (D / t)^{0.5} \quad (38)$$

Like all other models for unstirred dead-end filtration this model also predicts a $J_v \sim t^{-0.5}$ relationship.

The osmotic pressure models for stirred dead-end filtration and cross-flow filtration are essentially the same. Jonsson [28] describes stirred dead-end UF and Goldsmith [26] describes cross-flow filtration, both using the film theory (resulting in eq. 22) and the flux equation including the osmotic pressure (eq. 32) :

$$J_v = k . \ln (C_m / C_b) \quad (22)$$

$$J_v = L_p (\Delta P - \sigma\Delta\Pi) = (\Delta P - \sigma\Delta\Pi) / (\eta_0 . R_m) \quad (32)$$

From these equations and the dependence of the osmotic pressure on concentration from experimental data the mass transfer coefficient can be calculated. Jonsson [28] found a reasonable, but certainly not 100%, agreement with theoretical mass transfer data.

The experimental data, represented in a semi-logarithmic plot of J_v versus ln C_b, when extrapolated to $J_v \rightarrow 0$ gives a value for C_m, corresponding to an osmotic pressure which is

equal to the applied pressure ΔP. So instead of a 'fixed' gel concentration, as used in the gel-polarization models, a variable concentration $C_m = f(\Delta P)$ is assumed to be reached at the membrane interface.

Wijmans et al. [33] showed mathematically that the osmotic pressure model has many characteristics in common with the gel-polarization model. They used:

$$J_v = (\Delta P - \Delta\Pi) / \eta_0 . R_m \qquad (36)$$

and a relationship for the osmotic pressure as a function of concentration of the form:

$$\Delta\Pi = a . C^n \qquad (39)$$

where a is a constant and n an exponent larger than 1, together with eq. 13 and $\Delta\Pi = f(C_m)$ this results in

$$J_v = [\Delta P - a.(C_b)^n . \exp(n . J_v / k)] / \eta_0 . R_m \qquad (40)$$

From this equation it is clear that the flux will not increase linearly with the applied pressure. Furthermore, other filtration characteristics can be derived from the derivative $\partial J_v / \partial \Delta P$

$$\partial J_v / \partial \Delta P = [\eta_0 . R_m + (n/k).\Delta\Pi]^{-1} = [1 + (\Delta\Pi.n/ \eta_0 . R_m.k)]^{-1} / \eta_0 . R_m \qquad (41)$$

For high effective values of $\Delta\Pi$ the derivative $\partial J_v / \partial \Delta P$ will be almost zero (pressure independent filtration), while for $\Delta\Pi \approx 0$ the term $\partial J_v / \partial \Delta P$ will be near $1 / \eta_0 . R_m$ (as it i for pure water filtration). The term $\Delta\Pi.n/ \eta_0 . R_m.k$ was shown to be the ratio of the resistances caused by the osmotic pressure and the membrane itself. At high values of this ratio the solution is supposed to be very polarized at the membrane interface.
Another derivative, $\partial J_v / \partial \ln C_b$, is equal to

$$\partial J_v / \partial \ln C_b = - \{ 1/k + 1/[n\Delta P/ (\eta_0 . R_m - J_v)] \}^{-1} = - k [1 + (\eta_0 . R_m k)/(\Delta\Pi.n)]^{-1} \qquad (42)$$

At high values of the ratio $\Delta\Pi.n/ \eta_0 . R_m.k$ the term $\partial J_v / \partial \ln C_b$ will almost be equal to - k, which is also the predicted slope in plots of J_v versus $\ln C_b$ in the gel-polarization model.

The factors that can lead to a high $\Delta\Pi.n/ \eta_0 . R_m.k$ ratio (large flux decline by osmotic effects) were summarized as follows:

1 - high permeate fluxes, obtained by a large applied pressure or a small R_m-value,
2 - high bulk concentrations,
3 - low mass transfer coefficients: a small diffusion coefficient of the solute (a macro-molecular solute) and/or a low degree of mechanical mixing near the membrane interface,

4 - a high exponent n, i.e. a macromolecular solute,

5 - a high value of the constant a, i.e. a low molecular weight of the solute, which is the opposite of factors 3 and 4.

Thus, the generally in practice desired high degree of concentration of solutions, easily obtained at high fluxes, appears to be opposed by the same high flux and concentration.

IMPROVEMENT OF FLUXES

As indicated above flux enhancement is possible by destroying the concentrated layer near the membrane, but this is not the only way to improve the flux. Prevention of fouling phenomena might also give flux improvement. An extended review of methods to diminish the flux decline has been given by Matthiasson and Sivik [34].

The methods to improve the flux can be generally divided into 1) adapting the operating conditions in the existing equipment, 2) altering the solution, 3) using a different or pretreated membrane, 4) taking additional measures to prevent or decrease the flux decline.

1. Equipment related methods: unstirred dead-end filtration is always less favourable for the flux-behaviour than stirred dead-end filtration or cross-flow filtration, which can both be characterized by a mass transfer coefficient. It can be seen from theoretical considerations that a larger mass transfer coefficient will increase the flux. As the mass transfer coefficient is a function of both solute and equipment related parameters an improvement of the value of k can be realized, e.g. by increasing the cross-flow velocity, changing the flow channel or decreasing the viscosity, which is possible by increasing the temperature.

2. Solution related methods: when scaling is a problem, scaling-inhibitors can be added, ion exchange can be used to reduce the concentration of salts or the pH can be altered. Changing the value of the pH can also result in a decreased osmotic pressure and can increase the gel concentration. Sometimes a pH change is counteractive on the different parameters. Enzymatic hydrolysis of the feed can also result in an increased flux [35].

3. Membrane related methods: a chemical treatment can alter the surface of the membrane to make it less hydrophobic (less adsorption). Attaching hydrophilic chains on a hydrophobic membrane is also known to increase the flux during protein UF [36,37]. In situ removal of the concentrated layer is possible by immobilizing hydrolytic enzymes on the membrane surface [13]. The mass transfer coefficient can be increased by the use of corrugated membranes [38].

4. Additional measures: Prefiltration of a solution with serious fouling capacities can make a process much more economic. The use of special rotating equipment or membranes

can increase the mass transfer coefficient [39]. Also increased mass transfer coefficients and fluxes result from pulsing the feed solution flow [37], the use of a counter-current cascade [40] or the use of static mixers [41]. Recently a few methods have been described to improve the flux by the use of relatively small electrical current pulses [42,43]. When a deposit has been formed on the membrane surface backflushing a small amount of the permeate can improve the total efficiency [44,45]. Finally, membranes which have been fouled can be cleaned chemically or mechanically.

CONCLUSIONS

The flux decline during membrane filtration processes can be caused by many phenomena, mainly subdivided into fouling phenomena and concentration polarization. The concentration polarization phenomenon, which is always present when a membrane separation occurs, can be described by the film theory or a cake-filtration type of description. The effects of the increased concentration at the membrane interface has been described by several models. These concentration polarization models can be subdivided in resistance models (filtration and boundary layer resistance models), gel-polarization models and osmotic pressure models. Many of these models can describe the filtration phenomena (e.g. the $J_v \sim t^{-0.5}$ relationship for unstirred dead-end filtration). A limiting factor, however, is the difficulty to predict the mass transfer coefficient which is needed when stirred dead-end or cross-flow filtration is used. On the basis of an increase of the mass transfer coefficient or a pretreatment of the feed solution, to give a lower fouling potential, many methods are used in practice to improve the flux.

STRUCTURE OF THIS THESIS

The subjects described in this thesis are all, directly or indirectly, related to the problem of flux decline during membrane filtration processes. As indicated in this introductory *Chapter I* various models exist to describe (a part of) the problem, whether it is fouling or concentration polarization. In this thesis the concentration polarization phenomena are modelled using the boundary layer resistance model, filtration models and the osmotic pressure model. Many studies on the influence of the various parameters are done using dead-end ultrafiltration equipment, which implies a case of filtration which is not used in everyday's practice. The reasons are twofold: the description of a dead-end ultrafiltration process requires a one-dimensional analysis only and moreover the mass transfer in

cross-flow ultrafiltration still is an additional problem on top of the polarization description problem. The solutes studied are mostly proteins and some polysaccharides.

In *Chapter 2* the boundary layer resistance model is combined with film model equations to make computer predictions of an unstirred dead-end ultrafiltration experiment possible. The predictions are compared to experimental data of experiments with the protein BSA, at various circumstances, and estimations are made about the influence of several parameters on the flux behaviour of the solutions during ultrafiltration. The computer simulations lead to a number of additional data on the filtration phenomenon, such as the concentration at the membrane interface and the concentration profiles near the membrane.

In *Chapter 3* the flux declining effect of one positively and two types of negatively charged proteins, and of binary mixtures of these proteins, is investigated during unstirred dead-end ultrafiltration. The experimental flux behaviour of single protein solutions and of binary mixtures is compared to calculations based on specific resistances according to classical filtration laws. The additional effect of a denser packing of particles, when unequally sized particles are involved, is also included.

In *Chapter 4* the osmotic pressure of a protein solution is studied, which is directly related to the flux decline according to the osmotic pressure model. The monomer-dimer equilibrium of the protein involved (ß-lactoglobulin) appears to influence the magnitude of the osmotic pressure, as well as the retention during an ultrafiltration experiment. The dependence of the osmotic pressure on various parameters is calculated and is compared to actual osmotic pressure measurements.

In *Chapter 5* the mass transfer coefficients in cross-flow ultrafiltration are discussed. These coefficients are essentially necessary for the description of concentration polarization in cross-flow systems. The large number of mass transfer coefficient relations in literature, the various corrections which have to be applied for ultrafiltration circumstances and the large impact a small deviation will have on calculated flux data, make it difficult to choose the correct relation. Therefore, two methods are tested to determine the mass transfer coefficient experimentally, and its dependence on various experimental parameter: the velocity variation method and the method which uses the osmotic pressure difference across a membrane during the ultrafiltration experiment.

LIST OF SYMBOLS

a	constant in eqs. 39 and 40	(Pa)
A	membrane area	(m^2)
B_n	n^{th} virial coefficient	($m^{3(n-1)}.kg^{-n+1}$)

C_b	concentration in the bulk	(kg/m^3)
C_{bl}	(constant) concentration in the boundary layer	(kg/m^3)
C_g	gel concentration	(kg/m^3)
C_m	concentration at the membrane interface	(kg/m^3)
C_p	concentration of the permeate	(kg/m^3)
D	diffusion coefficient	(m^2/s)
d_s	diameter of the solute	(m)
F	quantity defined by eq. 35	(-)
J_v	flux	(m^3/m^2s)
J_w	pure water flux	(m^3/m^2s)
k	mass transfer coefficient	(m/s)
K_i	various constants, used in eqs. 20 and 21	($m^{3n}.kg^{-n}$)
L_p	pure water permeability	(m/Pa.s)
M	molecular weight	(kg/kmol)
m_s	mass of the deposit or concentrated layer	(kg)
n	exponent in eq. 26 and in eqs. 39-42	(-)
P	membrane permeability for solute	(m/s)
p	permeability of the boundary layer	(m^2)
R	gas constant	(J/mol.K)
$\Re$	intrinsic retention coefficient	(-)
R_a	resistance caused by adsorption	(m^{-1})
r_{bl}	specific resistance of the boundary layer	(m^{-2})
R_{bl}	total hydraulic resistance of the boundary layer	(m^{-1})
R_{cp}	resistance of the concentrated layer	(m^{-1})
R_g	gel layer resistance	(m^{-1})
R_m	hydraulic resistance of the membrane	(m^{-1})
$\Re_{obs}$	observed retention coefficient	(-)
R_p	resistance caused by pore-blocking	(m^{-1})
s	sedimentation coefficient	(s)
T	temperature	(K)
v_0	partial specific volume of the solvent	(m^3/kg)
v_1	partial specific volume of the solute	(m^3/kg)
V_p	(cumulative) permeate volume	(m^3)
x	coordinate perpendicular to the membrane	(m)
δ	thickness of the boundary layer	(m)
ε	porosity	(-)

ΔP	applied pressure	(Pa)
η_0	viscosity of the solvent	(Pa.s)
Π	osmotic pressure	(Pa)
ρ_s	density of the solute	(kg/m^3)
σ	reflection coefficient	(-)

REFERENCES

[1] E. Matthiasson, The role of macromolecular adsorption in fouling of ultrafiltration membranes, J. Membrane Sci., 16(1983)23-36.

[2] L.J. Zeman, Adsorption effects in rejection of macromolecules by ultrafiltration membranes, J. Membrane Sci., 15(1983)213-230.

[3] P. Aimar, S. Baklouti and V. Sanchez, Membrane-solute interactions: influence on pure solvent transfer during ultrafiltration, J. Membrane Sci., 29(1986) 207-224.

[4] T.B. Choe, P. Masse, A. Verdier and M.J. Clifton, Membrane fouling in the ultrafiltration of polyelectrolyte solutions: polyacrylic acid and bovine serum albumin, J. Membrane Sci., 26(1986)17-30.

[5] A. Suki, A.G. Fane and C.J.D. Fell, Modeling fouling mechanisms in protein ultrafiltration, J. Membrane Sci., 27(1986)181-193.

[6] S. Yagisawa, A method for observing protein-protein interaction, J. Biochem. 77(1975)605-616.

[7] A.G. Fane and C.J.D. Fell, A review of fouling and fouling control in ultrafiltration, Desalination, 62(1987)117-136.

[8] P. Aimar, Membrane fouling, Summer School on Engineering Aspects of Membrane Processes, Aarhus, Denmark, 1986.

[9] J.C. Schippers and J. Verdouw, The modified fouling index, a method of determining the fouling characteristics of water, Desalination, 32(1980)137-148.

[10] H. Reihanian, C.R. Robertson and A.S. Michaels, Mechanisms of polarization and fouling of ultrafiltration membranes by proteins, J. Membrane Sci., 16(1983)237-258.

[11] M.W. Chudacek and A.G. Fane, The dynamics of polarisation in unstirred and stirred ultrafiltration, J. Membrane Sci., 21(1984)145-160.

[12] P. Dejmek, Concentration polarization in ultrafiltration of macromolecules, Ph.D. Thesis, Univ. of Lund, Sweden, 1975.

[13] J.A. Howell and O. Velicangil, Theoretical considerations of membrane fouling and its treatment with immobilized enzymes for protein ultrafiltration, in: A.R. Cooper (Ed.), Polymer Science and Technology, Vol. 13, Plenum Press, New York, NY, 1980, pp. 217-229.

[14] R.J. Baker, A.G. Fane, C.J.D. Fell and B.H. Yoo, Factors affecting flux in crossflow filtration, Desalination, 53(1985)81-93.

[15] A.G. Fane, Ultrafiltration of suspensions, J. Membrane Sci., 20(1984)249-259.

[16] P.F. Mijnlieff and W.J.M. Jaspers, Solvent permeability of dissolved polymer material. Its direct determination from sedimentation measurements, Trans. Faraday Soc., 67(1971)1837-1854.

[17] J.G. Wijmans, S. Nakao, J.W.A. van den Berg, F.R. Troelstra and C.A. Smolders, Hydrodynamic resistance of concentration polarization boundary layers in ultrafiltration, J. Membrane Sci., 22(1985)117-135.

[18] S. Nakao, J.G. Wijmans and C.A. Smolders, Resistance to the permeate flux in unstirred ultrafiltration of dissolved macromolecular solutions, J.Membrane Sci., 26(1986)165-178.

[19] G.B. van den Berg and C.A. Smolders, The boundary layer resistance model for unstirred ultrafiltration, A new approach, accepted for publication by J. Membrane Sci., Chapter 2 of this thesis.

[20] V. Gekas and B. Hallström, Mass transfer in the membrane concentration polarization layer under turbulent cross flow. I. Critical literature review and adaption of existing Sherwood correlations to membrane operations. J. Membrane Sci., 30(1987)153-170.

[21] A.G. Fane, C.J.D. Fell, D. Wiley and R. McDonogh, Concentration polarization, mass transfer and fluid dynamics in membrane systems, Summer School on Engineering Aspects of Membrane Processes, Aarhus, Denmark, 1986.

[22] R.B. Bird, W.E. Stewart and E.N. Lightfoot, Transport Phenomena, J. Wiley and sons, New York, 1960.

[23] D.R. Trettin and M.R. Doshi, Ultrafiltration in an unstirred batch cell, Ind. Eng. Chem. Fundam., 19(1980)189-194.

[24] W.F. Blatt, A. Dravid, A.S. Michaels and L. Nelsen, Solute polarization and cake formation in membrane ultrafiltration: causes, consequences, and control techniques, in: J.E. Flinn (Ed.), Membrane Science and Technology, Plenum Press, 1970, pp. 47-97.

[25] M.C. Porter, Concentration polarization with membrane ultrafiltration, Ind. Eng. Chem. Prod. Res. Dev. 11(1972)234-248.

[26] R.L. Goldsmith, Macromolecular ultrafiltration with microporous membranes, Ind. Eng. Chem. Fundam., 10(1971)113-120.

[27] V.L. Vilker, C.K. Colton and K.A. Smith, The osmotic pressure of concentrated protein solutions: effect of concentration and pH in saline solutions of bovine serum albumin, J. Coll. Interf. Sci., 79(1981)548-566.

[28] G. Jonsson, Boundary layer phenomena during ultrafiltration of dextran and whey protein solutions, Desalination, 51(1984)61-77.

[29] G.B. van den Berg, J.H. Hanemaaijer and C.A. Smolders, Ultrafiltration of protein solutions; the role of protein association in rejection and osmotic pressure, J. Membrane Sci., 31(1987)307-320, Chapter 4 of this thesis.

[30] O. Kedem and A. Katchalsky, Permeability of composite membranes, Trans. Farad. Soc., 59(1963)1941-1951.

[31] K.S. Spiegler and O. Kedem, Thermodynamics of hyperfiltration (reverse osmosis): criteria for efficient membranes, Desalination, 1(1966)311-326.

[32] V.L. Vilker, C.K. Colton and K.A. Smith, Concentration polarization in protein ultrafiltration. Part II: Theoretical and experimental study of albumin ultrafiltered in an unstirred cell, AIChE Journal 27(4)(1981)637-645.

[33] J.G. Wijmans, S. Nakao and C.A. Smolders, Flux limitation in ultrafiltration: osmotic pressure model and gel layer model, J. Membrane Sci., 20(1984) 115-124.

[34] E. Matthiasson and B. Sivik, Concentration polarization and fouling, Desalination, 35(1980)59-103.

[35] J.L. Harris, Influence of gel layer rheology on ultrafiltration flux of wheat starch effluent, J. Membrane Sci., 29(1986)97-109.

[36] A.G. Fane, C.J.D. Fell and K.J. Kim, The effect of surfactant pretreatment on the ultrafiltration of proteins, Desalination, 53(1985)37-55.

[37] H. Bauser, H. Chmiel, N. Stroh and E. Walitza, Interfacial effects with microfiltration membranes, J. Membrane Sci., 11(1982)321-332.

[38] I.G. Rácz, J. Groot Wassink and R. Klaassen, Mass transfer, fluid flow and membrane properties in flat and corrugated plate hyperfiltration modules, Desalination, 60(1986)213-222.

[39] M. López-Leiva, Ultrafiltration in rotary annular flow, Ph.D. Thesis, Univ. of Lund, Sweden, 1979.

[40] R.A. Ward, E. Klein, P.A. Feldhoff and T.J. Turnham, Ultrafiltration: separation enhancement by counter-current cascading, J. Membrane Sci., 33(1987)97-111.

[41] J. Hiddink, D. Kloosterboer and S. Bruin, Evaluation of static mixers as convection promoters in the ultrafiltration of dairy liquids, Desalination, 35(1980)149-167.

[42] W.R. Bowen, R.S. Kingdon and H.A.M. Sabuni, Electrically enhanced separation processes-the basis of in-situ intermittent electrolytic membrane cleaning (IIEMC) and in-situ electrolytic membrane restoration (IEMR), submitted to J. Membrane Sci.

[43] R.J. Wakeman and E.S. Tarleton, Membrane fouling in crossflow microfiltration by the use of electric fields, Chem. Eng. Sci., 42(1987)829-842.

[44] B.R. Breslau, E.A. Agranat, A.J. Testa, S. Messinger and R.A. Cross, Hollow fiber ultrafiltration, Chem. Eng. Prog., 71(1975)74-80.

[45] K.H. Kroner, H. Schütte, H. Hustedt and M.R. Kula, Cross-flow filtration in the downstream processing of enzymes, Process Biochemistry, April 1984, 67-74.

CHAPTER 2

THE BOUNDARY LAYER RESISTANCE MODEL FOR UNSTIRRED ULTRAFILTRATION. A NEW APPROACH.

G.B. van den Berg and C.A. Smolders

SUMMARY

The possibility to analyse concentration polarization phenomena during unstirred dead-end ultrafiltration by the boundary layer resistance theory has been shown by Nakao et al. [1]. Experimental data on the ultrafiltration of BSA at pH=7.4, at various concentrations and pressures, were analysed by this model and by a new version of the model in this paper. Instead of the assumption of the cake filtration theory the new version of the model uses the unsteady state equation for solute mass transport to predict flux data, by computer simulations. This approach requires no assumptions concerning the concentration at the membrane, the concentration profile or the specific resistance of the boundary layer. The computer simulations agree very well with the experimental data. Many agreements with Nakao's analyses are confirmed and some new data on the concentration polarization phenomena are obtained.

INTRODUCTION

The phenomenon of flux decline in protein ultrafiltration has been studied by several investigators, usually each of them emphasizing one of the aspects of membrane fouling. The subjects studied most, in relation to the flux decline, are adsorption [2], pore-blocking [3], deposition of solute [4] and concentration polarization phenomena, for which several models have been developed [5-9]. The latter models make use of one or more of the properties of the solute: an increased osmotic pressure difference [5,6], formation of a gel layer [8,9] or a limited permeability of the concentrated layer near the membrane which can be described by the boundary layer resistance model [7]. One of the problems in the study of the cross-flow ultrafiltration process is to describe the mass transfer coefficient

properly. The numerous relations for the mass transfer coefficient are all (semi-)empirical and in some cases show large deviations when checked with experimental data. To overcome this problem the study of concentration polarization can be simplified to the case of unstirred dead-end ultrafiltration. Nakao et al. [1] used the boundary layer resistance model adapted to a cake-filtration type of description to analyse the experimental flux behaviour during the ultrafiltration of dextrans and polyethylene glycols. This model gave some promising results but it could not describe some of the experimentally obtained flux data. Furthermore the model was unable to predict the experimental flux behaviour without doing several other experiments to obtain the necessary parameters.

The objectives of this investigation are to develop a more accurate and predictive description of the flux behaviour in ultrafiltration. This has been achieved by adapting the boundary layer resistance model, now using dynamic equations for describing the phenomena near the membrane interface. Besides, the validity of the model has been extended to the filtration of protein solutions (BSA). The simulated flux data have been compared to both the experimental ultrafiltration results and to the results obtained with the model of Nakao et al.

With the improved model more information can be obtained about the ultrafiltration proces, while less parameters are necessary to describe the flux behaviour than with the original model of Nakao et al.

The newly developed boundary layer resistance model has been succesfully applied (and experimentally verified) to various applied pressures in the ultrafiltration process, to several concentrations and to different types of membranes.

THEORY

This section on the theory of dead-end ultrafiltration consists of three parts: 1. the general principles of the boundary layer resistance model, 2. the adaption of these principles to a cake-filtration type of description and 3. the adaption to a dynamic model, which is the new approach.

1. The general principles of the boundary layer resistance model.

According to the boundary layer resistance model the permeate-flux J_v can be described by:

$$J_v = \Delta P / [\eta_0 \cdot (R_m + R_{bl})] \qquad (1)$$

where R_m and R_{bl} are the hydraulic resistances of the membrane and the concentrated boundary layer respectively, ΔP is the applied pressure and η_0 is the dynamic viscosity of the solvent. The resistance R_{bl} is a cumulative effect of the diminished permeability of the concentrated layer near the membrane and it can be described by

$$R_{bl} = {}_0\int^{\delta} r_{bl}(x)dx = {}_0\int^{\delta} p(x)^{-1}dx \qquad (2)$$

where $r_{bl}(x)$ is the specific resistance of a thin concentrated layer dx and p(x) is the permeability of that layer. The basic principle of the boundary layer resistance theory is the correspondence of the permeability of a concentrated layer for the solvent near a membrane interface and the permeability of a solute in a stagnant solution, as occuring during a sedimentation experiment. This latter relationship can be described by [10]

$$p = (\eta_0 * s(C)) / (C * (1-v_1/v_0)) \qquad (3)$$

where p is the permeability, s(C) is the sedimentation coefficient at concentration C and v_0 and v_1 are the partial specific volumes of the solvent and the solute respectively.

2. The boundary layer resistance model adapted to the cake-filtration type of description [1]

Following the cake filtration description one represents the concentration profile near the membrane as given in figure 1.

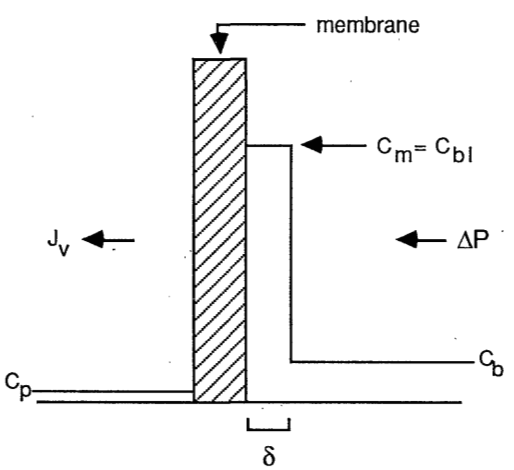

Figure 1. The concentration-profile according to the cake-filtration model.

The thickness of the boundary layer δ, having a constant concentration C_{bl}, can be obtained from the mass balance

$$C_b * \Re_{obs} * V_p = \delta * A * C_{bl} \quad (4)$$

in which C_b is the bulk concentration, $\Re_{obs}$ is the observed retention, V_p is the accumulative permeate volume and A is the membrane area. Now the resistance of the boundary layer can be calculated by

$$R_{bl} = \delta * r_{bl} \quad (5)$$

in which the specific resistance r_{bl} is constant over the boundary layer δ. Combining equations 1, 4 and 5 results in

$$1/J_v = 1/J_w + (\eta_0 * C_b * \Re_{obs} / \Delta P) * (r_{bl} / C_{bl}) * (V_p / A) \quad (6)$$

in which (r_{bl}/C_{bl}) is a quantity called the flux decline index and (V_p/A) is the specific cumulative permeate volume.

In order to analyse experimental results, where usually $1/J_v$ is plotted as a function of (V_p/A), eq. 6 is transformed into

$$d(1/J_v) / d(V_p / A) = (\eta_0 * C_b * \Re_{obs} / \Delta P) * (r_{bl} / C_{bl}) \quad (7)$$

With the known values of C_b, η_0, $\Re_{obs}$ and ΔP the flux decline index r_{bl}/C_{bl} can be determined from one set of experiments. From this value the boundary layer concentration C_{bl} can be calculated making use of the relation for the sedimentation coefficient (eq. 8).

$$r_{bl} / C_{bl} = (1 - v_1 / v_0) / (\eta_0 * s(C_{bl})) \quad (8)$$

provided the dependence of s on the concentration is known.

In the discussion section results obtained in this way will be compared with the simulated ultrafiltration flux data.

3. The new approach to the boundary layer resistance model

Contrary to the former model, the concentration profile near the membrane interface will be calculated without making any assumptions concerning the concentration at the

membrane or the shape of the concentration profile. In this situation the general mass balance equation for the solute reads

$$\partial C / \partial t = - J_v.\partial C/\partial x + D.\partial^2 C / \partial x^2 \qquad (9)$$

where $-J_v.\partial C/\partial x$ represents the convective solute transport towards the membrane ($\partial C/\partial x$ negative, x is the distance into the boundary layer) and $D.\partial^2 C/\partial x^2$ represents the back-diffusion as a result of the concentration gradient.

The boundary and initial conditions are:

$$t = 0 \quad : \quad C = C_b \qquad (10)$$

$$x = \delta \quad : \quad C = C_b \qquad (11)$$

$$x = 0 \quad : \quad J_v.C_m = D \,.\, (\partial C/\partial x)_{x=0} + (1 - \Re_{obs}) \,.\, J_v \,.\, C_b \qquad (12)$$

where δ is the thickness of the concentration polarization layer.

Using the equations mentioned above the shape of the concentration profile can be expected to be as shown in figure 2.

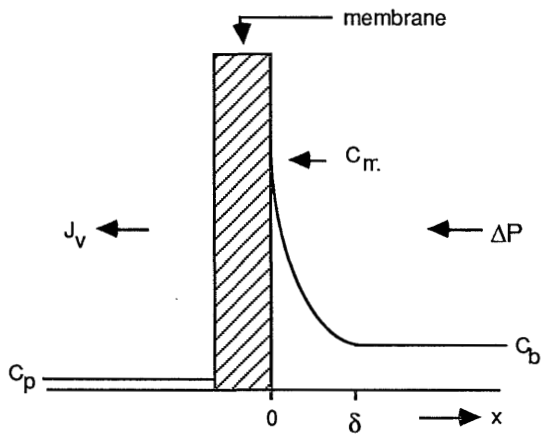

Figure 2. The concentration profile during dead-end ultrafiltration according to the new approach.

If the diffusion coefficient and the concentration of the bulk solution were constant this set of equations could be solved analytically [11]. However in the realistic situation many

variables are a function of concentration hence the differential equation can be solved numerically only.

The concentration dependence of the viscosity was not used for correction of the increased viscosity near the membrane interface. This is not necessary because we use the appropriate sedimentation coefficients (i.e. at the actual boundary layer concentrations) to calculate the resistance of the concentrated layer.

The equations used to solve the problem numerically are the equations 1, 2, 3 and 9, where the dependence of the diffusion coefficient and the sedimentation coefficient on the concentration has to be included. Without any assumptions concerning the concentration at the membrane or the specific resistance of the concentrated layer, all ultrafiltration characteristics can be calculated including the concentration profile near the membrane. The only experimental data needed for simulating an ultrafiltration experiment are the retention and the hydraulic resistance of the membrane.

The comparison between the results of this model and Nakao's model will be made for the major part by comparing the $d(1/J_v)/d(V_p/A)$-values, which can be calculated easily from the computed flux-data.

EXPERIMENTAL

Materials

All experiments were performed using bovine serum albumin (BSA) Cohn fraction V from Sigma Chemical Company, lot nº 45F-0064 as a solute. The solutions of BSA were prepared in a phosphate buffer at pH = 7.4 ± 0.05 with 0.1 M NaCl added, to give a solution with ionic strength I = 0.125 N. The concentrations of the BSA solutions were determined, after producing a calibration curve, using a Hitachi Perkin Elmer double beam spectrophotometer model 124, operating at 280 nm. Normally the extinction coefficient E^{280} was 0.66. The water used was demineralized by ion exchange, ultrafiltered and finally hyperfiltered.

The membranes used in the dead-end ultrafiltration experiments were Amicon Diaflo membranes. In most experiments YM-30 membranes (regenerated cellulose-acetate, cut-off 30,000 D) were used and also experiments were performed using PM-30 membranes (polysulfone, cut-off 30,000 D).

Equipment

The unstirred dead-end ultrafiltration experiments were performed in an Amicon cell, type 401S, which was adapted to make thermostatting at 20°C possible. The total

membrane surface was 38.48 cm^2. To avoid fouling in the blank experiment, by e.g. colloids present in the system, the water was filtered in-line through a 0.22 μm PVDF Millipore microfiltration membrane. The amount of permeate was determined gravimetrically, while the amount of permeate collected in time was registered by a recorder.

Figure 3 gives a general outline of the equipment.

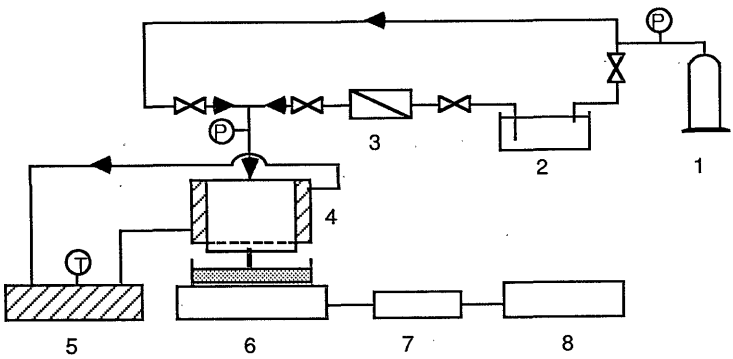

Figure 3. The dead-end ultrafiltration equipment.
1. technical air, 2. pressure vessel, 3. prefilter, 4. ultrafiltration-cell, 5. thermostat-bath, 6. balance, 7. D/A-converter, 8. recorder.

The simulations of ultrafiltration experiments were performed by using either a DEC-2060 computer or a VAX-8650 computer, in both cases with the help of several library routines to solve the differential equations. The main routine used is the D03PBF-NAG FORTRAN library routine document, which integrates a system of linear or nonlinear parabolic partial differential equations in one space variable [12].

The sedimentation and diffusion experiments were performed in a Beckman analytical ultracentrifuge, model E, equipped with a Schlieren optics and a temperature control system. Centerpieces of 1.5, 3 and 12 mm were used, the temperature was 20°C and the rotation speed was 40,000 rpm during the sedimentation experiments and 3400 rpm during the diffusion experiments. The concentration range measured was from 2.5 to 450 kg/m^3 for the sedimentation experiments and 6 to 215 kg/m^3 for the diffusion experiments.

Methods

To obtain the experimental flux-data the following procedure was employed :

a/ determine the water flux, b/ replace the water by the BSA solution at 20°C , c/ register the cumulative permeate weight as a function of time, d/ remove the BSA solution and rinse the ultrafiltration-cell radically, e/ determine the water flux again. To calculate the permeate volume the density of the permeate was taken as 1000 kg/m^3. In order to determine the protein retention the protein concentration of the feed, the retentate and the permeate solutions was measured spectrophotometrically.

RESULTS AND DISCUSSION

In the calculations to come and in the simulation computer-program some properties of BSA solutions will be used: the partial specific volume, the sedimentation coefficient and the diffusion coefficient. The values used for the partial specific volume are $v_1 = 1/(1.34\ 10^3) = 0.75\ 10^{-3}$ m^3/kg [5] and $v_0 = 1.0\ 10^{-3}$ m^3/kg. The values for the concentration dependent sedimentation coefficient were determined experimentally (Results section A). Some measurements were also performed to determine the diffusion coefficient of BSA at high concentrations (Results section B).

A. The sedimentation coefficient

The sedimentation coefficients of BSA had to be measured because of the very limited number of literature data on these coefficients. Mostly these coefficients were determined at very low concentrations or a different pH, while for our model knowledge of the sedimentation coefficients over a large concentration range is needed. The coefficients as determined at pH = 7.4 and I = 0.125 N, at 20°C, are given in figure 4.

The dependence on the concentration can best be described by

$$1/s = (1 / 4.412\ 10^{-13}) * (1 + 7.051\ 10^{-3}\ C + 3.002\ 10^{-5}\ C^2 + 1.173\ 10^{-7}\ C^3) \qquad (14)$$

The line in figure 4 is drawn according to eq. 14. A comparison of literature data with our consistent measurements is difficult: Kitchen et al. [13] find a qualitatively similar dependence on the concentration up to 80 kg/m^3 starting at $(s_{20,w})_0 = 4.1\ 10^{-13}$ s, for unbuffered BSA-solutions, according to Anderson et al. [14] the value of the pH will be around 6.5 then. A value found by Cohn et al. [15] is $s(1\%) = 4.0\ 10^{-13}$ s, measured at pH = 7.7. Our value of $4.12\ 10^{-13}$ s for s(10 kg/m^3) at pH = 7.4 is in good agreement with this literature value.

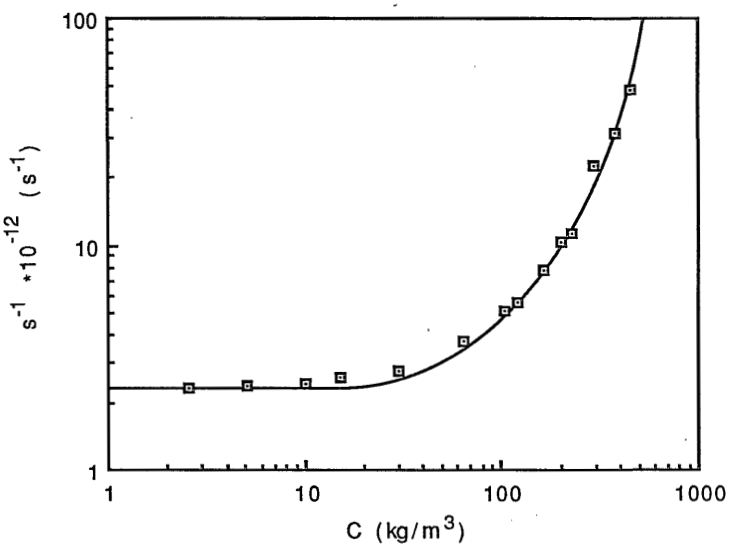

Figure 4. The (apparent, reciprocal) sedimentation coefficient of BSA as a function of concentration (pH = 7.4, I = 0.125 N and T = 20 °C)

B. The diffusion coefficient

The data on the diffusion coefficient of BSA at pH = 7.4 at high concentrations are limited: in the literature on modelling concentration polarization during ultrafiltration constant values are used for high concentrations. Trettin and Doshi [9] use D = 6.91 10^{-11} m^2/s, while this value was originally determined at a low concentration. Shen and Probstein [16] use D = 6.7 10^{-11} m^2/s , a value which was derived from ultrafiltration experiments and represents the diffusion coefficient at the "gel concentration" of 580 kg /m^3. We determined the value of the diffusion coefficient up to 210 kg/m^3.

In figure 5 our data are compared to those obtained by several other authors:

/1/ Phillies et al. [17]: these data were determined at pH = 7.2 to 7.5,

/2/ Anderson et al. [14], data at pH = 6.5, their equation D = 5.9 10^{-11} * (1 + 6.10^{-4}*C) was extrapolated to higher concentrations,

/3/ Fair et al. [18] obtained data at pH= 7.4,

/4/ Van Damme et al. [19] obtained data at pH = 7.2 up to 327 kg /m^3 and finally /5/ Kitchen et al. [13] used unbuffered BSA-solutions up to 240 kg /m^3.

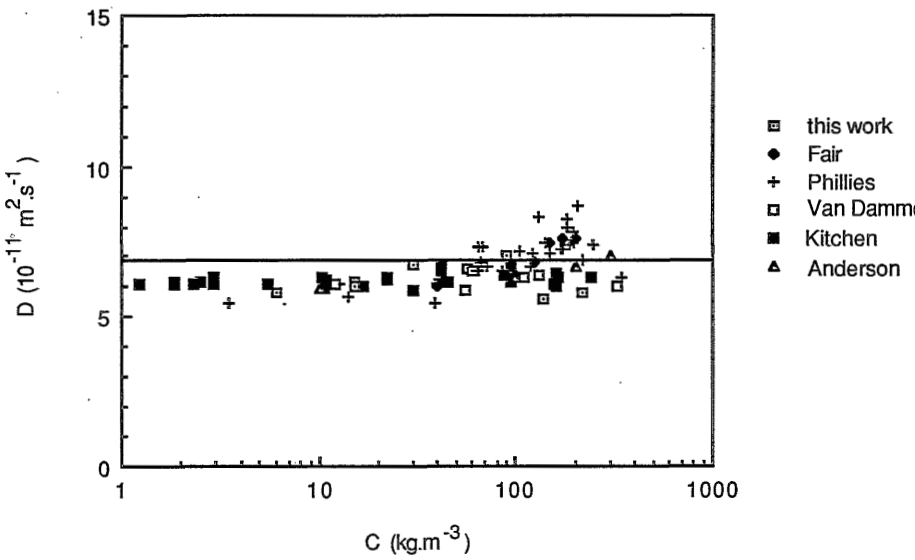

Figure 5. The diffusion coefficient of BSA as a function of concentration, data from several authors, ——: D = 6.9 10^{-11} m^2/s.

All solutions mentioned had an ionic strength of at least I = 0.1 N . The total review of data on diffusion coefficients of BSA at pH-values around 7.4 and at moderate to high concentrations shows that the diffusion coefficient is not significantly depending on the concentration of the solution. In our calculations we used D = 6.9 10^{-11} m^2/s over the entire range of concentrations. In the last part of section D the sensitivity of the model to the value of the diffusion coefficient will be discussed.

C. The flux behaviour during dead-end ultrafiltration: analysis using the 'cake-filtration' model

The results of some typical dead-end ultrafiltration experiments are given in figures 6 and 7, by plotting the reciprocal flux ($1/J_v$) as a function of the specific cumulative permeate volume (V_p/A). In figure 6 the dependence on the concentration is shown at constant pressure, while in figure 7 the concentration is constant and the pressure varies.

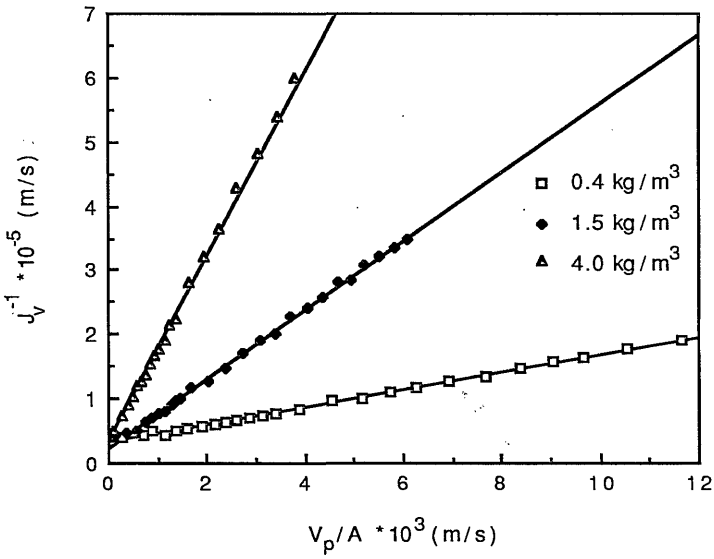

Figure 6. The reciprocal flux as a function of the specific cumulative permeate volume at different concentrations (Ultrafiltration of BSA at $\Delta P = 1.0\ 10^5$ Pa, YM-30 membrane)

A linear relation does exist in all cases, where the $1/J_v$-value at $V_p/A = 0$ represents the reciprocal clean water flux. This clean water flux varied only slightly before and after the experiment, i.e. 0-5% decline for the YM-30 membrane and for the PM-30 membrane only those experiments were used where the flux decline was less than 10%. This very small effect of adsorption or pore-blocking on a YM-30 membrane was also observed by Reihanian et al. [20].

The linear relationship between the reciprocal flux and the cumulative permeate volume is a well known phenomenon in unstirred dead-end ultrafiltration, however it is better known as the $V_p \sim t^{0.5}$ relationship. This relationship can be derived easily from the boundary layer theory: eq. 6 simplifies to eq. 15 when the resistance of the membrane is neglected compared to the resistance of the concentrated layer.

$$1/J_v = dt / d(V_p / A) = (\eta_0 * C_b * \Re_{obs} / \Delta P) * (r_{bl} / C_{bl}) * (V_p / A) \qquad (15)$$

from which the time-permeate volume relationship can be derived by integration

$$t = (\eta_0 * C_b * \Re_{obs} / 2.\Delta P) * (r_{bl} / C_{bl}) * (V_p / A)^2 \qquad (16)$$

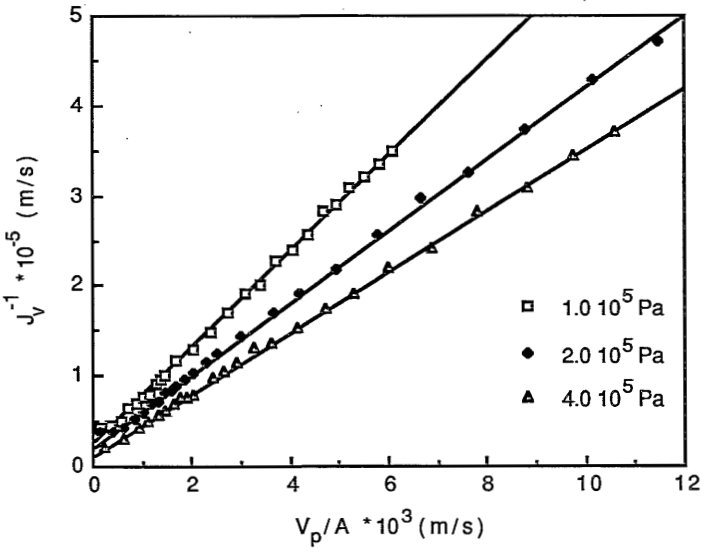

Figure 7. The reciprocal flux as a function of the specific cumulative permeate volume at different applied pressures (Ultrafiltration of BSA with C_b = 1.5 kg/m^3, YM-30 membrane)

This $V_p \sim t^{0.5}$ dependence is also found by Vilker et al. [5], Trettin and Doshi [9], Reihanian et al. [20] and Chudacek and Fane [21], each using a different theory.

A strong dependence of the reciprocal flux on both the concentration and the applied pressure is obvious from the slopes of the various lines. The flux decline indices r_{bl}/C_{bl} are calculated from these slopes according to eq. 7. In figure 8 r_{bl}/C_{bl} is plotted as a function of the bulk concentration for both the YM-30 membrane and the PM-30 membrane. The results show that the flux decline index tends to reach a constant value for higher concentrations, at each applied pressure, after a slight increase at concentrations below 2 kg/m^3.

From the figure it may be concluded that the build up of a concentrated "cake" layer near the membrane surface obtained through the analysis of the experimental data yields the same result for different membranes. However, these results are a little different from Nakao's results who found only a linear dependence on the concentration. Nakao performed experiments with dextrans and polyethylene glycols only at low concentrations (smaller than 0.6 kg/m^3). The influence of the retention, which was 95% or more in our case, is implemented in the calculations as represented by eq. 7.

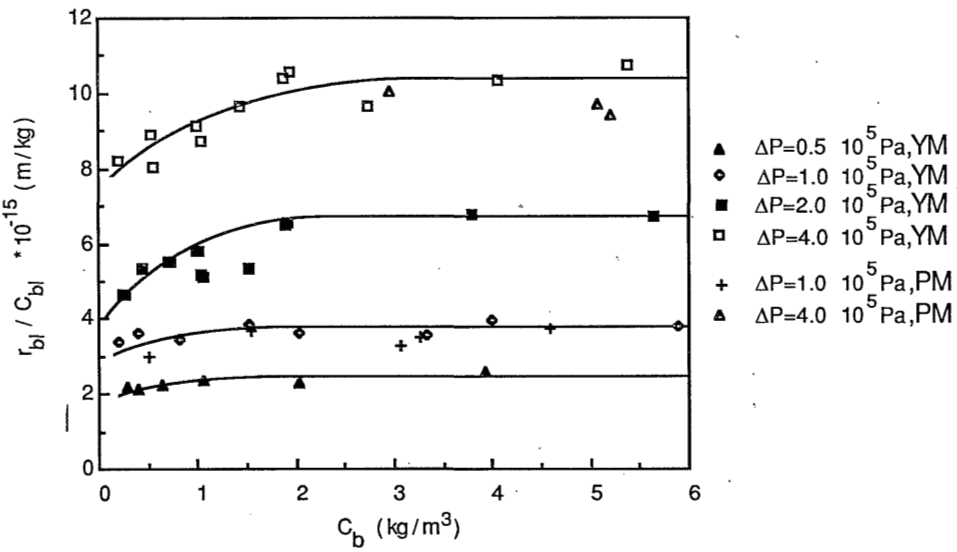

Figure 8. The flux decline index r_{bl}/C_{bl} as a function of concentration at several applied pressures. (YM-30 and PM-30 membranes used)

Taking the plateau value of r_{bl}/C_{bl} at each pressure the influence of the applied pressure on these values is given in figure 9.

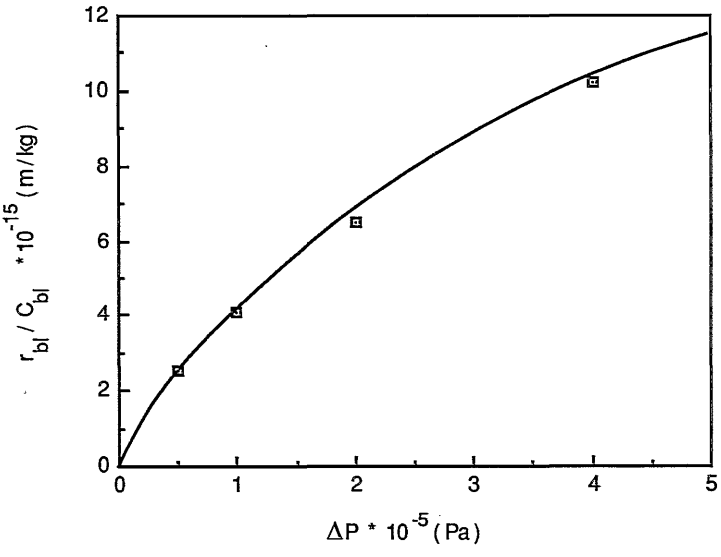

Figure 9. The plateau values of the flux decline index r_{bl}/C_{bl} as a function of the applied pressure.

From the r_{bl}/C_{bl}-values the 'cake' concentrations in the boundary layer C_{bl} can be calculated via the $s(C_{bl})$-values using eq. 8 and eq. 14. The resulting boundary layer concentrations are given in figure 10 as a function of the initial concentration of the bulk and the applied pressure.

As for the flux decline index a plateau value for the boundary layer 'cake' concentration also appears here, although the influence of the concentration of the bulk is not as clear as it was for the r_{bl}/C_{bl}-values. The calculated C_{bl} concentrations, varying from 180 to 440 kg/m^3, are all smaller than the gel concentration of 585 kg/m^3 which was obtained for BSA at pH = 7.4 (in fact a solubility limit was determined) [22]. According to this gel concentration and the model used there will be no gelation yet in the boundary layer.

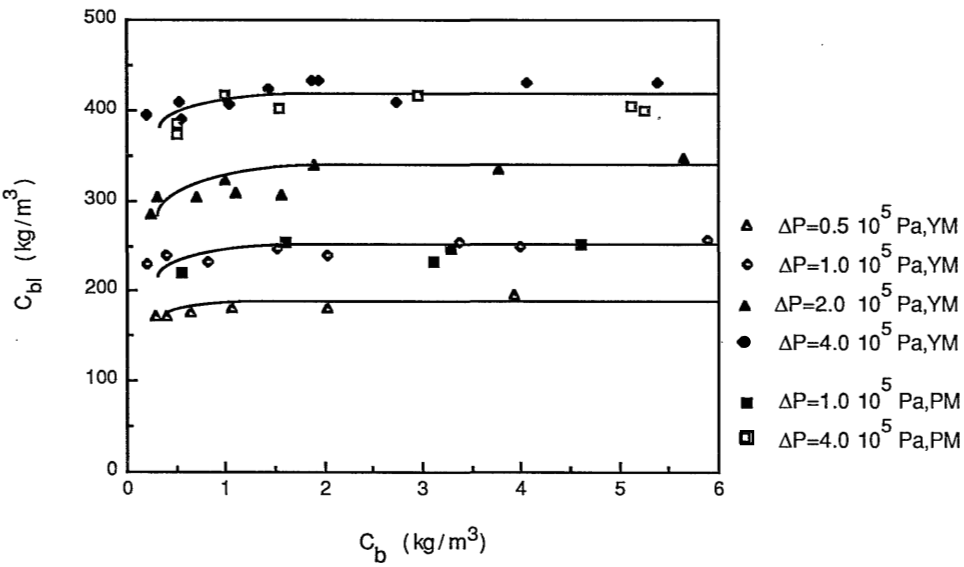

Figure 10. The calculated boundary layer concentration C_{bl} as a function of the initial bulk concentration and the applied pressure.

Knowing the r_{bl}/C_{bl}-values and the C_{bl}-values at the various applied pressures the values of the specific resistance r_{bl} can be calculated easily, the results of which are given in figure 11.

From these experimental data it is clear that the specific resistance is linearly dependent on the applied pressure as given in eq. 17. The dependence of the boundary layer concentration on the applied pressure is given in eq. 18, from which the dependence of the flux decline index on the applied pressure can be calculated (eq. 19).

$$r_{bl} = 9.9\ 10^{17}\ (10^{-5}.\Delta P) = 9.9\ 10^{12}\ \Delta P \quad (17)$$

$$C_{bl} = 260\ (10^{-5}.\Delta P)^{1/3} = 5.60\ (\Delta P)^{1/3} \quad (18)$$

$$r_{bl} / C_{bl} = 3.8\ 10^{15}\ (10^{-5}.\Delta P)^{2/3} = 1.76\ 10^{12}\ (\Delta P)^{2/3} \quad (19)$$

The dependence of r_{bl} and δ (via C_{bl}) on ΔP results in boundary layer resistance values (R_{bl}) which are proportional to $\Delta P^{2/3}$. This result indicates directly that the flux $J_v = \Delta P / [\eta_0 .(R_m + R_{bl})]$ is not linearly depending on ΔP, as is commonly known. In fact the flux is proportional to $\Delta P^{1/3}$ at equal cumulative permeate volumes V_p for the case where the membrane resistance can be neglected.

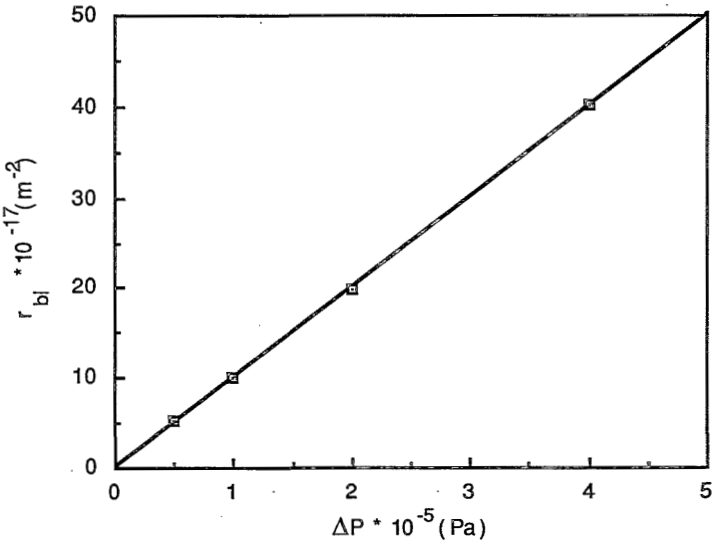

Figure 11. The specific resistance r_{bl} as a function of the applied pressure.

Other concentration polarization models concerning dead-end ultrafiltration have also lead to values for the specific resistance of the layer near the membrane, sometimes as a function of the applied pressure. Unfortunately a different meaning is sometimes given to the term specific resistance; however, by analysing the dimensions of the quantities given a comparison can be made:

- Reihanian et al. [20] determined gel layer permeabilities, using $C_{bl} = C_g = 590$ kg/m^3 (BSA at pH = 7.4), resulting in $r_{bl} = 6.7 - 33\ 10^{17}$ m^{-2}.
- Chudacek and Fane [21], using BSA at pH = 7.4 and C_g-values of 30-40%, found values of r_{bl}/C_{bl} strongly depending on the the applied pressure and also slightly on the concentration. The values for 2 kg/m^3 can be represented by $r_{bl}/C_{bl} \approx 4.0\ 10^{15}$ $(10^{-5}.\Delta P)^{0.55}$, which is in fair agreement with eq. 19.
- Finally Dejmek [23] after very many experiments at various pH-values found a relation, which was independent of the pH-value and which described the dependence of his 'specific resistance' of the gel layer (with dimension s^{-1}) on the pressure by $(\Delta P)^{0.72}$. Recalculation of his data showed that he calculated a quantity equivalent to our r_{bl}/C_{bl}-values, apart from a constant factor, which result is also in rather good agreement with eq. 19.

D. The new approach of the boundary layer resistance dead-end ultrafiltration model.

Before comparing the results of the analysis of experimental data according to Nakao's dead-end ultrafiltration model and the results of the computer simulations it will be shown that the computer simulations indeed agree with the experimental data. In figure 12 the data of two different experiments are compared with the data as calculated by the computer. For one experiment the initial concentration is 2.032 kg/m^3 and ΔP=1.0 10^5 Pa, while for the other experiment the initial concentration is 1.423 kg/m^3 and ΔP=4.0 10^5 Pa.

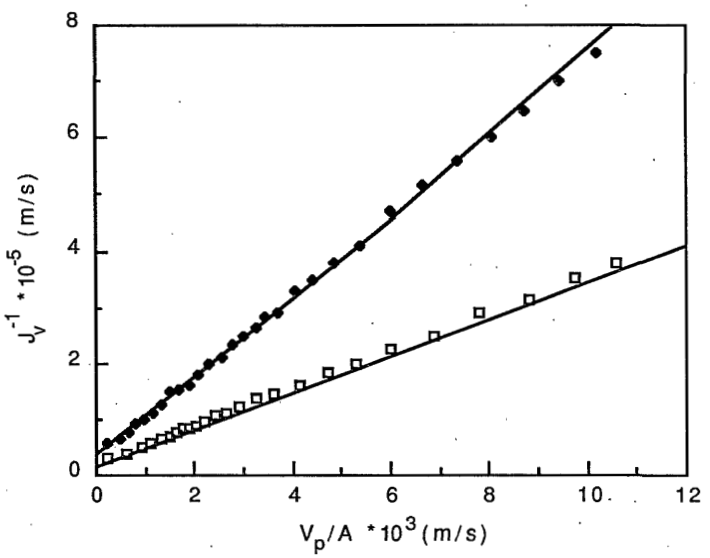

Figure 12. Comparison between reciprocal flux data obtained from ultrafiltration experiments and the computer simulation of these experiments.

simulation : ———

experiments : ♦ : ΔP=1.0 10^5 Pa, R_m=2.78 10^{12} m^{-1}, $\Re_{obs}$ =0.977, C_b =0.994 kg/m^3,

❑ : ΔP=4.0 10^5 Pa, R_m=4.55 10^{12} m^{-1}, $\Re_{obs}$ =1.0, C_b =1.423 kg/m^3.

From both comparisons it may be concluded that the simulations approximate the experimental results very well. Despite the different initial concentrations, different retentions and resistances of the membrane and especially the different applied pressures

the difference between the experimental data and the simulation data is smaller than 5%. This same result was obtained for a large number of experiments.

It is characteristic for the simulations that the slope of the 'straight' line approaches the experimental slopes very well, whereas at the first part of the simulated line a small non-linear relationship exists. Depending on the resistance of the membrane and the applied pressure the reciprocal flux is initially less than linear with the specific cumulative permeate volume. This can be observed especially when large membrane resistances and/or small applied pressures are used and it indicates that the simulation of the first few seconds underpredicts the resistance build up. Probably this is a result of the initial pore obstruction, and the resulting increase in the effective R_m-value, during an experiment.

Some results derived from the simulations.

During the simulations of the experiments it is possible to show the concentration profile near the membrane at every desired moment. For a number of time intervals this has been done to obtain an impression of the development of the profile with time (figure 13).

A number of characteristic phenomena (valid for all simulations) can be observed:

a/ even after a very short time interval high concentrations are reached at the membrane interface: $C_m \approx 260$ kg/m^3, after 10 seconds in figure 13, while the initial concentration was 4.0 kg/m^3. The thickness of the layer δ built up after 10 seconds is very small: $\delta \approx$ 20 μm.

b/ the concentration at the membrane interface continues to increase: 350 kg/m^3 after 50 sec. up to 385 kg/m^3 after 500 sec., while now the thickness δ increases clearly ($\delta \approx 120$ μm after 500 sec.).

c/ at longer times the concentration at the membrane interface reaches a plateau value, which is different for each applied pressure, and which is approximately 405 kg/m^3 for $\Delta P = 1.0\ 10^5$ Pa. In figure 14 the increase of the concentration at the membrane interface is plotted as a function of time.

d/ having reached the stationary state concentration at the membrane interface the concentration profile only expands away from the membrane. This expansion will proceed more and more slowly in time because of the decreased supply of the solute through diminished flux values.

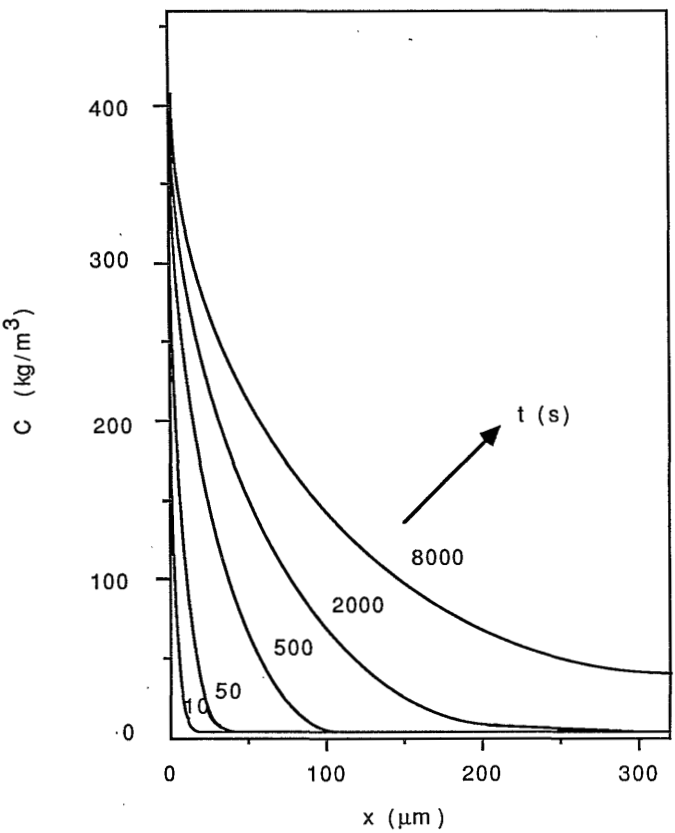

Figure 13. Simulated concentration profiles near the membrane interface as a function of time and distance from the membrane.
(ΔP=1 10^5 Pa, R_m=3.76 10^{12} m^{-1}, $\Re_{obs}$=1.0, C_b=4.00 kg/m^3)

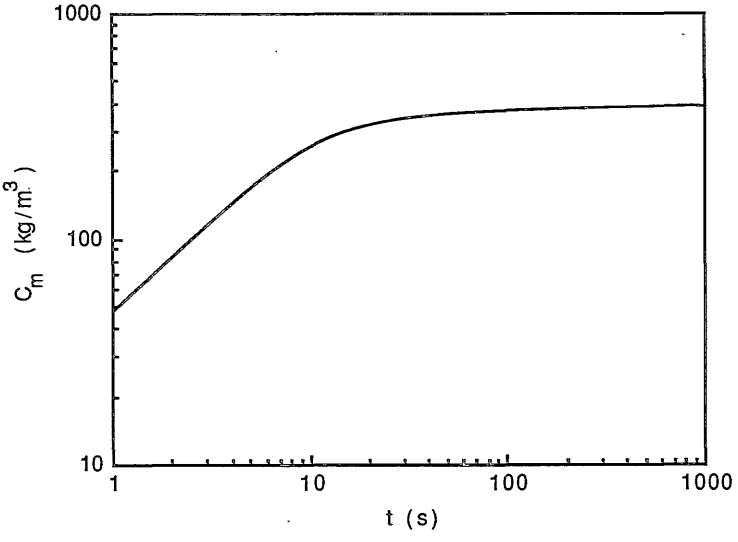

Figure 14. The concentration at the membrane interface as a function of time. (data obtained by simulation : ΔP=1 10^5 Pa, R_m=3.76 10^{12} m^{-1}, $\Re_{obs}$=1.0, C_b=4.00 kg/m^3)

The stationary state concentration at the membrane interface mentioned at point c appears to be very dependent on the applied pressure (figure 15).

From this figure it is clear that the concentration at the membrane interface first will increase strongly with increasing pressure but later-on the dependence on the pressure decreases. The calculated concentrations do increase up to values larger than the generally known gelconcentration of 585 kg/m^3 for BSA at pH = 7.4. This gelconcentration value is reached already at $\Delta P \approx 3.0\ 10^5$ Pa. However, despite these extremely high concentrations the flux behaviour is calculated very well in accordance with experiments.

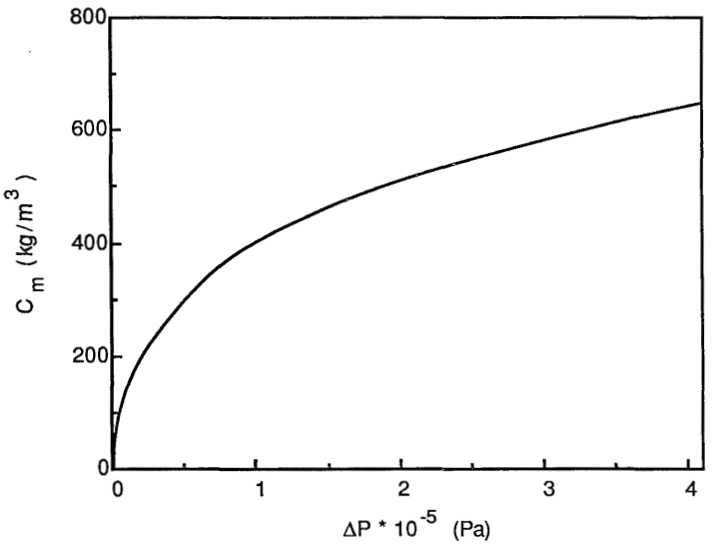

Figure 15. The stationary state concentration at the membrane interface as a function of the applied pressure. (data obtained by simulation : R_m=4.0 10^{12} m^{-1}, $\Re_{obs}$=1.0, C_b=1.0 kg/m^3)

Comparison of the results obtained from computer simulations and from the analysis of the experimental data by Nakao's model.

The comparison between the two versions of the boundary layer resistance model for dead-end ultrafiltration of BSA at pH = 7.4 is possible by comparing the slope α, which is proportional to the flux decline, and which is defined by

$$\alpha = d(1/J_v) / d(V_p/A) \qquad (20)$$

according to Nakao et al. this slope is given by (eq. 7)

$$\alpha = (\eta_0 * C_b * \Re_{obs} / \Delta P) * (r_{bl} / C_{bl})$$

In case of the simulations the slope of the straight part of the line will be calculated from the data between V_p/A is 5.10^{-3} and 10^{-2} m (compare figure 12).

The influence of the initial bulk concentration.

Both for the experimental data and the computer simulated data an initial increase in the $\alpha.\Delta P/C_b$ value (= $(r_{bl}/C_{bl}).\Re_{obs}.\eta_0$) can be observed with increasing bulk concentration,

starting from $\alpha.\Delta P/C_b = 0$ at $C_b = 0$ for the simulated data (figure 16). This starting value seems very reasonable as in the absence of solute no extra resistance or a concentrated layer can be formed at all. When the bulk concentration is still very low the equilibrium concentration at the membrane interface also reaches rather small values, resulting in relatively small $\alpha.\Delta P/C_b$ or r_{bl}/C_{bl}-values. After the initial increase the $\alpha.\Delta P/C_b$ values reach plateau values.

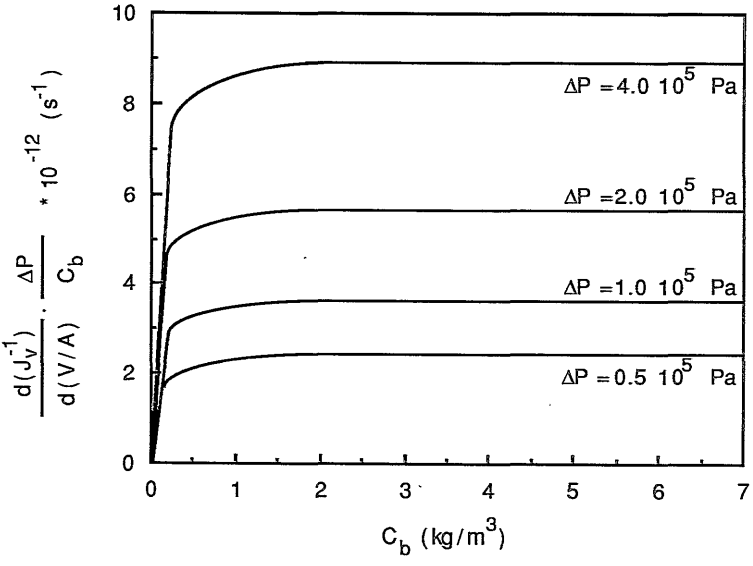

Figure 16. The influence of the initial bulk concentration on the calculated value of $\alpha.\Delta P / C_b$.(data obtained by simulation : ΔP=0.5, 1 or 2 10^5 Pa, R_m=4.0 10^{12} m^{-1}, $\Re_{obs}$=1.0)

Unlike these simulated and the experimental results, it follows from Nakao's model (eq. 7) that α is proportional to C_b, which was only valid for higher concentrations. As shown above the new model can predict this phenomenon correctly.

The influence of the observed retention.

According to Nakao's model α is proportional to the observed retention. This could not be confirmed or denied by experimental data because of the retention values being larger than 95% and so having too little influence. From the simulations it followed that the slope α indeed is proportional to the retention (figure 17).

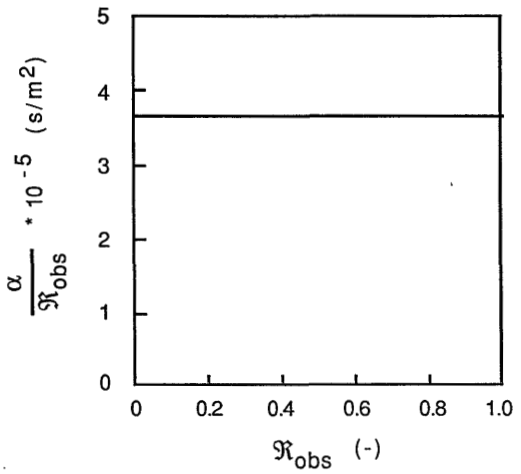

Figure 17. The influence of the retention on the $\alpha/\Re_{obs}$-value.
(data obtained by simulation : $\Delta P=1\ 10^5$ Pa, $R_m=4.0\ 10^{12}\ m^{-1}$)

The influence of the applied pressure.

It is rather difficult to describe directly the influence of the applied pressure in the new version of the model, which is due to the absence of terms like C_{bl} and r_{bl}. However, it followed from the analysis of the experimental data by Nakao's model that $r_{bl} = k * \Delta P$ (figure 11) from which it can be derived that $\alpha * C_{bl}$ is a constant for one set of $\Re_{obs}$ and C_b values since $\alpha * C_{bl} = (\eta_0 * C_b * \Re_{obs} / \Delta P) * (k * \Delta P)$, which is proportional to k. So α is proportional to $1/C_{bl}$.

The data from the simulations of experiments at various pressures showed that α is also proportional to $1/C_m$ ($\alpha * C_m$ is a constant in figure 18, C_m being the concentration at the membrane interface in a stationary state situation). Furthermore it may be concluded that C_m is only dependent on the pressure, which follows from all simulations with different parameters.

As mentioned before the dependence of C_{bl} on ΔP, according to Nakao's model, can be described as $C_{bl} \approx 260\ (10^{-5}\ \Delta P)^{1/3}$. According to the computer simulations this dependence is $C_m \approx 405\ (10^{-5}\ \Delta P)^{1/3}$. Apart from a constant factor an identical dependence on the pressure appears. The reason for this difference is simply the shape of the profile which is assumed for the case of the cake-filtration type of description: the constant concentration in the boundary layer is an average of a relatively thin layer with a higher concentration (and a higher C_m-value) and a layer with a lower concentration.

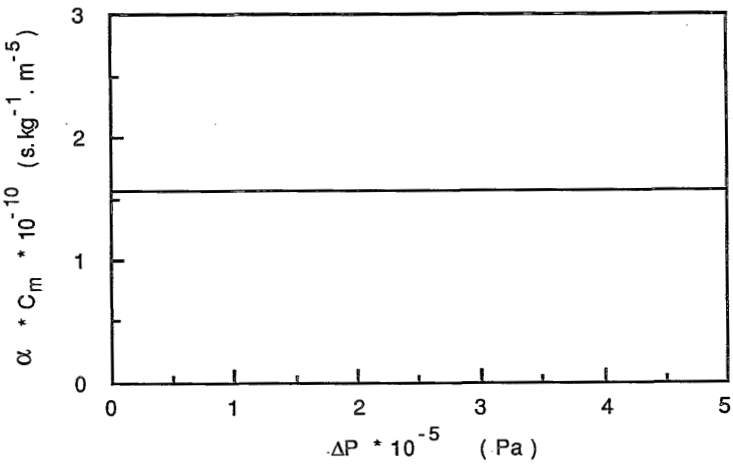

Figure 18. The influence of the applied pressure on the $\alpha * C_m$-value. (data obtained by simulation : R_m=4.0 10^{12} m^{-1}, $\Re_{obs}$ =1.0, C_b=1.00 kg/m^3)

The influence of the hydraulic resistance of the membrane.

Unlike for real experiments it is very simple to vary the hydraulic resistance of the membrane in a computer simulation, while the other parameters are kept constant. Figure 19 shows the results of simulating two different ultrafiltration experiments each using three different R_m-values. The influence of the R_m-values seems of minor importance. Especially when the resistance of the boundary layer increases as a result of more solute-supply from the bulk, by increasing the pressure or the concentration, the influence of the membrane is minimized.

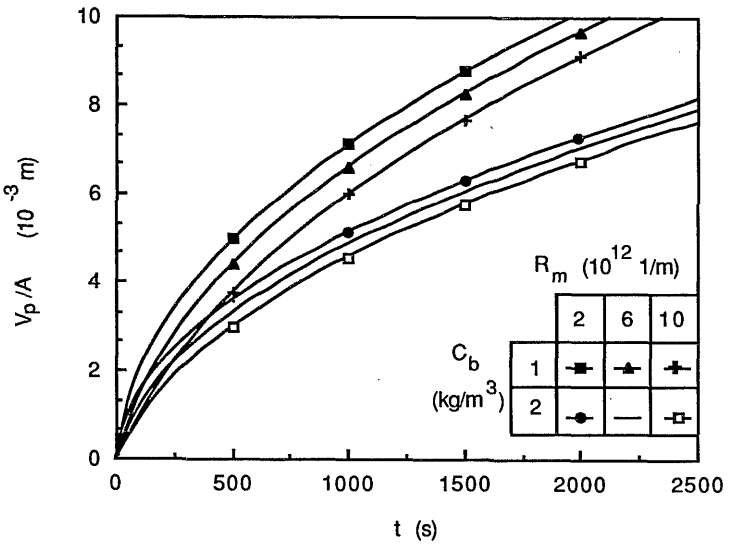

Figure 19. The influence of the resistance of a membrane on the flux behaviour in two different situations (data obtained by simulation : C_b=1 kg/m^3 and C_b=2 kg/m^3, ΔP=1 10^5 Pa, $\Re_{obs}$=1.0)

The sensitivity of the model to the value of the diffusion coefficient

It was shown in section B that the diffusion coefficient of BSA is rather constant over a large range of concentrations. At very high concentrations (100 kg/m^3 and more) there appeared to be a number of experimental data which were not exactly this constant value but were in the range from 5 to 9 10^{-11} m^2/s. Up to now all the computer calculations were done using one constant value of the diffusion coefficient. In this part of the discussion the influence of using a certain value will be demonstrated.

By using values of the diffusion coefficient of 6 10^{-12} to 2 10^{-10} m^2/s the flux decline index and the concentration at the membrane interface were calculated, as well as the concentration profile near the membrane after 1000 seconds filtration. The other physico-chemical properties will be kept constant during the simulations.

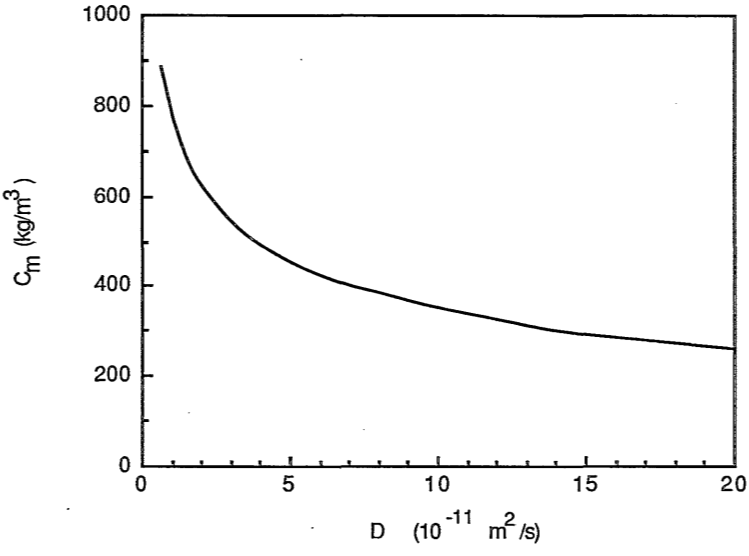

Figure 20. The concentration at the membrane interface as a function of the diffusion coefficient, data obtained by simulation.
(ΔP=1 10^5 Pa, R_m=3.76 10^{12} m^{-1}, $\Re_{obs}$=1.0 and C_b=4.00 kg/m^3)

As can be felt intuitively, the concentration at the membrane will increase with decreasing values of the diffusion coefficient because of the decreased back-diffusion away from the concentrated phase. The concentrations increase when the diffusion coefficient is very small, up to very high values like 800 kg/m^3 or even more (figure 20), while the value of the concentration at the membrane interface is very dependent on the diffusion coefficient. On the other hand, when the diffusion coefficent is 5 10^{-11} m^2/s or more the concentration at the membrane interface appears to be much less dependent on the diffusion coefficient. The increased concentrations at the membrane interface at smaller diffusion coefficients also result in increased resistances of the concentrated layer (eq. 8 and 14). And as can be expected from these equations the effect of the changing value of the diffusion coefficient is even more pronounced than in the case of the concentration at the membrane interface (figure 21). The relatively small effect of the change in diffusion coefficient in the region 5 10^{-11} m^2/s and higher shows that the exact value of the diffusion coefficient, within reasonable limits, is of minor importance.

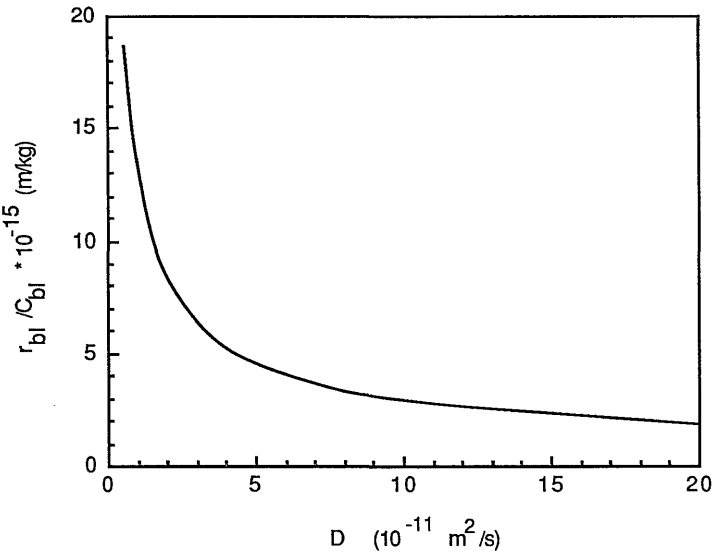

Figure 21. The calculated flux decline index as a function of the diffusion coefficient, data obtained by simulation. ($\Delta P=1\ 10^5$ Pa, $R_m=3.76\ 10^{12}\ m^{-1}$, $\Re_{obs}=1.0$ and $C_b=4.00\ kg/m^3$)

Finally, the effect of the changing diffusion coefficient is also represented in the concentration profile after a certain filtration-period. Figure 22 shows the concentration profiles after 1000 seconds in the case of 6 different diffusion coefficients. The increasing concentration with decreasing diffusion coefficient can be seen again as well as a very steep concentration gradient at small diffusion coefficients and a weak concentration gradient at larger diffusion coeffiicients. Though the amount of solute (equal to the surface under the graph and linear to the calculated cumulative permeate volume) increases with increasing diffusion coefficient the flux decline index and the total resistance decrease. This is due to the concentration dependence of the sedimentation coefficient, needed in eq. 8 and 14.

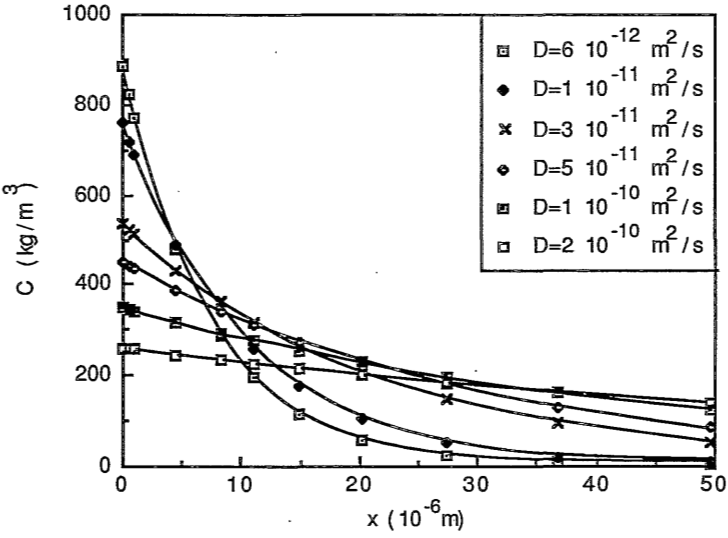

Figure 22. The concentration profiles after 1000 seconds filtration using different values of the diffusion coefficient, data obtained by simulation. (ΔP=1 10^5 Pa, R_m=3.76 10^{12} m^{-1}, $\Re_{obs}$=1.0 and C_b=4.00 kg/m^3)

CONCLUSIONS

The use of the boundary layer resistance model principles in combination with a dynamic model which describes the formation of a concentrated layer near the membrane interface can predict the experimental flux behaviour very well. Analysis of the experimental dead-end ultrafiltration data for BSA at various conditions with Nakao's boundary layer resistance/cake filtration model yields relations concerning the dependence on the applied pressure, which agree with literature values. In comparing our experimental data with those of Nakao et al. some deviations were found probably because of the extended range of concentrations used in this study. The simulations of ultrafiltration experiments yielded a similar dependence on the applied pressure and the concentration, as found by analysis with Nakao's model, but the calculated concentrations at the membrane reach extremely high values. Even so the predicted flux behaviour agrees with the experiments. These calculations also resulted in some interesting conclusions concerning the build up of the concentrated layer near the membrane interface. Extended simulations showed a linear

dependence of the flux decline index on the retention and only a limited influence of the hydraulic resistance of the membrane itself.

ACKNOWLEDGEMENTS

Thanks are due to Ms. Gonlag and Mr. Smit who performed the dead-end ultrafiltration experiments.

LIST OF SYMBOLS

A	membrane area	(m^2)
C_b	concentration of the bulk	(kg/m^3)
C_{bl}	(constant) concentration in the boundary layer	(kg/m^3)
C_g	gel concentration	(kg/m^3)
C_m	concentration at the membrane interface	(kg/m^3)
C_p	concentration of the permeate	(kg/m^3)
D	diffusion coefficient	(m^2/s)
J_v	flux	(m^3/m^2s)
J_w	clean water flux	(m^3/m^2s)
p	permeability of the boundary layer	(m^2)
r_{bl}	specific resistance of the boundary layer	(m^{-2})
$\Re_{obs}$	observed retention coefficient	(-)
R_{bl}	total hydraulic resistance of the boundary layer	(m^{-1})
R_m	hydraulic resistance of the membrane	(m^{-1})
s	sedimentation coefficient	(s)
T	temperature	(°C)
v_0	partial specific volume of the solvent	(m^3/kg)
v_1	partial specific volume of the solute	(m^3/kg)
V_p	(cumulative) permeate volume	(m^3)
x	coordinate perpendicular to the membrane	(m)
α	slope $d(1/J_v) / d(V_p/A)$	(s/m^2)
δ	thickness of the boundary layer	(m)
ΔP	applied pressure	(Pa)
η_0	viscosity of the solvent	(Pa.s)

REFERENCES

[1] S. Nakao, J.G. Wijmans and C.A. Smolders, Resistance to the permeate flux in unstirred ultrafiltration of dissolved macromolecular solutions, J. Membrane Sci., 26(1986)165-178.

[2] E. Matthiasson, The role of macromolecular adsorption in fouling of ultrafiltration membranes, J. Membrane Sci., 16(1983)23-36.

[3] M.S. Le and J.A. Howell, Alternative model for ultrafiltration, Chem. Eng. Res. Des., 62(6)(1984)373-380.

[4] A. Suki, A.G. Fane and C.J.D. Fell, Modeling fouling mechanisms in protein ultrafiltration, J. Membrane Sci., 27(1986)181-193.

[5] V.L. Vilker, C.K. Colton and K.A. Smith, Concentration polarization in protein ultrafiltration, Part II:Theoretical and experimental study of albumin ultrafiltered in an unstirred batch cell, AIChE Journal, 27(4)(1981)637-645.

[6] G. Jonsson, Boundary layer phenomena during ultrafiltration of dextran and whey protein solutions, Desalination, 51(1984)61-77.

[7] J.G. Wijmans, S. Nakao and C.A. Smolders, Hydrodynamic resistance of concentration polarization boundary layers in ultrafiltration, J. Membrane Sci., 22(1985)117-135.

[8] W.F. Blatt, A. Dravid, A.S. Michaels and L. Nelsen, Solute polarization and cake formation in membrane ultrafiltration: causes, consequences and control techniques, in J.E. Flinn (Ed.), Membrane Science and Technology, Plenum Press, New York, 1970, 47-97.

[9] D.R. Trettin and M.R. Doshi, Ultrafiltration in an unstirred batch cell, Ind. Eng. Chem. Fundam., 19(1980)189-194.

[10] P.F. Mijnlieff and W.J.M. Jaspers, Solvent permeability of dissolved polymer material. Its direct determination from sedimentation experiments, Trans. Faraday Soc., 67(1971)1837-1854.

[11] J.A. Howell and O. Velicangil, Theoretical considerations of membrane fouling and its treatment with immobilized enzymes for protein ultrafiltration, J. Appl. Pol. Sci., 27(1982)21-32.

[12] Fortran Library Manual, Mark 11, Volume 2, Numerical Algorithms Group, 1984.

[13] R.G. Kitchen, B.N. Preston and J.D. Wells, Diffusion and sedimentation of serum albumin in concentrated solutions, J. Polymer Sci., Polym. Symp., 55(1976)39-49.

[14] J.L. Anderson, F. Rauh and A. Morales, Particle diffusion as a function of concentration and ionic strength, J. Phys. Chem., 82(1978)608-616.

[15] E.J. Cohn, J.A. Luetscher, J.L. Oncley, S.H. Amstrong and B.D. Davis, Preparation and properties of serum and plasma proteins: part III, J. Am. Chem. Soc., 62(1940)3396-3400.

[16] J.J.S. Shen and R.F. Probstein, On the prediction of limiting flux in laminar ultrafiltration of macromolecular solutions, Ind. Eng. Chem. Fundam., 16(4)(1977) 459-465.

[17] G.D.J. Phillies, G.B. Benedek and N.A. Mazer, Diffusion in protein solutions at high concentrations: A study by quasielastic light scattering spectroscopy, J. Chem. Phys., 65(1976)1883-1892.

[18] B.D. Fair, D.Y. Chao and A.M. Jamieson, Mutual diffusion coefficients in Bovine Serum Albumen solutions measured by quasielastic laser light scattering, J. Coll. Interf. Sci., 66(1978)323-330.

[19] M.I. Van Damme, W.D. Comper and B.N. Preston, Experimental measurements of polymer unidirectional fluxes in polymer + solvent systems with non-zero chemical-potential gradients, J. Chem. Soc., Faraday Trans., 78(1982)3357-3367.

[20] H. Reihanian, C.R. Robertson and A.S. Michaels, Mechanisms of polarization and fouling of ultrafiltration membranes by proteins, J. Membrane Sci., 16(1983) 237-258.

[21] M.W. Chudacek and A.G. Fane, The dynamics of polarisation in unstirred and stirred ultrafiltration, J. Membrane Sci., 21(1984)145-160.

[22] A.A. Kozinski and E.N. Lightfoot, Protein ultrafiltration: a general example of boundary layer filtration, AIChE Journal, 18(1972)1030-1040.

[23] P. Dejmek, Concentration polarization in ultrafiltration of macromolecules, Ph.D. Thesis, Lund (Sweden), 1975.

CHAPTER 3

CONCENTRATION POLARIZATION PHENOMENA DURING DEAD-END ULTRAFILTRATION OF PROTEIN MIXTURES. THE INFLUENCE OF SOLUTE-SOLUTE INTERACTIONS.

G.B. van den Berg and C.A. Smolders

SUMMARY

The flux decline behaviour of some charged proteins and of binary mixtures of charged solutes during unstirred dead-end ultrafiltration has been studied. The mixtures consisted of the proteins BSA, α-lactalbumin and/or lysozyme. Of special interest were α-lactalbumin and lysozyme because these proteins are physico-chemically identical, except for the sign of their charge at the conditions used (pH = 7.4, I = 0.125 N and T = 20 °C). The ultrafiltration properties were studied using the boundary layer resistance model. Ultrafiltration of single protein solutions of α-lactalbumin and of lysozyme showed identical characteristics. The fouling behaviour during ultrafiltration of binary mixtures of the three components appeared to be dependent on both the charge of the solutes and on the (unequal) dimensions of the solutes. A mixture of oppositely charged proteins (i.e. BSA/lysozyme or α-lactalbumin/ lysozyme) showed sometimes a considerable increase of the resistance of the concentrated layer near the membrane, depending on the mixing ratio of the two proteins. When equally charged (i.e. BSA/ α-lactalbumin) proteins are ultrafiltered a small decrease of the resistance could be observed, again depending on the mixing ratio of the proteins. The charge of the proteins, especially opposite charges, appeared to influence the flux behaviour more than the slightly denser packing of the solutes (as a result of unequal dimensions) would allow for.

INTRODUCTION

Concentration polarization phenomena during membrane filtration have been described extensively in the last few decades. Several models have been proposed and these all

appeared to be useful for the specific solutes under study. The models often were adequate for one class of solutes and could not explain the phenomena which occurred during filtration of other types of solutes. The appearance of a variety of other flux declining phenomena like adsorption, pore-blocking and gel-layer formation may have been the reason for this imperfection. The inappropriate background of a model could also be at the origin of its failure, e.g. the use of specific characteristics of one solute may not be applicable to all solutes. The osmotic pressure model will not apply, as an example, in case of filtration of colloidal suspensions. Sometimes the analysis of concentration polarization phenomena is done by more than one model at a time: e.g. Choe et al. [1] used the osmotic pressure model for dextrans and the classic (compressible) filter-cake model for the colloidal suspension of bentonite to distinguish the two types of filtration behaviour of dextrans and bentonite. On the other hand several models have been used to describe the dead-end ultrafiltration behaviour of one protein, i.e. Bovine Serum Albumin (BSA): Vilker et al. [2] proposed the osmotic pressure model, Trettin and Doshi [3] the gel-polarization model, Reihanian et al. [4] and Chudacek et al. [5] a particle filtration model and Van den Berg et al. [6] the boundary layer resistance model. The difference often is the number of assumptions concerning the concentration profile, the permeability of the concentrated layer and/or the presence of a gel-layer. The nature of these models can vary from being more or less descriptive [4] to predictive [6].

Apart from the problem of choosing the best model for only one solute, there is the problem of describing the flux decline during the filtration of a complex fluid like milk or fruitjuice. These liquids consist of many different solutes which each can have a different effect on flux decline. As shown by Ingham et al. [7] and Fane [8], the presence of large solutes can influence the retention of smaller solutes. Changing the ionic strength or the pH-value of the solution, while using the same amount of macro-solute, can change the flux, which was also shown by Fane [8]. It will be clear that these changes can influence the properties of the solute and so the flux behaviour, indicating the importance of interactions between the micro- and macro-solutes in a solution. An example of macro-/ macro-solute interaction can also be found: an increase in concentration of the protein ß-lactoglobulin will result in an increasing retention because of association [9].

These examples clearly illustrate the problems which can arise when a number of solutes is brought together to simulate a complex fluid. The number of possible interactions, which may occur during the filtration, will increase exponentially with the increasing number of solutes. Therefore, the total effect of the solutes on flux decline will be very difficult to predict quantitatively or even qualitatively.

The aim of this work is to show the effect of interactions between two different proteins

during dead-end ultrafiltration. For that purpose experimental filtration data will be analysed using the boundary layer resistance model as described by Nakao et al. [10,11]. The proteins studied were BSA, lysozyme and α-lactalbumin. Of particular interest are the proteins lysozyme and α-lactalbumin because these two proteins are almost identical (in structure and geometry) but they have totally different iso-electric points. The result is that, at the conditions used (pH = 7.4), lysozyme is positive (net charge = +7 groups per molecule) and α-lactalbumin is negative (net charge = -7). A mixture of these proteins, or a mixture of BSA (net charge = -22) with one of these proteins, can therefore be interesting for a study of the interactions of proteins during dead-end ultrafiltration. Except for charge interactions also an additional effect can be expected to occur when mixtures are ultrafiltered: a different packing during the solute build-up near the membrane interface. Therefore some model considerations for the packing of binary mixtures will be given.

THEORY

A. The data analysis by the Wijmans-Nakao model.

In their articles on the hydraulic boundary layer resistance model for ultrafiltration Wijmans et al. [10] and Nakao et al. [11] showed that the analogy between permeation through a concentrated layer and sedimentation of a concentrated solution led to a model which could describe some concentration polarization phenomena near the membrane interface. Van den Berg et al. [6] adapted the boundary layer resistance model to the film theory and solved the differential equations involved numerically. The latter approach made it possible to predict the flux as a function of solute concentration, applied pressure, time and/or permeate volume as well as predicting other flux decline related phenomena like the build-up of the concentrated layer near the membrane interface. The only experimental data needed were the resistance of the membrane for pure water flow and the independently determined diffusion- and sedimentation coefficients of the solute as a function of concentration. However, when a mixture of solutes is used the diffusion- and sedimentation coefficients are hard to determine and when also interactions occur it is impossible to calculate these coefficients. Johnston and Ogston [12] reported that for a mixture of solutes in the absence of interaction the sedimentation coefficient of each solute as a function of concentration is dependent on the total amount of solutes: when the mixture contains x g/l of solute A and y g/l of solute B the sedimentation coefficients are calculated like $s_A = s_A(x+y)$ and $s_B = s_B(x+y)$, where $s_A(C)$ and $s_B(C)$ normally are different functions of concentration. When interactions occur, and more complex particles

are formed, this kind of description is not valid anymore. For this reason the analysis of the experimental data will be done using the cake filtration approach [11].

The flux is given by:

$$J_v = \Delta P / [\eta_0 . (R_m + R_{bl})] \quad (1)$$

where ΔP is the applied pressure, η_0 the viscosity of the solvent, R_m the resistance of the membrane and R_{bl} the resistance of the concentrated boundary layer.

The equivalent thickness of the boundary layer δ, having a constant concentration C_{bl} in the cake filtration approach, can be obtained via the mass balance, resulting in

$$C_b * \Re_{obs} * V_p = \delta * A * C_{bl} \quad (2)$$

in which C_b is the bulk concentration, $\Re_{obs} = 1 - (C_p/C_b)$ is the observed retention, V_p is the accumulated permeate volume and A is the membrane area. Now the resistance of the boundary layer can be described by

$$R_{bl} = \delta * r_{bl} \quad (3)$$

in which the specific resistance r_{bl} is assumed constant over the boundary layer δ. Combining equations 1, 2 and 3 results in

$$1/J_v = 1/J_w + (\eta_0 * C_b * \Re_{obs} / \Delta P) * (r_{bl} / C_{bl}) * (V_p / A) \quad (4)$$

in which (r_{bl}/C_{bl}) is a quantity called the *flux decline index* and (V_p/A) is the specific cumulative permeate volume.

In order to analyse the experimental results, for which slopes in the plot of $1/J_v$ as a function of (V_p/A) are required, eq. 4 is transformed into

$$d(1/J_v) / d(V_p / A) = (\eta_0 * C_b * \Re_{obs} / \Delta P) * (r_{bl} / C_{bl}) \quad (5)$$

For known values of C_b, η_0, $\Re_{obs}$ and ΔP the flux decline index r_{bl}/C_{bl} can be determined from one set of experiments.

Eventually, from this r_{bl}/C_{bl} -value and the relationship between the permeability p of the boundary layer and the sedimentation coefficient s(C)

$$p = 1 / r_{bl} = (\eta_0 * s(C)) / (C * (1-v_1/v_0) \quad (6)$$

the boundary layer concentration C_{bl} can be calculated via

$$r_{bl} / C_{bl} = (1 - v_1 / v_0) / (\eta_0 * s(C_{bl})) \quad (7)$$

provided the dependence of s on the concentration is known.

B. Solute-solute interactions

The interactions which can occur in a mixture of proteins in a buffer are both micro-/macro-solute interactions and macro-/macro-solute interactions. Since we use the same buffer (phosphate-buffer at pH = 7.4) and the same amount of salt (0.1 N NaCl) in all experiments in this work the micro-/macro-solute interactions will be considered to be constant. The remaining (changing) interactions are the protein-protein interactions. These interactions can be subdivided into interactions which occur between proteins of one kind (self-association) and interactions which occur between different proteins.

When looking at the properties of the proteins used (Table 1) a number of characteristics can be observed. First of all the striking resemblance of the proteins lysozyme and α-lactalbumin is obvious; in this study hen's egg-white lysozyme and bovine α-lactalbumin are used. These proteins have similar amino acid sequences, identical chain folds but different functions [21]. The physico-chemical properties of these two proteins therefore are almost identical, except for the iso-electric point (I.E.P.) and therefore the net charge at pH = 7.4. The consequence is that the filtration behaviour of the proteins separately has to be identical because the values of s(C), D(C) and v_1 are the same and those are the only parameters necessary to describe the dead-end filtration phenomena with the boundary layer resistance model.

In Table 1 the radius r_s of the proteins is calculated using the Stokes-Einstein equation for spherical particles

$$D_{c=0} = kT / (6\pi.\eta.r_s) \quad (8)$$

	lysozyme	α-lactalbumin	BSA
M_w (Dalton)	14,200 [13] 14,100 [14]	14,400 [15]	69,000 [16]
I.E.P.	11.0 [13]	5.1 [17]	4.7 [18]
net charge at pH = 7.4	+ 7 [13]	- 7 [19]	- 22 [20]
$D_{c=0}$ (10^{-11} m^2/s)	10.7 [21]	10.6 [22]	5.9 [6]
$s_{c=0}$ (10^{-13} s)	1.86 [21]	1.83 [17]	4.41 [6]
v_1 (10^{-4} m^3/kg)	7.26 [23]	7.35 [22]	7.34 [18]
r_s (nm)	2.00	2.02	3.64

Table 1. Physico-chemical properties of the proteins lysozyme, α-lactalbumin and BSA (data are at pH = 7.4, T = 20 °C and I = 0.125 N, or closest data available)

Self-association of the lysozyme molecules at high concentrations could introduce some problems when calculating the concentration in the boundary layer via eq. 7, but since we use the measured sedimentation coefficient as a function of the actual concentration the 'actual' boundary layer concentration will be calculated. The self-association constant for lysozyme is K = 0.489 m^3/mol at pH = 7.0 and I = 0.2 N [23].

Association between positively and negatively charged proteins can be expected to be substantially larger. Steiner et al. [24] found for the association-constant of BSA and lysozyme at pH = 7.0 and I = 0.01 N the value of 40 m^3/mol. Though direct comparison between the association constants is not allowed because of the difference in ionic strength the association constant for the BSA-lysozyme couple seems to be considerably larger than for the self-association of the lysozyme proteins. No data were found in literature concerning the association of α-lactalbumin with other or identical proteins. The fact that mixtures of proteins carrying opposite charges form stable solutions indicates that not only these charge interactions are important, but also other factors like for instance hydration of the protein molecules.

C. The build-up of a layer of particles of unequal size

Apart from the difference in charge the solutes can also have different dimensions. When the Stokes radius (3.64 nm for BSA and 2.02 nm for α-lactalbumin and lysozyme) is taken as a reference the diameter-ratio is 0.55 when BSA is in the mixture and is 1.00 otherwise. From literature [e.g. 25] it is known that mixing particles of different size will increase the overall packing density and it therefore will enhance the resistance to permeation of solvent. The extent of this effect depends on the particle diameter ratio and the way of packing.

The packing density changes with the regularity of the lattices built up. For packing of equal spheres the cubic-close-packed (c.c.p.) structure is the most dense with only 25.9% porosity. In case of filtration a randomly packed layer of particles is more likely to be formed. Many experiments and computer simulations have been performed to calculate the porosity ε of layers of spheres of equal size in random packing (see Rodriguez et al. [25] for a review). Depending on the coordination number, the packing density varies from 0.58 ($\varepsilon = 0.42$) for 'loose random packing' to 0.64 ($\varepsilon = 0.36$) for 'dense random packing' of equal spheres.

The packing of spheres of unequal size depends on the diameter ratio of the particles. For the case of a binary mixture both experiments [26] and computer simulations [25,27] have been performed for various diameter ratios. In general the porosity or density is calculated as a function of the volume fraction ϕ_1 of the smaller particles. Ben Aïm et al. [26] showed experimentally that the porosity of a binary mixture of spheres with diameter ratio 0.52 (which is very close to our ratio of 0.55 for BSA and α-lactalbumin or lysozyme) first decreases rapidly from $\varepsilon = 0.36$, at $\phi_1 = 0$, to a minimum value for the porosity $\varepsilon = 0.31$ at $\phi_1 = 0.25$ and increases slowly again to the original value of $\varepsilon = 0.36$, at $\phi_1 = 1$. A very similar behaviour is found in calculations by Dodds [27] for several diameter ratios (0.17 to 0.71) though in this reference it was stated that "the absolute values of porosity were not realistic" ($\varepsilon \approx 0.2$). The calculations by Rodriguez et al. [25] c the packing density (= 1 - ε) as a function of ϕ_1, at diameter ratio 0.3, and their comparison with several experimental data showed rather large mutual deviations. The maximum density, at $\phi_1 \approx 0.25$, increases from 0.64 (calculated [25,28]) to 0.74 (experimental [26]). Although this difference seems to be relatively small, when the Kozeny-Carman equation is used to calculate the specific resistance of such a layer the effect of the deviating density is very large. The Kozeny-Carman equation describes the specific resistance as [29]

$$r_{KC} = [5 * (S_0)^2] * [(1 - \varepsilon)^2 / \varepsilon^3] \qquad (9)$$

where S_0 is the specific area of the particles (= 3 / r_s). For a given mixture with a fixed ϕ_1 S_0 is constant, so that the specific resistance at (1 - ε) = 0.74 is about 3.5 times larger than at (1 - ε) = 0.64.

An estimation of the influence of the composition in a mixture of BSA (larger particles) and α-lactalbumin or lysozyme (smaller particles) on the porosity and the specific resistance can be made using the experimental data for uncharged particles of Ben Aïm et al. [26]. In this analysis we use the molar fraction as the main variable, as will be done in the plots in the section with results of ultrafiltration experiments. In figure 1 the porosity and the specific resistance are given as a function of the molar fraction of small particles, assuming no interaction (a detailed description of mixtures with unequally sized, uncharged solutes is given in Appendix 1). The porosity clearly changes with the changing fraction of smaller particles x_1, with a minimum value near $x_1 = 0.6$, and the calculated specific resistance of a mixture of BSA and α-lactalbumin or lysozyme seems to be an almost linear function of x_1. In this case (i.e. charge effects are excluded), the calculations for a mixture of α-lactalbumin and lysozyme would result in a constant porosity (ε = 0.36) and a constant specific resistance ($r \approx 1\ 10^{20}\ m^{-2}$).

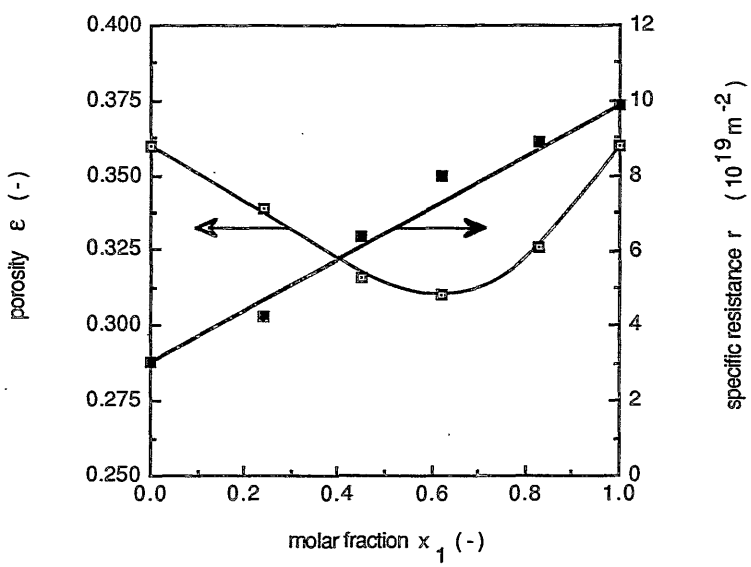

Figure 1. The porosity and specific resistance (the latter according to the Kozeny-Carman equation) in a binary mixture of hard spheres as a function of the molar fraction of small particles. For the big particles the dimension of BSA (d_p = 7.28 nm) is taken and for the small particles the dimension of α-lactalbumin or lysozyme (d_p = 4.0 nm) is taken. Interactions due to charge are supposed to be absent.

An estimation concerning the behaviour of the flux decline index r_{bl}/C_{bl} of a mixture of particles with the dimensions of BSA and α-lactalbumin or lysozyme can be made also, while noticing that the computed values of the specific resistance are at least one order of magnitude too large (compare the values of the specific resistance given in figure A.1 with calculated values from the figures 3 and 4). This can only be a very general estimation, the reasons are the unknown dependence of the quantity r_{bl}/C_{bl} on the applied pressure and the unknown boundary layer concentration C_{bl}. Assuming C_{bl} to be constant, which is true for $x_1 = 0$ and $x_1 = 1$ (see hereafter and ref. [6]), the flux decline index also is a linear function of the molar fraction x_1. If the flux decline index of a mixture of BSA and another protein as a function of the molar fraction of BSA follows a linear relationship we can write:

$$r_{bl}/C_{bl}(\text{mixture of BSA + protein x}) = x_{BSA}*r_{bl}/C_{bl}(\text{BSA}) + (1-x_{BSA})*r_{bl}/C_{bl}(\text{protein x}) \quad (10)$$

When the porosity decreases a little because of the unequal size of the solutes, e.g. like Ben Aïm [26] described, the flux decline index will increase significantly, but as the concentration C_{bl} will increase the flux decline index will also show a small decrease in comparison to eq. 10. For the diameter-ratio 0.52 the decrease in porosity and r_{bl}/C_{bl} will be at most some 14 %.

EXPERIMENTAL

The proteins used were bovine serum albumin (BSA), hen's egg-white lysozyme and bovine α-lactalbumin. The BSA was a Cohn fraction V from Sigma Chemical Company. The crystallized lysozyme was from FLUKA A.G. The α-lactalbumin was prepared from casein whey and was kindly supplied by the Netherlands Institute for Dairy Research (NIZO). The protein solutions were prepared in a phosphate buffer at pH = 7.4 ± 0.05 with 0.1 M NaCl added, resulting in a solution with ionic strength I = 0.125 N.

The concentration of each protein in the mixture was determined using a Waters HPLC system. The column used was a PROTEIN-PAK 125 column (GPC), the detection wavelength was 280 nm and the buffer was a phosphate buffer at pH = 7.4 with 0.15 N Na_2SO_4 added (for the separation of the equal molecular-weight proteins α-lactalbumin and lysozyme a buffer at pH = 4.5 was used).

The unstirred dead-end ultrafiltration experiments and the experiments to determine the sedimentation coefficient of lysozyme as a function of concentration were carried out as described previously [6]. The membranes used in the ultrafiltration experiments were

Amicon YM-5 membranes (regenerated cellulose-acetate, cut-off 5,000 D). The retention for BSA was 100% and 99.5+% for the other proteins. The concentration range for the determination of the sedimentation coefficients was 5 to 310 kg/m^3.

RESULTS AND DISCUSSION

1. The sedimentation coefficient of lysozyme

When the concentration in the layer near the membrane interface is calculated the sedimentation coefficient as a function of concentration has to be known (eq. 7). The sedimentation coefficient of lysozyme had to be determined experimentally because of the very scarce data on these coefficients in the literature. Especially at higher concentrations no data were available. The values of the reciprocal sedimentation coefficient, as determined at pH = 7.4, I = 0.125 N and T = 20 °C, are represented in figure 2.

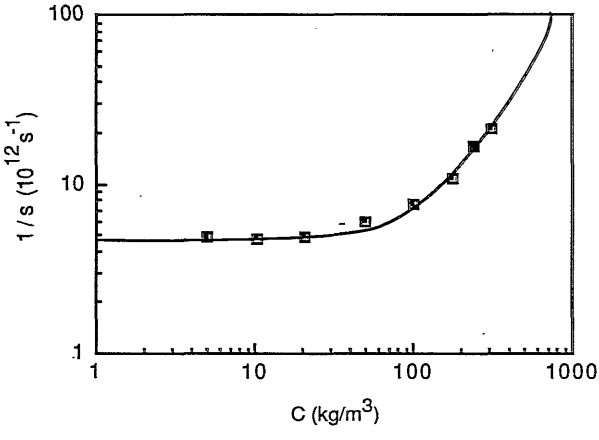

Figure 2. The measured reciprocal sedimentation coefficient of lysozyme as a function of concentration (pH = 7.4, I = 0.125 N and T = 20 °C)

Curve fitting of the experimental data resulted in

$$1/s = (1 + 1.067\ 10^{-3} * C + 5.537\ 10^{-5} * C^2 - 1.341\ 10^{-7} * C^3 + 1.856\ 10^{-10} * C^4) / (2.042\ 10^{-13}) \quad (11)$$

Following the strong analogy in physico-chemical properties of α-lactalbumin and lysozyme the sedimentation coefficient of α-lactalbumin is assumed to have the same dependence on the concentration as is the case for lysozyme. This dependence was not determined experimentally because of the limited amount of pure α-lactalbumin available and its extraordinary high purchase price.

2. Dead-end ultrafiltration of single protein solutions

Ultrafiltration experiments with single protein solutions of lysozyme and α-lactalbumin were performed to compare the filtration characteristics to those of BSA and to each other. The pressures used were 1.0 or 4.0 10^5 Pa, the temperature was 20 °C and the concentration range was 0 to 4 kg/m^3 for α-lactalbumin and 0 to 6 kg/m^3 for lysozyme.

As described in the theoretical section the flux decline index r_{bl}/C_{bl} can be calculated from the slope $d(1/J_v)/d(V_p/A)$. In figure 3 the values of this index are given as a function of the concentration in the bulk for both the proteins lysozyme and α-lactalbumin at the two applied pressures, 1.0 and 4.0 10^5 Pa.

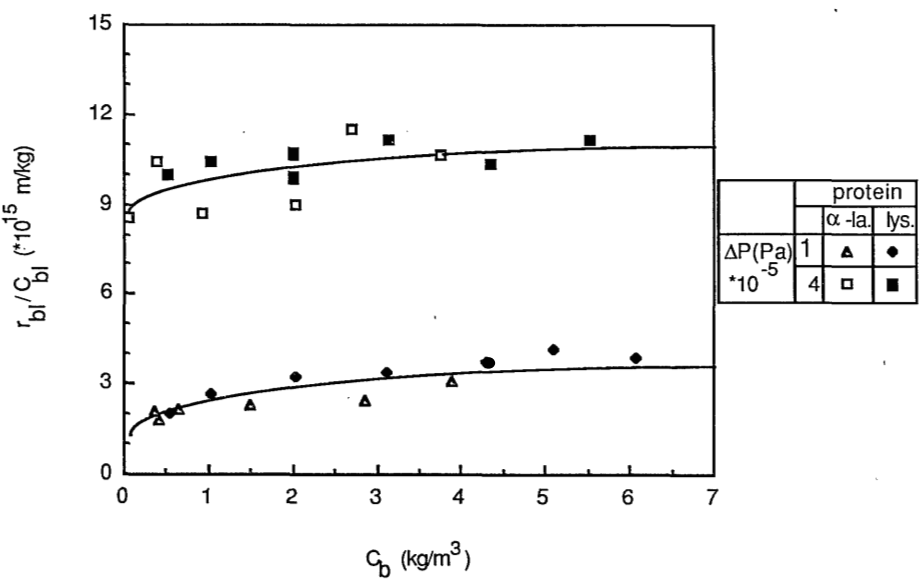

Figure 3. The flux decline index r_{bl}/C_{bl} as a function of concentration in the bulk for the proteins α-lactalbumin and lysozyme. ΔP = 1.0 or 4.0 10^5 Pa.

From this figure it can be concluded that the flux decline indices indeed are equal for the two proteins, as could already be expected from the almost identical physico-chemical properties. As shown in our previous work [6] for BSA the flux decline index also first increases with concentration at low concentration in the bulk but soon it reaches a plateau value. These plateau values are about 3.9 and 10.8 $*10^{15}$ m/kg respectively for the applied pressures 1.0 and 4.0 10^5 Pa. For BSA values of 3.8 and 10.5 $*10^{15}$ m/kg respectively were found at the pressures mentioned [6]. As these values do not differ very much for these three proteins, the question arises whether the flux decline index could perhaps be about the same for all solutes at a given pressure. In Table 2 a number of flux decline indices is given for different kinds of solutes at applied pressures $\Delta P = 1.0$ and 4.0 10^5 Pa (most data were obtained from data-points in plots which makes them approximate values).

solute	ΔP (10^5 Pa)	$\frac{r_{bl}}{C_{bl}}$ (10^{15} m/kg)	Reference
lysozyme or α- lactalbumin	1 4	3.9 10.8	this work
BSA	1 4	3.8 10.5	[6]
hemoglobin	1 4	3.8 11.5	[30]
ß - lactoglobulin	1 4	3.1 9.4	[30]
Dextran T500	1 4	13.5 24.0	[11]
PEG 600	1 4	16.5 23.5	[11]
silica colloids	1	0.15 - 0.9	[31]

Table 2. The flux decline index of several solutes at applied pressures $\Delta P = 1.0$ and 4.0 10^5 Pa, most data taken from literature.

Dejmek [30] found almost identical values for the specific 'gel' resistance (m) of the proteins hemoglobin and ß-lactoglobulin ($r_{bl}/C_{bl} = (m)/\eta_0$). Nakao et al. [11] calculated much higher values for the flux decline index of the solutes Dextran T500 and PEG 600. On the other hand, data by McDonogh et al. [31] for silica colloids with varying zeta potentials show much lower values.

The almost identical values for the proteins and the different values for the other solutes seem to lead to the conclusion that the permeability of a concentrated boundary layer depends on the compactness and type of packing of these solutes. A concentrated layer of the rather compact and impermeable protein molecules is more permeable than a layer of entangled polymers (Dextrans and PEG), but less permeable than a layer of very compact but rather loosely packed silica colloids. The observation by McDonogh et al. that a higher zeta potential (more open structure) decreases the specific resistance of colloids agrees with this conclusion. In the case of Dextran T70 and PEG 600 (above the overlap concentration which is about 5%) the transport of the solvent water probably occurs through the molecular coils (intramolecular) while the transport is around the particles (intermolecular) in the case of proteins and colloids [32].

When the data from figure 3 are used to calculate the concentration in the boundary layer, with help of eq. 7 and 11, it can be seen that these concentrations can reach rather high values (figure 4). In these calculations eq. 11 is used both for lysozyme and for α-lactalbumin.

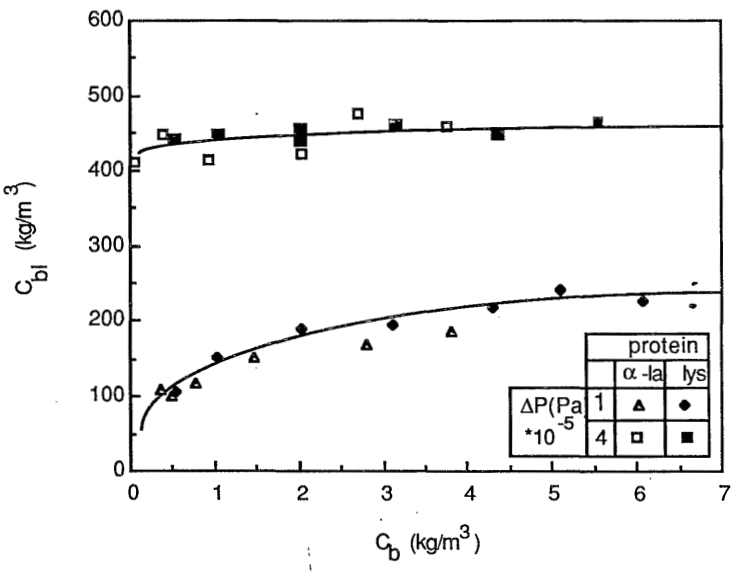

Figure 4. The calculated boundary layer concentration C_{bl} as a function of the initial bulk concentration and the applied pressure.

The plateau values of the boundary layer concentrations are about 240 and 450 kg/m^3 for

the applied pressures $\Delta P = 1.0$ and $4.0\ 10^5$ Pa respectively. It will be clear that at these high concentrations rather large resistances for permeation can be expected. The real value of the concentration at the membrane interface will be different from those mentioned here because of the assumption that the concentration in the boundary layer is constant, i.e. independent of the distance. In our previous work [6] we showed that a decreasing concentration profile into the bulk solution is more realistic and can be calculated from basic equations for the case of a solution with one solute. In that case the concentration at the membrane interface was shown to be somewhat higher. There is a maximum possible concentration of course, which is determined by the density of the particles, the shape and size of the particles and the inter-particle distance as a result of attraction or repulsion.

3. Dead-end ultrafiltration of mixtures of proteins

The flux decline indices of mixtures of proteins are calculated in the same way as for solutions of single proteins. To make allowance for the specific properties of each kind of protein (e.g. charge and molecular weight) the flux decline index is represented as a function of the number of moles present in the solutions: the molar fraction of one of the proteins is used as composition variable.

As mentioned in the theoretical section, the flux decline index of a mixture of BSA and another protein as a function of the molar fraction of BSA possibly follows a linear relationship, given by eq. 10. Obviously when the experimental data should follow this linear relationship there would be no significant difference between the interaction of a protein with a protein of the same kind and the interaction with a differently charged and differently sized protein (e.g. diameter ratio 0.55 for the proteins used).

In figure 5 the indices are given as a function of the molar fraction BSA present in mixtures with either lysozyme or α-lactalbumin. The data at $x = 0$ and $x = 1$ are the plateau values for the flux decline indices of the single proteins.

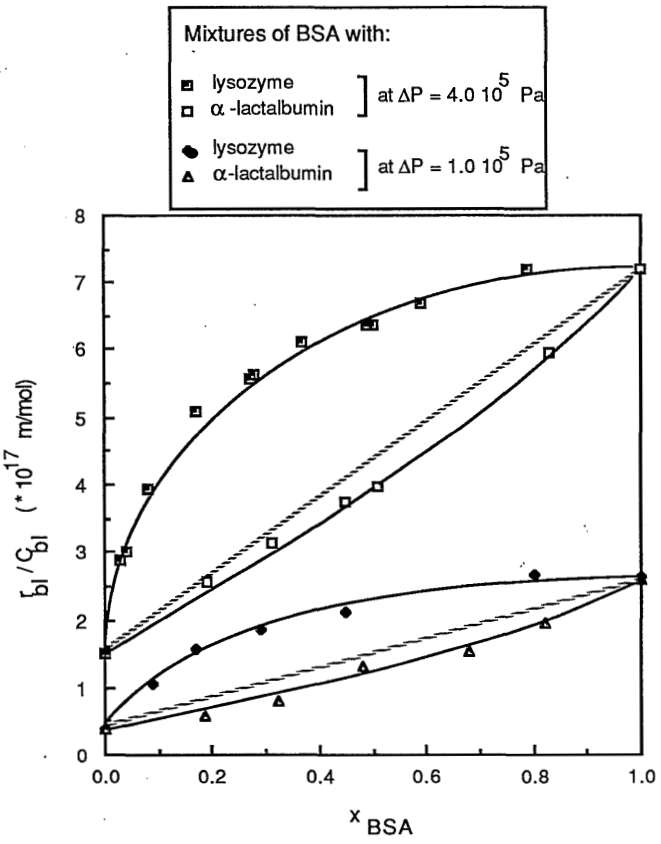

Figure 5. The flux decline index r_{bl}/C_{bl} (on molar basis) for mixtures of BSA with α-lactalbumin or lysozyme, as a function of the molar fraction BSA in the solution. $\Delta P = 1.0$ and $4.0\ 10^5$ Pa, $T = 20$ °C, pH = 7.4 and $I = 0.125$ N. The concentration in the bulk solution was between 1 and 5 kg/m^3.

For the two pressures studied the values for the flux decline index of a mixture of BSA and α-lactalbumin (both negatively charged) show slightly smaller values than the linear curve representing eq. (10). In view of the theoretical considerations given above this would mean that the BSA and α-lactalbumin molecules have built up a concentrated layer during filtration with a slightly decreased flux decline index in comparison with two non-interacting proteins in the mixture. The repulsion between these different molecules is almost equal to the repulsion between the proteins of only one kind of protein. The deviation to a more loosely packed boundary layer could perhaps be due to the

non-spherical dimensions of the BSA molecule. Even so, our conclusion is that essentially the experimentally determined flux decline indices show the same tendency here with changing molar fraction x_1 as derived in the theoretical section, indicating that the equations originally meant for much larger spherical particles can also be applied to hard semi-spherical solutes such as proteins.

The data on the mixtures of BSA and lysozyme show a quite different flux behaviour. The flux decline index is larger than the linear relationship between the indices of the single protein solutions (eq. 10). The index can reach values up to twice the predicted value (i.e. for $x_{BSA} \approx 0.1$ to 0.2). The origin of the larger resistance than that predicted for non-interacting particles may be found in a tighter packing of the concentrated layer. This is possible because of the oppositely charged particles. It can be imagined that a boundary layer of positively and negatively charged proteins can be packed more densely than a layer of protein-molecules with just one type of charge, resulting in a much higher specific resistance. While the flux decline index r_{bl}/C_{bl} increases more than linearly with x_{BSA}, the specific resistance r_{bl} will have to increase still more strongly, since the concentration C_{bl} also can be expected to increase as a result of the attraction. These observations also can be described theoretically for the analogous case of single lysozyme solutions, using the equations for the calculation of the specific resistance (eqs. 7 and 11). When the concentration in the boundary layer increases, e.g. from 300 to 360 kg/m^3 (= 20%), the specific resistance will increase more strongly because of the exponential equation for the (reciprocal) sedimentation coefficient (in this example 30%) resulting in a higher value for the flux decline index (in this example 8%).

In figure 6 the results for the experiments using mixtures of the equally sized but oppositely charged α-lactalbumin and lysozyme are shown. For these mixtures the flux decline index again is considerably larger than the values for the single protein solutions and seems to indicate a maximum near $x_{\alpha\text{-lactalbumin}} = 0.5$. Here the flux decline index appears to be about 2.3 times as large as in the case of single protein solutions. The packing of the positively and negatively charged protein molecules will again be much more dense than in the case of the single protein solutions.

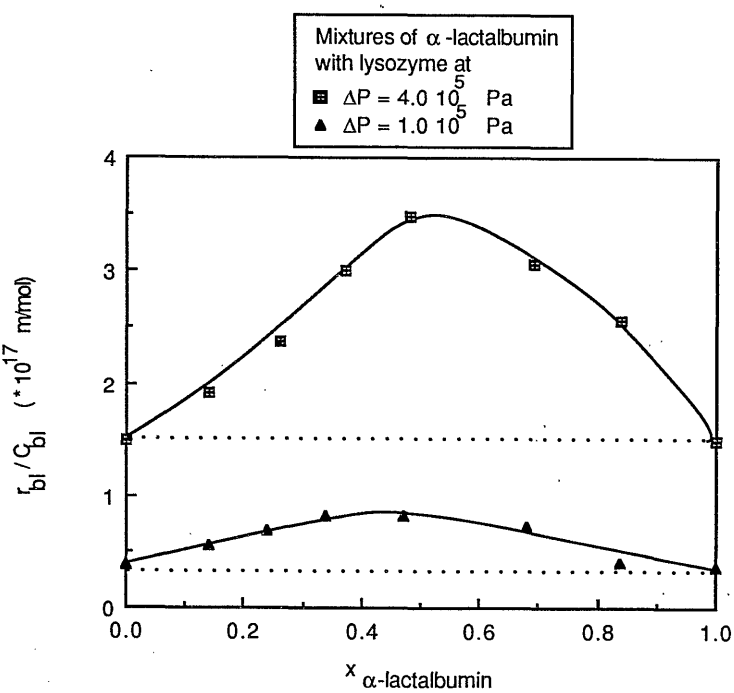

Figure 6. The flux decline index r_{bl}/C_{bl} (on molar basis) for mixtures of α-lactalbumin with lysozyme, as a function of the molar fraction α-lactalbumin in the solution. ΔP = 1.0 and 4.0 10^5 Pa, pH = 7.4, T = 20°C and I = 0.125 N.

Except for the sign of the charge these molecules are totally identical as to the physico-chemical properties and the flux behaviour (Table 1 and fig. 3). Hence the specific resistance or the flux decline index could be expected to be totally constant if the attraction were not present. The effect of oppositely charged but further identical molecules in a network can only be an enhanced packing density and an increasing resistance, probably with a maximum in resistance at $x_{\alpha\text{-lactalbumin}} = 0.5$ because of the numerically equal charge for lysozyme and α-lactalbumin respectively and identical dimensions for these proteins. Looking only at mutual charge compensation for the effect on packing density (and not at the influence of particle dimensions) the maximum relative increase in resistance for the case of mixing lysozyme and BSA could be expected at $x_{BSA} = 0.25$. This is not too far off from the actual situation found in fig. 5.

The observation that the flux decline indices and specific resistances of mixtures with oppositely charged particles only increase indicates that no coagulation or flocculation

occurs in the solution before the particles settle in the concentrated layer near the membrane interface. When this would have occured the structure of the concentration polarization layer would have been much more open with a lower resistance as the result [31]. The reason for this phenomenon probably is the presence of stabilizing hydration shells around the proteins.

The inter-particle distance can be estimated for both the single protein solutions and the mixtures (see Appendix 2). The distance between molecules in a single protein solution is calculated to be 0.92 nm, whereas the minimum distance in a mixture of α-lactalbumin and lysozyme, at $x_{\alpha\text{-lactalbumin}} = 0.5$, is only 0.44 nm. Apparently a considerable decrease can occur due to the attraction of the oppositely charged proteins.

When the charge of the proteins changes, e.g. as a result of a change in pH, a different behaviour can be expected: when the charge of the positive lysozyme proteins is twice the charge of the negative α-lactalbumin proteins the maximum resistance can be expected at $x_{\alpha\text{-lactalbumin}} = 0.67$. Though this example can be calculated easily, much more complicated calculations can be expected when also the size of the solutes is unequal or when (many) more solutes are in the solution. Then the total fouling capacity has to be determined using all the different interactions between the solutes, while their different sizes have to be taken into account as well, which probably results in a too complex set of equations. The only way left then is the experimental way to determine the flux decline index, which will also be of more use when other practical circumstances (e.g. the temperature) are changed.

CONCLUSIONS

The flux behaviour of mixtures of proteins during unstirred dead-end ultrafiltration can be very different from the behaviour of the single proteins. Both larger and about equal flux decline indices can be determined for solutions with mixtures of solutes, compared to the single solute solutions. The net charge of the molecules can give essential information of the kind of interactions which will lead to a different fouling behaviour. When oppositely charged proteins (lysozyme with α-lactalbumin or BSA) are present in a mixture during ultrafiltration the permeability of the concentrated boundary layer near the membrane interface can decrease drastically, this depends on the mixing ratio of the proteins. When equally charged proteins are present in a solution (BSA with α-lactalbumin) the resistance or flux decline index decreases only slightly. The effect of opposite charges seems to be much more effective than the difference in size of the solute molecules. The changing packing of layers of unequal size particles certainly influences the

resistance of such a layer but not as much as the difference in charge does. Simulating the ultrafiltration of a complex liquid, like milk or whey with many differently sized and charged molecules, therefore will be very difficult. From the observations described above it will be clear that the fouling capacity of a mixture of solutes can not be described by simply adding up the fouling behaviour of the single solutes. When the total fouling capacity of a complex mixture has to be determined the calculations probably will be too complex because of all the interactions between the solutes and the different sizes which have to be taken into account. The only way left then is the experimental way, which will also be of more use when other practical circumstances like a changing pH-value etc. are considered.

ACKNOWLEDGEMENTS

The authors wish to thank the Netherlands Institute for Dairy Research for supplying us with the α-lactalbumin sample. Thanks also to Ms. A. Gonlag and Ms. M. Veldhuis for performing the experiments and analyses and to Dr. I.G. Rácz and Dr. Th. van den Boomgaard for helpful discussions.

APPENDIX 1

The porosity and specific resistance as a function of x_1.

The experimental data (the porosity ε as a function of the volume fraction ϕ_1 of small glass particles), as obtained from data-points in a plot of Ben Aïm et al. [26] are given in Table A.1. These data were used to estimate the specific resistance r of a concentrated layer of BSA (largest protein, r_s = 3.64 nm) and α-lactalbumin or lysozyme (smallest proteins, r_s = 2.02 nm). These results can also be found in the table and it will be explained in this appendix how we obtained these results. For reasons of convenience in this appendix the layer will be assumed to consist of BSA and α-lactalbumin (the same results, only about 1% difference, will be obtained for a layer with BSA and lysozyme when the dimensions of the particles are taken into account only, and not the charge).

Ben Aïm [26] (experimental)		calculated		
ϕ_1	ε	x_1	r_{KC} ($10^{19}m^{-2}$)	r_H ($10^{19}m^{-2}$)
0	0.360	0	3.05	2.78
0.06	0.339	0.24	4.27	4.06
0.14	0.316	0.45	6.36	6.36
0.25	0.310	0.62	8.00	8.11
0.50	0.326	0.83	8.91	8.71
1	0.360	1	9.88	9.00

Table A.1. Experimental and calculated characteristics of a binary mixture of α-lactalbumin (r_s = 2.02 nm) and BSA (r_s = 3.64 nm). For explanations see text.

Assuming no mutual interaction (attraction or repulsion), neglecting effects from the applied pressure and assuming the proteins to be spheres with radii equal to the Stokes-radius the specific resistance and the porosity will be calculated for such a layer of unequal-sized particles as a function of the molar fraction of small particles x_1.

The molar fraction x_1 is used as the main variable in this appendix because x_1 is the most convenient parameter to use when the experimental flux decline indices r_{bl}/C_{bl} have to be represented. For the mixture α-lactalbumin/BSA the x_1-value can be calculated from the ϕ_1-value, since the specific volumes or densities are equal, using

$$\phi_1 = V_1 / (V_1 + V_2) = m_1 / (m_1 + m_2) \qquad (A1)$$

where V_1 and V_2 are the volumes occupied in the layer by the small and large particles respectively, and m_1 and m_2 are the masses of these particles. The molar fraction x_1 can now be described by

$$x_1 = [m_1 / 14000] / \{[m_1 /14000] + [m_2 / 69000]\} = m_1 / [m_1 + 0.203*m_2] \qquad (A2)$$

The specific resistance can easily be calculated using the general Kozeny-Carman equation

$$r_{KC} = [5 * (S_0)^2] * [(1-\varepsilon)^2 / \varepsilon^3] \qquad (9)$$

now calculating the specific area S_0 as [33]

$$S_0 = 3 \{ \phi_1 / r_{s,1} + \phi_2 / r_{s,2} \} = 3 \{ \phi_1 / r_{s,1} + (1 - \phi_1) / r_{s,2} \} \qquad (A3)$$

The results of the calculations are given in Table A.1, while the specific resistance and the porosity as a function of x_1 are plotted in figure 1 (theoretical section). The almost linear dependence of the specific resistance on x_1 is quite remarkable.

A more fundamental way to calculate the specific resistance is by the (theoretical) Happel's resistance law, which incorporates a stagnant layer around the particles [34]

$$r_H = [18 \varphi_e / (d_p)^2] * [(1 - \varepsilon)^2 / \varepsilon^3] \qquad (A4)$$

where φ_e is a rather complicated function of the porosity and the particle diameter. This term can be described accurately, for $0 \leq \varepsilon \leq 0.6$, by the empirical relation [33]

$$\varphi_e = 9.0 + [\varepsilon^3 / (1 - \varepsilon)^2] \qquad (A5)$$

For the case that the resistance of a mixture with varying porosity has to be calculated an additional (empirical) term $(\varepsilon / \varepsilon_m)^{0.75}$ has to be added [33], where ε_m is the porosity of the mixture and ε the original porosity.

The total resistance of a mixture can now be described by

$$r_H = [18 / (d_m)^2] * [(1 - \varepsilon_m)^2 / \varepsilon_m^3] * \{9.0 + [\varepsilon_m^3 / (1 - \varepsilon_m)^2]\} * (\varepsilon / \varepsilon_m)^{0.75} \qquad (A6)$$

where d_m is calculated as

$$d_m = 1 / \{\phi_1 / d_1 + (1 - \phi_1) / d_2\} \qquad (A7)$$

The calculated values of r_H as a function of x_1 are also given in Table A.1. In figure A.1 a comparison is given between the data on the specific resistance according to the two models.

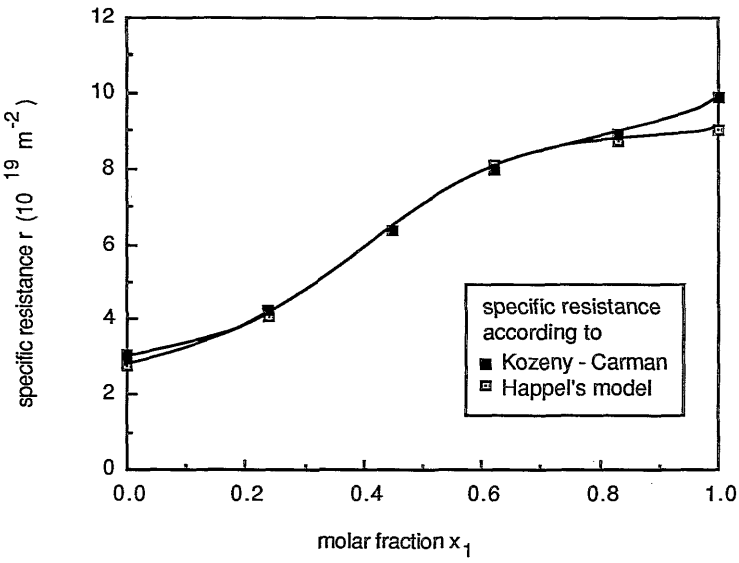

Figure A.1. The specific resistance of a mixture of BSA and α-lactalbumin as a function of the molar fraction of α-lactalbumin according to two models: the Kozeny-Carman model and Happel's model.

Apparently the two models result in about the same specific resistance in the porosity range used. Large deviations can only be expected when $\varepsilon_m > 0.6$, i.e. when φ_e becomes much larger than the value represented by eq. A.5. For reasons of convenience the more simple Kozeny-Carman model will be used to compare 'theoretical' and experimental data.

Though the calculations show an almost linear dependence of the specific resistance on the molar fraction, this might be difficult to understand because of the declining average particle diameter of the mixture d_m and the decrease in porosity as well. To show the effect of only a decrease in the d_m-value, in figure A.2 the specific resistance is plotted as a function of the molar fraction x_1 for a constant ε-value of 0.36 and for the 'actual' variation in porosity, using the experimental values of Ben Aïm [26]. (The calculations are done using the Kozeny-Carman equation).

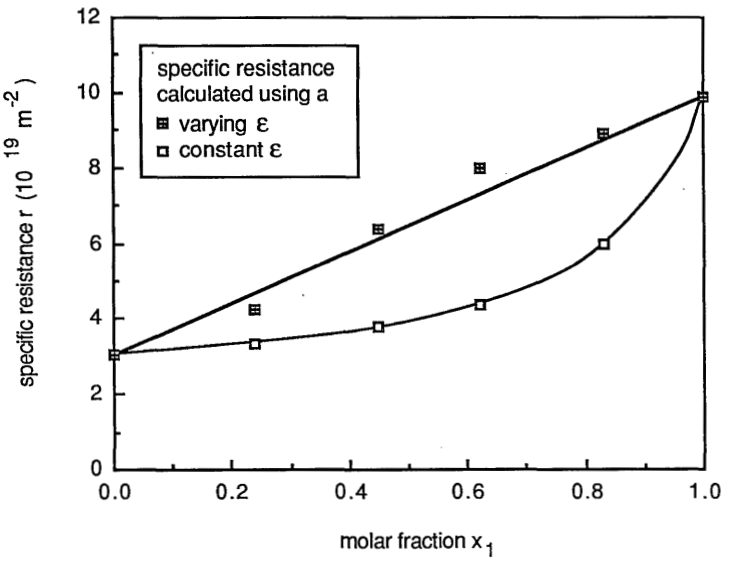

Figure A.2. The specific resistance as a function of the molar fraction of small particles, using a varying porosity and a constant porosity.

From the figure it can be concluded that the specific resistance decreases indeed, compared to a linear dependence, when only the average particle diameter d_m decreases (lower set of data-points).

APPENDIX 2

Estimation of the inter-particle distance in single protein solutions and in mixtures.

In this appendix the change in packing density, as a result of the charge interactions, will be estimated using the experimental ultrafiltration results. As shown in fig. 6 the flux decline index of a mixture of lysozyme and α-lactalbumin can be substantially larger than the flux decline index of the single protein solutions of lysozyme or α-lactalbumin. Therefore it is very likely that the porosities and the inter-particle distances are also different. They are calculated as follows: using eq. 7 the sedimentation coefficient of the solutions can be calculated from the flux decline index, assuming the sedimentation coefficient of the mixture is equal to the sedimentation coefficient of a single protein with

the same (total) concentration. From the value of the sedimentation coefficient the concentration in the boundary layer can be calculated (eq. 11) and so the specific resistance r_{bl}. By using the Kozeny-Carman equation (eq. 9), taking $r_{KC} = r_{bl}$, the apparent porosity ε_{app} can be calculated. Now the minimum distance between the proteins can be estimated, using the representation of figure A.3. for two particles in a protein layer.

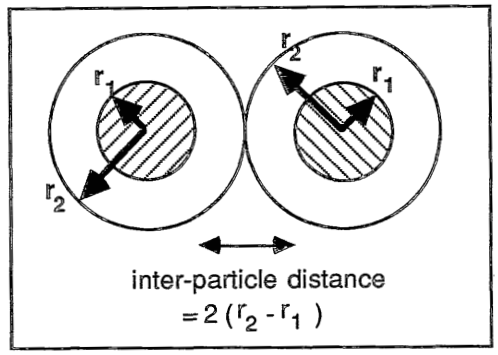

Figure A.3. Representation of the radii and the inter-particle distance of two particles, for details see text.

Knowing that the size of α-lactalbumin is identical to that of lysozyme a rather simple model can be derived for the total porosity: assume the layer to consist of randomly packed spheres, in which the particles are present plus an extra voidage which prevents the particles to touch (caused by intercharge interactions, hydration shells or mixed forms). If the particles have a radius r_1 and the spheres have a radius r_2, the minimum interparticle distance will be $2*(r_2-r_1)$. The porosity of this system can be described like the porosity of a randomly packed layer of equal spheres ($\varepsilon = 0.36$) plus the extra voidage inside the spheres, $0.64 * (1 - V_1/V_2)$, where V_1 and V_2 are the volumes of the particles and the spheres respectively. This results in:

$$\varepsilon_{tot} = 0.36 + 0.64 * [1 - V_1/V_2] = 0.36 + 0.64 * [1 - (r_1)^3/(r_2)^3] \qquad (A8)$$

Taking $\varepsilon_{app} = \varepsilon_{tot}$, the radius r_2 can be calculated like

$$r_2 = r_1 * [0.64 / (1 - \varepsilon_{tot})]^{1/3} \qquad (A9)$$

from which the inter-particle distance ($= 2[r_2 - r_1]$) can be calculated.

For $\Delta P = 4.0\ 10^5$ Pa the experimental values of the flux decline index are $1.5\ 10^{17}$ m/mol for single protein solutions of α-lactalbumin or lysozyme and $3.5\ 10^{17}$ m/mol (maximum) for mixtures of α-lactalbumin and lysozyme. Using these values and eq. 7 the sedimentation coefficients will be $2.52\ 10^{-14}$ and $1.08\ 10^{-14}$ s respectively, from which the concentration in the boundary layer can be calculated, via eq. 11, being 450 and 625 kg/m^3. The resulting specific resistances r_{bl} will then be $4.82\ 10^{18}$ and $1.56\ 10^{19}$ m^{-2}. With $r_{bl} = r_{KC}$ the porosity ε_{app} can be calculated to be 0.655 and 0.537 for the single protein solutions and the mixture respectively.

Using eq. A9 the radius r_2 can be calculated, these values are $1.23*r_1$ and $1.11*r_1$ respectively. With $r_1 = 2.0$ nm the inter-particle distance will be 0.92 nm for the single protein solutions and 0.44 nm for the mixture. The latter value is the minimum value for the mixture: when other molar fractions are used the distance will be larger. In case the applied pressure is $1.0\ 10^5$ Pa the distances can be calculated to be 2.48 nm for the single protein solutions and 1.36 nm as a minimum distance in a mixture of positive and negative proteins.

At the moment the inter-particle distance is subject of further research. Based on theories on the electrostatic interactions of particles [35-38], eventually followed by coagulation, the distance will be estimated. Some problems can be expected however:

1. only a limited number of the required parameters used to calculate the potential functions is readily available,
2. the particles are very small, so that the boundary conditions normally used in these theories will not be satified and
3. the fact that the particles are not ideal spherical particles, but proteins, will make the application of these theories more complicated: most proteins are ellipsoidal and the net charge of the proteins will be a result of partly positive and negative domains on the protein-particle surface.

LIST OF SYMBOLS

A	membrane area	(m^2)
C_b	concentration in the bulk	(kg/m^3)
C_{bl}	(constant) concentration in the boundary layer	(kg/m^3)
C_p	concentration in the permeate	(kg/m^3)
d_p	particle-diameter	(m)
D	diffusion coefficient	(m^2/s)
I	ionic strength	(N)

I.E.P.	iso-electric point	(-)
J_v	flux	(m^3/m^2s)
J_w	clean water flux	(m^3/m^2s)
$m_{1,2}$	mass of smaller and larger particles, respectively	(kg)
(m)	specific gel resistance defined by Dejmek [30]	(s^{-1})
p	permeability of the boundary layer	(m^2)
r_{bl}	specific resistance of the boundary layer	(m^{-2})
r_H	specific resistance according to Happel's model	(m^{-2})
r_{KC}	specific resistance according to the Kozeny - Carman eq.	(m^{-2})
$\Re_{obs}$	observed retention coefficient = 1 - (C_p / C_b)	(-)
R_{bl}	total hydraulic resistance of the boundary layer	(m^{-1})
R_m	hydraulic resistance of the membrane	(m^{-1})
r_s	radius of a solute	(m)
s	sedimentation coefficient	(s)
S_0	specific area	(m^2/m^3)
T	temperature	(°C)
v_0	partial specific volume of the solvent	(m^3/kg)
v_1	partial specific volume of the solute	(m^3/kg)
V_p	(cumulative) permeate volume	(m^3)
$V_{1,2}$	volume of smaller and larger particles, respectively	(m^3)
x	molar fraction	(-)
x_1	molar fraction of small particles in a binary mixture	(-)

δ	thickness of the boundary layer	(m)
ε	porosity	(-)
ε_{app}	apparent porosity (calculated from experimental data)	(-)
ε_m	porosity of a mixture	(-)
ε_{tot}	total porosity of a layer of randomly packed partly filled spheres	(-)
ϕ_1	volume fraction of the small particles in a binary mixture	(-)
φ_e	term used in eqs. A4 and A5	(-)
ΔP	applied pressure	(Pa)
η_0	viscosity of the solvent	(Pa.s)

REFERENCES

[1] T.B. Choe, P. Masse, A. Verdier and M.J. Clifton, Flux decline in batch ultrafiltration: concentration polarization and cake formation, J. Membrane Sci., 26(1986)1-15.

[2] V.L. Vilker, C.K. Colton and K.A. Smith, Concentration polarization in protein ultrafiltration, Part II: Theoretical and experimental study of albumin ultrafiltered in an unstirred batch cell, AIChE Journal, 27(4)(1981)637-645.

[3] D.R. Trettin and M.R. Doshi, Ultrafiltration in an unstirred batch cell, Ind. Eng. Chem. Fundam., 19(1980)189-194.

[4] H. Reihanian, C.R. Robertson and A.S. Michaels, Mechanisms of polarization and fouling of ultrafiltration membranes by proteins, J. Membrane Sci., 16(1983) 237-258.

[5] M.W. Chudacek and A.G. Fane, The dynamics of polarisation in unstirred and stirred ultrafiltration, J. Membrane Sci., 21(1984)145-160.

[6] G.B. van den Berg and C.A. Smolders, The boundary layer resistance model for unstirred ultrafiltration. A new approach., accepted for publication by J. Membrane Sci., Chapter 2 of this thesis.

[7] K.C. Ingham, T.F. Busby, Y. Sahlestrom and F. Castino, Separation of macromolecules by ultrafiltration: influence of protein adsorption, protein-protein interactions and concentration polarization, in: Ultrafiltration membranes and applications, A.R. Cooper (ed.), Plenum Press, New York, NY, 1980, p.141-158.

[8] A.G. Fane, Factors affecting flux and rejection in ultrafiltration, J. Separ. Proc. Technol., 4(1)(1983)15-23.

[9] G.B. van den Berg, J.H. Hanemaaijer and C.A. Smolders, Ultrafiltration of protein solutions; the role of protein association in rejection and osmotic pressure, J. Membrane Sci., 31(1987)307-320, Chapter 4 of this thesis.

[10] J.G. Wijmans, S. Nakao, J.W.A. van den Berg, F.R. Troelstra and C.A. Smolders, Hydrodynamic resistance of concentration polarization boundary layers in ultrafiltration, J. Membrane Sci., 22(1985)117-135.

[11] S. Nakao, J.G. Wijmans and C.A. Smolders, Resistance to the permeate flux in unstirred ultrafiltration of dissolved macromolecular solutions, J. Membrane Sci., 26(1986)165-178.

[12] J.P. Johnston and A.G. Ogston, A boundary anomaly found in the ultracentrifugal sedimentation of mixtures, Trans. Farad. Soc., 42(1946)789-799.

[13] C. Tanford and M.L. Wagner, Hydrogen ion equilibria of lysozyme, J. Am. Chem. Soc., 76(1954)3331-3336.

[14] J.R. Colvin, The size and shape of lysozyme, Can. J. Chem. 30(1953)831-834.

[15] K.E. Hopper and H.A. McKenzie, Minor components of bovine α-lactalbumin A and B, Bioch. Bioph. Acta, 295(1973)352-363.

[16] G. Scatchard, I.H. Scheinberg and S.H. Amstrong, Physical chemistry of protein solutions. IV. The combination of Human Serum Albumin with chloride ion, J. Am. Chem. Soc., 72(1950)535-540.

[17] H. Klostergaard and R.A. Pasternak, Electrophoresis and ultracentrifuge studies of milk proteins. II. α-lactalbumin, J. Am. Chem. Soc., 79(1957)5674-5676.

[18] V.L. Vilker, C.K. Colton and K.A. Smith, The osmotic pressure of concentrated protein solutions: effect of concentration and pH in saline solutions of Bovine Serum Albumin, J. Coll. Interf. Sci., 79(1981)548-566.

[19] F.M. Robbins, R.E. Andreotti, L.G. Holmes and M.J. Kronman, Inter- and intramolecular interactions of α-lactalbumin. VII. The hydrogen ion titration curve of α-lactalbumin, Bioch. Bioph. Acta, 133(1967)33-45.

[20] C. Tanford, S.A. Swanson and W.S. Shore, Hydrogen ion equilibria of Bovine Serum Albumin, J. Am. Chem. Soc., 77(1955)6414-6421.

[21] Y. Looze, E.D. Maes, A.O. Barel and J. Leonis, Hydrodynamic studies of some lysozymes and α-lactalbumins, Protides of the biological fluids. Proceedings of the Colloquium, 19(1971: publ. 1972)409-411.

[22] W.C. Gordon and W.F. Semmett, Isolation of crystalline α-lactalbumin from milk, J. Am. Chem. Soc., 75(1957)328-330.

[23] R.C. Deonier and J.W. Williams, Self-association of muramidase (lysozyme) in solution at 25°, pH = 7.0 and I = 0.20, Biochemistry, 9(1970)4260-4267.

[24] R.F. Steiner, Reversible association processes of globular proteins. II. Electric complexes of plasma albumin and lysozyme, Arch. Biochem. Bioph., 47(1953) 56-75.

[25] J. Rodriguez, C.H. Allibert and J.M. Chaix, A computer method for random packing of spheres of unequal size, Powder Technology, 47(1986)25-33.

[26] R. Ben Aïm and P. Le Goff, Effet de paroi dans les empilements désordonnés de sphères et application à la porosité de mélanges binaires, Powder Technology, 1(1967)281-290.

[27] J.A. Dodds, The porosity and contact points in multicomponent random sphere packings calculated by a simple statistical geometric model, J. Coll. Interf. Sci., 77(2)(1980)317-327.

[28] W.M. Visscher and M. Bolsterli, Random packing of equal and unequal spheres in two and three dimensions, Nature, 239(1972)504-507.

[29] P.C. Carman, Fundamental principles of industrial filtration, Trans. Inst. Chem. Eng., 16(1938)168-188.

[30] P. Dejmek, Concentration polarization in ultrafiltration of macromolecules, Ph.D. Thesis, Lund Institute of Technology, Lund, Sweden, 1975.

[31] R.M. McDonogh, C.J.D. Fell and A.G. Fane, Surface charge and permeability in the ultrafiltration of non-flocculating colloids, J. Membrane Sci., 21(1984)285-294.

[32] P.F. Mijnlieff and W.J.M. Jaspers, Solvent permeability of dissolved polymer material. Its direct determination from sedimentation measurements, Trans. Farad. Soc., 67(1971)1837-1854.

[33] H. Brauer, Grundlagen der Einphasen- und Mehrphasenströmungen, Chapter 8, Verlag Sauerländer, Aarau (Switzerland), 1971.

[34] J. Happel, Viscous flow in multiparticle systems; Slow motion of fluids relative to beds of spherical particles, AIChE Journal, 4(1958)197-201.

[35] R. Hogg, T.W. Healy and D.W. Fuerstenau, Mutual coagulation of colloidal dispersions, Trans. Farad. Soc., 62(1966)1638-1651.

[36] E. Barouch, E. Matijevic, T.A. King and J.M. Finlan, Heterocoagulation. II. Interaction energy of two unequal spheres, J. Coll. Interf. Sci., 67(1978)1-9 and 70(1979)400.

[37] D.Y.C. Chan and L.R. White, The electrostatic interaction between spherical colloidal particles - A comment on the paper by Barouch et al., J. Coll. Interf. Sci., 74(1980)303-305.

[38] B.K.C. Chan and D.Y.C. Chan, Electrical double-layer interaction between spherical colloidal particles: an exact solution, J. Coll. Interf. Sci., 92(1983) 281-283.

CHAPTER 4

ULTRAFILTRATION OF PROTEIN SOLUTIONS; THE ROLE OF PROTEIN ASSOCIATION IN REJECTION AND OSMOTIC PRESSURE

G.B. van den Berg, J.H. Hanemaaijer* and C.A. Smolders

SUMMARY

The monomer-dimer equilibrium of the protein ß-lactoglobulin under neutral conditions appears to influence the rejection and the osmotic pressure build-up, both phenomena closely related to ultrafiltration. Rejection measurements indicate different rejections for the ß-lactoglobulin monomers and dimers: the membrane rejects the dimer almost completely and the monomer only partially. The osmotic pressure turns out to be highly dependent on the protein concentration. A good agreement, up to high concentrations, is found between experimental data and theoretical osmotic pressures, calculated by taking into account the state of association, the excluded volume and the Donnan effects. The effect of changes in pH on the osmotic pressure has been measured: a minimum was found around pH = 4.5 where, according to literature, maximum protein-protein interaction occurs.

INTRODUCTION

During the past few decades whey, a liquid produced when milk is processed into cheese or casein, has developed from dairy waste into a valuable dairy product. In particular the whey proteins and lactose are valuable components of whey and the isolation and the purification of the protein fraction has gained particular interest. Whey protein concentrates (WPC) can be made in various compositions, depending on the process used, with a wide range of nutritional and functional properties [1]. The major component of the whey proteins is the protein ß-lactoglobulin. One of the methods of processing whey is by

* Netherlands Institute for Dairy Research (NIZO), P.O. Box 20, 6710 BA Ede.

ultrafiltration. An important aspect of ultrafiltration is the protein rejection, which is influenced by both membrane and solute characteristics. In case of a solute such as ß-lactoglobulin, which shows a concentration dependent association, different rejections may be expected for the different states of association. Osmotic pressure measurements may give information on the association equilibria of ß-lactoglobulin under ultrafiltration conditions.

The osmotic pressure is also related to ultrafiltration in another way: in addition to solute adsorption, pore-blocking etc. the permeate flux is limited by the difference in the osmotic value of the solutions at each side of the membrane. The osmotic pressure difference $\Delta\Pi$, which is further increased by concentration polarization at the membrane surface, decreases the flux by decreasing the effectiveness of the applied transmembrane pressure [2,3,4].

The objectives of this paper are:

- to present osmotic pressure data, measured under actual ultrafiltration process conditions, for the associating protein ß-lactoglobulin,
- to explain these data by considering protein association, excluded volume and Donnan effects; and
- to show the relation between protein association and rejection.

THEORY

1. The association of ß-lactoglobulin [5]

Several genetic variants of the protein ß-lactoglobulin exist, each with slightly different properties. Variants A and B are present in milk and whey obtained from Frisian cows. The protein tends to form oligomers, mostly dimers and some octamers, while other n-mers are present in negligible amounts. These oligomer formations seem to be the result of non-covalent bonds, which are probably based on hydrophobic interactions. Normally these interactions are maximal around the iso-electric point, which for ß-lactoglobulin is at pH = 5.2. Both at lower and higher pH-values (until pH ≈ 8, above which denaturation occurs) the state of association changes to form more monomers, fewer dimers and far fewer octamers.

This state of association of ß-lactoglobulin has been the subject of extensive research [6-11]. Although the influence of several parameters such as pH, ionic environment, concentration and temperature has been investigated no data were available for practical (ultrafiltration) use. Georges et al. [6] gave monomer-dimer equilibrium constants (K_{eq}) for several combinations of pH and temperature, obtained from light-scattering

measurements. For pH = 6.6 and T = 323 K a value of K_{eq} (= $(c_{monomers})^2/c_{dimers}$) can be obtained from their data by interpolation: $K_{eq} = 2.90 * 10^{-5}$ kmol.m^{-3}. Using this equilibrium constant the percentage of dimer ß-lactoglobulin in solution can be calculated as a function of the total concentration. This dependence of the state of association of ß-lactoglobulin on the solute concentration will be used in the equations below.

The state of association of ß-lactoglobulin appears to depend not only on concentration but also on temperature and pH. In Table 1 the association equilibrium constants for ß-lactoglobulin B and C are given, as found by several investigators. They are summarized as a function of temperature, pH and method of determining the equilibrium constant. The ionic strength I is 0.1 N in all cases.

Genetic variant	T (K)	pH	$K_{eq} * 10^6$ (kmol/m^3)	Technique	Ref.
C	293	2.5	95	sedimentation	[9]
C	293	4.7	0.52	sedimentation	[8]
B	293	2.6	160	sedimentation	[10]
B	293	2.7	51	light scattering	[11]
B	293	7.0	5.6	light scattering	[6]
B	313	7.0	30	light scattering	[6]
B	333	7.0	129	light scattering	[6]

Table 1. Equilibrium constants for two genetic variants of ß-lactoglobulin at different temperatures and pH (ionic strength I = 0.1 N)

In figure 1 the dependence of the fraction of dimers of ß-lactoglobulin B on temperature and concentration is given. The fraction of dimers clearly declines with increasing temperature.

To compare the monomer-dimer equilibrium of the B and the C variant at the same pH, equilibrium constants of several investigators were used, each using different measuring techniques. Though the data do not match exactly the calculated fraction of dimers seems to be roughly the same (curves a, b and c in figure 2). Also, the method of determining the equilibrium constant seems of little importance.

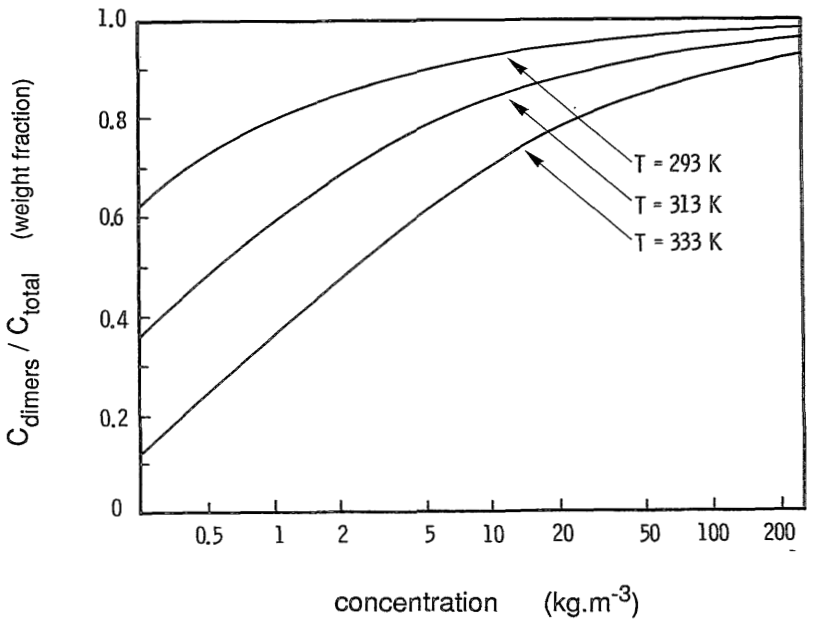

Figure 1. The fraction of dimers of ß-lactoglobulin B as a function of temperature and concentration (pH = 7.0 and I = 0.1 N)

In figure 2 the fraction of dimers of the two variants of ß-lactoglobulin (B and C) is also given as a function of pH and concentration at 293 K and I = 0.1 N, making use of the listed K_{eq}-values. To illustrate solely the monomer-dimer equilibrium at different pH-values, ß-lactoglobulin C was used at the iso-electric point, because the C variant is the only variant which is unable to form oligomers larger than dimers, such as octamers, at pH-values around the iso-electric point [5]. Now the fraction of dimers increases with increasing pH, when going from pH ≈ 2.6 to pH = 4.7, and decreases again when pH is increasing further to pH = 7.0. This corresponds with the decreasing charge of ß-lactoglobulin when changing the pH from 2.6 to about 5 and increasing charge at higher pH-values [12].

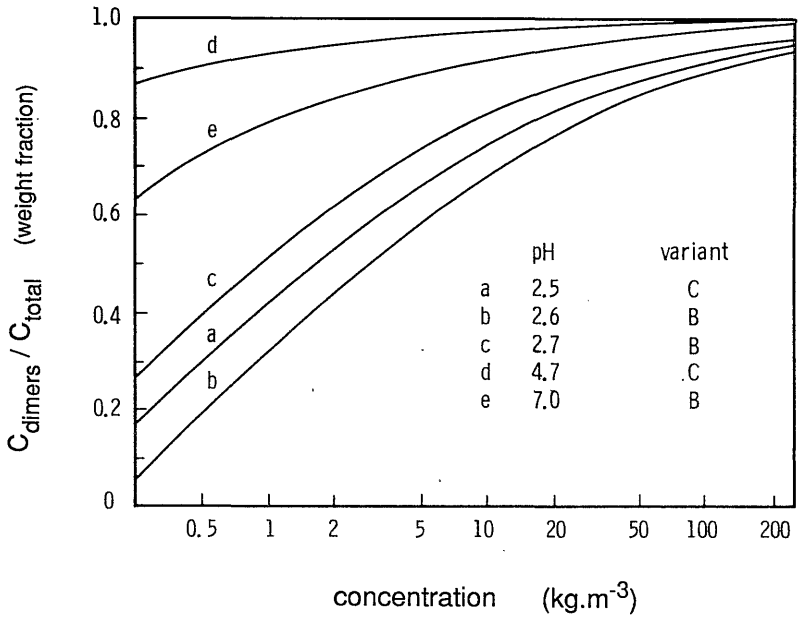

Figure 2. The fraction of dimers of ß-lactoglobulin B and C as a function of pH and concentration (T = 293 K and I = 0.1 N). Equilibrium constants from literature (see Table 1).

2. Rejection in ultrafiltration

The rejection of a solute in protein ultrafiltration, at constant pressure, is known to be dependent on the membrane-type (pore size and pore distribution), on the solute-adsorption [13] and the presence of a concentration polarization and gel layer [14]. The rejection as observed in an experiment is defined as:

$$\Re_{obs} = 1 - (C_p/C_b) \qquad (1)$$

where C_p is the concentration of the permeate and C_b is the concentration of the bulk (concentrate). In fact, the true rejection should be calculated from the concentration at the membrane interface, which is much higher than the bulk concentration because of the concentration polarization. This interfacial concentration can not be measured directly. The

state of association of ß-lactoglobulin will add one more variable to the set of parameters which determine the overall rejection-value $\Re_{obs}$, because protein association can be expected to increase the protein rejection.

3. Osmotic pressure

Several relations have been proposed to describe the osmotic pressure of macromolecular solutions at different concentrations [4,15,16].

The basic thermodynamic equation for non-ideal solutions is (e.g. ref. [17]):

$$\Pi = \frac{RT}{M}(C + B_2C^2 + B_3C^3 + ...) \qquad (2)$$

in which the virialcoefficients B_2 ($m^3.kg^{-1}$) and B_3 ($m^6.kg^{-2}$) can be calculated as a function of several parameters, such as the excluded volume, the hydration and the Donnan effects.

In this work we shall calculate the osmotic pressure to a certain extent like Vilker et al. [18] have proposed: the osmotic pressure is calculated taking into account the ideal Donnan effects (the first term in eq. 3) and the excluded volume (the second term in eq.3):

$$\Pi = 10^3.R.T\,[2\{(Z.C/2M)^2 + I^2\}^{0.5} - (2 * I)] + \frac{(RT)}{M} * (C + B_2^{ev}C^2 + B_3^{ev}C^3) \qquad (3)$$

where Z is the net charge of the proteins and I is the ionic strength of the protein solution. To calculate the Donnan effect term we will use Z=-12 and M=35,500, as found by Basch and Timasheff [12] at pH = 6.6. The value of Z=-12 is an average for ß-lactoglobulin A and B. The Donnan effects will, of course, be calculated by using the total protein concentration.

The excluded volume-based virialcoefficients B_2^{ev} and B_3^{ev} will be calculated as functions of the molecular volume v_m and the shape-dependent parameters R_1 and S_1 [19] :

$$B_2^{ev} = (v_m + R_1S_1).(10^3.N_{av} / M) \qquad (4)$$

$$B_3^{ev} = [(v_m)^2 + 2.R_1S_1v_m + \frac{1}{3}(R_1S_1)^2]\,(10^3.N_{av} / M)^2 \qquad (5)$$

where N_{av} is Avogadro's number.

To calculate v_m, R_1 and S_1 we have made use of the fact that the ß-lactoglobulin monomer is a globular protein, while the dimeric ß-lactoglobulin is rod-like [5]. For the monomer r = 1.8 nm is used and for the cylindric dimer r = 1.8 nm and l = 7.2 nm [5]. Table 2 shows the equations necessary to calculate the virial coefficients. Based on eq. 3,

$\Pi_{(total)}$ can be calculated according to

$$\Pi_{(total)} = \Pi^{e.v.}{}_{(monomers)} + \Pi^{e.v.}{}_{(dimers)} + \Pi_{D(mixture)} \qquad (6)$$

where $\Pi^{e.v.}{}_{(monomers)}$ and $\Pi^{e.v.}{}_{(dimers)}$ are the excluded volume terms of the osmotic pressure of the monomers and the dimers, respectively, and Π_D is the Donnan effect term on the osmotic pressure using the total concentration of the mixture.

	For spheres	For cylinders
v_m	$\frac{4}{3}\pi r^3$	$\pi r l^2$
R_1	r	$(l + r)/4$
S_1	$4 \pi r^2$	$2 \pi r (l + r)$

Table 2. Shape-dependent parameter equations used to determine the virialcoefficients B_2^{ev} and B_3^{ev}.

4. Determination of the state of association by reduced osmotic pressure measurements.

The reduced osmotic pressure (Π/C) can give more information about the state of association of ß-lactoglobulin. When the reduced osmotic pressure (Π/C) is plotted versus the concentration, according to Van 't Hoff's law, the molecular weight M can be determined by extrapolating Π/C to C = 0 (i.e., when an ideal situation is approached), then:

$$\lim_{C \to 0} \Pi / C = RT / M \qquad (7)$$

Or reversed, when the molecular weight is known the state of association of ß-lactoglobulin can be deduced. For ß-lactoglobulin: Π/C = 146.7 $Pa.m^3.kg^{-1}$ for monomers with M=18,300 and Π/C = 73.3 $Pa.m^3.kg^{-1}$ for dimers with M=36,600.

The value for the reduced osmotic pressure of a mixture of monomeric and dimeric protein molecules can easily be derived, knowing the contributions of both the monomers and the dimers and the Donnan effects for the entire mixture:

$$(\Pi / C)_{mixture} = [\Pi^{e.v.}{}_{(monomers)} + \Pi^{e.v.}{}_{(dimers)} + \Pi_D] / (C_{monomers} + C_{dimers}) \qquad (8)$$

MATERIALS AND METHODS

1. ß-lactoglobulin

The ß-lactoglobulin was prepared at NIZO from casein whey. After desalting, clarification [20], ultra- and diafiltration the whey protein mixture was fractionated on a Pharmacia Stack KS 370/15 pilot-plant column, using DEAE Sepharose Fast Flow anion exchanger. The pure fractions were concentrated by ultrafiltration and freeze dried.

Protein solutions were made by dissolving the ß-lactoglobulin in a Jenness and Koops-buffer (I=0.1 N) of the desired pH [21]. Adjustments were made by adding 0.1 N HCl or 0.1 N NaOH to the solutions.

The water used was distilled and prefiltered using a reverse osmosis membrane module (Nitto NTR 7250).

2. Osmotic pressure measurements

The osmotic pressure as a function of concentration and solution pH was determined using a high-pressure osmometer [22], thermostatted at 50.0 ± 0.5 °C. This osmometer is capable of measuring osmotic pressures larger than 0.5 kPa.

Both Abcor HFK-131 membranes (M_w cut-off 5000 D, rejection 99.9+% for ß-lactoglobulin) and Amicon Diaflo UM-30 membranes (M_w cut-off 30,000 D with 99+% rejection for ß-lactoglobulin) were used in the osmometer. In order to obtain information on the influence of pH, osmotic pressure measurements were performed at 323 K with solutions at various pH and concentrations of 100 $kg.m^{-3}$.

3. Rejection measurements and ultrafiltration experiments

The ultrafiltration experiments were performed with a Amicon TCF-10A thin channel cell. The experimental conditions were: T = 323 K, ΔP = 150 kPa and tangential flow velocity v = 1.63 $m.s^{-1}$. The membrane used was a Rhône Poulenc Iris 3038 membrane (M_w cut-off 30,000 D).

4. Analytical procedures

The concentration of the ß-lactoglobulin solutions, used for the osmotic pressure experiments, was determined chemically by the Kjeldahl-method [23]. As a control the ß-lactoglobulin concentration of the solution at the solvent side of the osmometer was also determined.

To determine the concentration during ultrafiltration of both the concentrate and the permeate (very low concentrations), and also to control purity of the protein, high performance gel permeation chromatography (HP-GPC) was used. The column used was

a Dupont GF250 column, the detection wavelength was 280 nm and the buffer : 0.1 M potassium phosphate/0.15 M sodium phosphate at pH = 6.0; the flow rate was 1.0 $ml.min^{-1}$.

RESULTS AND DISCUSSION

1. Rejection

From seven independent, batch-wise performed ultrafiltration experiments a number of rejection-data were gathered at different degrees of concentration. Each experiment was performed with a new Iris 3038 membrane. This resulted in the rejection as a function of the concentration as plotted in figure 3. Because all data are situated on one curve, even though starting concentrations ranging from 0.1 to 4.0 $kg.m^{-3}$ were used, it can be concluded that any shifts of association equilibria do not influence the rejection significantly. For comparison the fraction of dimers at the experimental conditions (using $K_{eq} = 2.90\ 10^{-5}$ $kmol.m^{-3}$) is given by the dashed line.

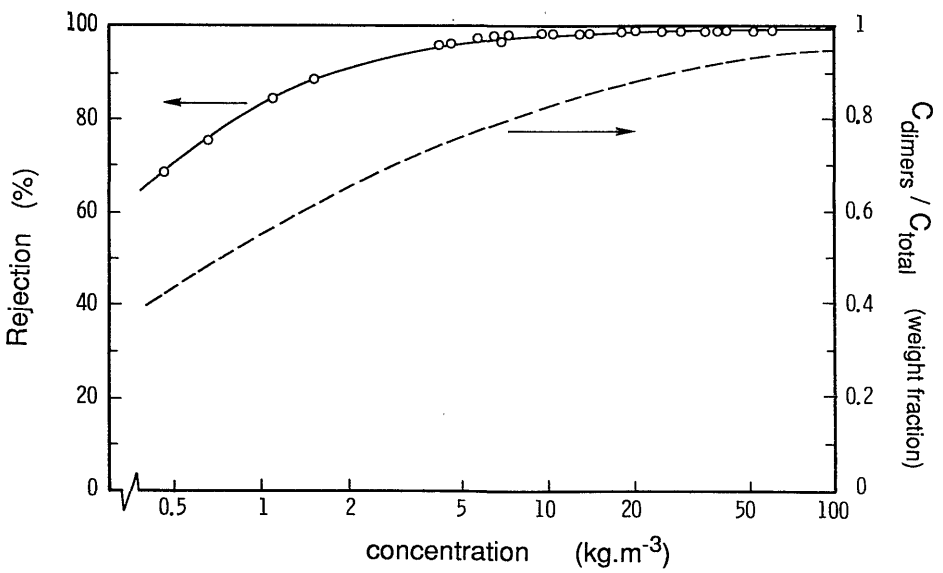

Figure 3. Solid curve: rejection of ß-lactoglobulin as a function of feed concentration (Iris 3038 membrane, pH = 6.6, T = 323 K and I = 0.1 N). Dashed curve: fraction of dimers at the same conditions.

The rejection increases clearly with the protein concentration of the retentate. This is also to be predicted from the increasing fraction of dimers, resulting from the monomer-dimer equilibrium of ß-lactoglobulin. The rejection of the dimers will be higher than the rejection of the smaller monomers, so the total rejection will increase.

Though knowing the quantities of monomers and dimers and the total rejection, the exact rejection of both the monomers and the dimers can not be calculated yet. The explanation must probably be found in the additional phenomena of protein rejection in ultrafiltration: partitioning of solute in the pore entrance area, solute adsorption, pore-blocking and eventually the formation of a gel layer. These phenomena are functions of time, protein concentration and the membrane characteristics, which are quite complex altogether and have not been exactly under control until now.

When at the start of an experiment and at very low concentrations, the rejection is measured, it appears that this rejection is higher than could be expected from rejection of dimers only. At this point the above mentioned additional phenomena will be of minor influence, so that the rejection of monomers will be higher than zero. For instance a rejection of ca. 50% for monomers and 100% for dimers at initial conditions (low concentrations, no proteins adsorbing or pore blocking) can explain the initial overall rejection quite well. At higher concentrations the rejection then increases as a result of the phenomena mentioned above.

2. The osmotic pressure of ß-lactoglobulin

Results of osmotic pressure measurements using both the HFK 131 membrane and the UM 30 membrane are reported in figure 4. The small permeability for ß-lactoglobulin when using the UM 30 membrane did not seem to effect the measurements. The maximum concentration at the "pure-solvent" side was 0.5 $kg.m^{-3}$ which results in a (very small) osmotic pressure of about 40 Pa.
Curve-fitting of the data by the non-linear least-squares method resulted in:

$$\Pi = 79.4\ C + 0.419\ C^2 + 2.5\ 10^{-3}\ C^3 \qquad (10)$$

where C is in $kg.m^{-3}$. Though there is a small difference between the experimental osmotic pressures (the drawn curve in figure 4) and theoretical values based on the theoretical model (the dashed curve in figure 4), we think the agreement is remarkable. Thus, using simple theoretical equations, the osmotic pressure can be predicted rather accurately, even at higher concentrations.

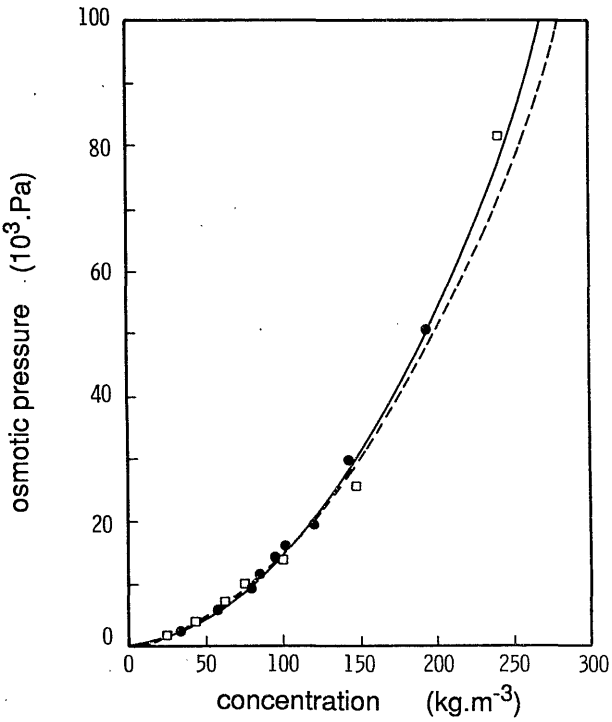

Figure 4. The osmotic pressure of ß-lactoglobulin as a function of concentration. (pH = 6.6, T = 323 K and I = 0.1 N). Solid curve: measured osmotic pressures (eq. 10); the membranes used were (❑) Amicon Diaflo UM 30 and (●) Abcor HFK 131. Dashed curve: calculated osmotic pressures (eq. 3).

At high concentrations, such as appear at the membrane during ultrafiltration, the osmotic pressure can reach rather high values: e.g. $\Pi \approx 85$ kPa at 250 kg.m^{-3} and $\Pi \approx$ 260 kPa at 400 kg.m^{-3}. According to the osmotic pressure model these osmotic pressures will reduce the driving force ($\Delta P - \Delta\Pi$) considerably, resulting in much lower product fluxes.

3. The state of association of ß-lactoglobulin

In figure 5 the reduced osmotic pressure is plotted against the concentration. The drawn line is derived from the curve-fit equation (eq. 10). Extrapolation to C = 0 yields a value of 79.4 Pa.m^3.kg^{-1}. This value approaches the value of 73.3 Pa.m^3.kg^{-1} for dimers quite well, so that from these osmotic pressure measurements it can be concluded that

ß-lactoglobulin, at the concentrations used, mainly consists of dimers.

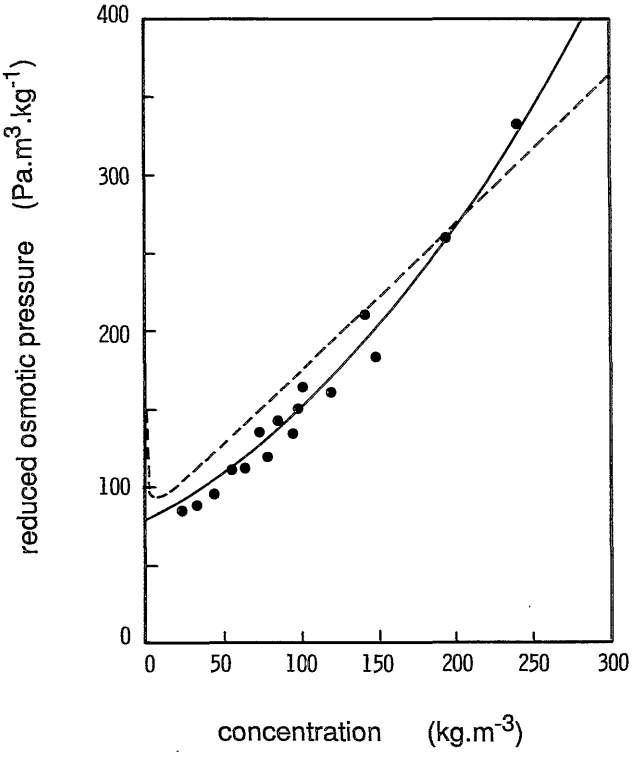

Figure 5. The reduced osmotic pressure of ß-lactoglobulin as a function of concentration. (pH = 6.6, T = 323 K, I = 0.1 N). Solid curve: experimental curve, using eq. (10). Dashed curve: theoretical curve, using eq. (8).

Because osmotic pressures were measured only of solutions with moderately high to very high concentrations, this conclusion corresponds with the calculations made before. From data on the equilibrium constant it was shown that at low concentrations the ß-lactoglobulin mainly consists of monomers. This seems to contradict with the experiments where ß-lactoglobulin seems to consist only of dimers, and therefore also the theoretical reduced osmotic pressures were also calculated using eq. (8) . The result is the dashed curve in figure 5. Starting from the value of Π/C = 146.7 $Pa.m^3.kg^{-1}$ for monomers, according to Van 't Hoff's law, the reduced osmotic pressure decreases rapidly, reaches a minimum at a rather low protein concentration and increases again.

4. The influence of pH on the osmotic pressure

In figure 6 a comparison is given of the osmotic pressure, measured at various pH-values, with the expected osmotic pressure at pH = 6.6. A minimum was found around pH = 4.5. It should be noticed that this region is not the locus of the ß-lactoglobulin iso-electric point, which is at 5.2. However, this minimum corresponds with the minimum (pH = 4.40 -4.65) in free enthalpy of the association reaction, derived from sedimentation and light scattering experiments [7,24], resulting in maximal protein-protein interactions in this region.

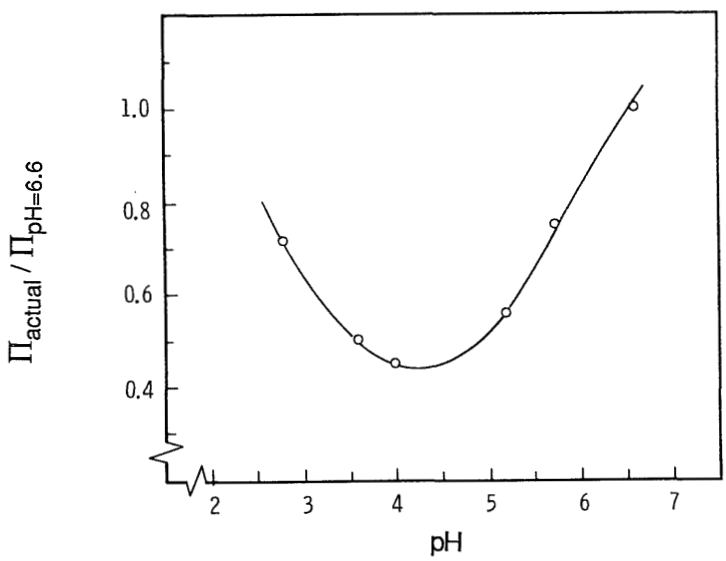

Figure 6. The osmotic pressure of ß-lactoglobulin as a function of pH (concentration = 100 kg.m^{-3}, T = 323 K and I = 0.1 N).

At both lower and higher pH the osmotic pressure increases quite symmetrically around pH = 4.5, suggesting a relation with the degree of protein association. At pH values much higher than 6.6 ß-lactoglobulin will readily denature and therefore this high pH region was not investigated.

CONCLUSIONS

During ultrafiltration of ß-lactoglobulin solutions both protein rejection and osmotic pressure are influenced by the state of association of the protein.

The increasing rejection with the protein concentration appears to be related to the increasing degree of protein association, although not exclusively. Probably also other phenomena like solute adsorption and pore blocking also increase the rejection.

The osmotic pressure data support the data on the association of ß-lactoglobulin, derived from literature. Under common process conditions during ultrafiltration of sweet whey (T = 323 K, pH = 6.6) most of the ß-lactoglobulin is present as dimers. During ultrafiltration of acid whey (T = 323 K, pH = 4.5) oligomerization probably takes place.

Taking protein association, the excluded volume and Donnan effects into account, the osmotic pressure at various concentrations and process conditions can be predicted rather well.

Especially during ultrafiltration of sweet whey at high concentrations at the membrane surface the considerable contributions of the osmotic pressure to limitation of the flux must be expected.

ACKNOWLEDGEMENTS

We would like to thank Mr. G. Klarenbeek for preparing the ß-lactoglobulin samples, Mr. C. Brons for performing the HP-GPC analyses and Ms. M. Acda, Ms. W. Versluis and Mr. J. Leenders for performing the numerous additional analyses.

LIST OF SYMBOLS

B_n	n^{th} virialcoefficient	$(m^{3(n-1)}.kg^{-n+1})$
C	concentration	$(kg.m^{-3})$
I	ionic strength	$(kmol.m^{-3})$
K_{eq}	association equilibrium constant	$(kmol.m^{-3})$
l	length (in Table 2)	(m)
M	molecular weight	$(kg.kmol^{-1})$
N_{av}	Avogadro's number	(mol^{-1})

P	applied pressure	(Pa)
r	radius	(m)
$\Re_{obs}$	rejection (retention)	(-)
R	gas constant	($J.mol^{-1}.K^{-1}$)
R_1	shape-dependent parameter in eqs. 4 and 5	(m)
S_1	shape-dependent parameter in eqs. 4 and 5	(m^2)
T	temperature	(K)
v	cross-flow velocity	($m.s^{-1}$)
v_m	molecular volume (in Table 2)	(m^3)
Z	charge number	(-)
Π	osmotic pressure	(Pa)

Subscripts:

b	bulk (concentrate)
D	Donnan effect term
p	permeate

Superscript:

ev	excluded volume

REFERENCES

[1] J.N. de Wit, Functional properties of whey proteins in food systems, Neth. Milk Dairy J., 38(1984)71-89.

[2] J.G. Wijmans, S. Nakao and C.A. Smolders, Flux limitation in ultrafiltration: osmotic pressure model and gel layer model, J. Membrane Sci., 20(1984)115-128.

[3] R.L. Goldsmith, Macromolecular ultrafiltration with microporous membranes, Ind. Eng. Chem. Fundam., 10(1971)113-120.

[4] V.L. Vilker, C.K. Colton, K.A. Smith and D.L. Green, The osmotic pressure of concentrated protein and lipoprotein solutions and its significance to ultrafiltration, J. Membrane Sci., 20(1984)63-77.

[5] H.A. McKenzie, in: H.A. McKenzie (Ed.), Milk proteins, Chemistry and Molecular Biology, Vol. II, Academic Press, New York, NY , 1971.

[6] C. Georges, S. Guinand and J. Tonnelat, Étude thermodynamique de la dissociation de la ß-lactoglobuline B pour pH supérieurs à 5.5. Biochim. Bioph. Acta, 59(1962) 737-739.

[7] R. Townend and S.N. Timasheff, The pH-dependence of the association of ß-lactoglobulin, Arch. Biochem. Biophys., 63(1956)482-484.

[8] J.L. Sarquis and E.T. Adams, Self-association of ß-lactoglobulin C in acetate buffers, Biophys. Chem., 4(1976)181-190.

[9] J.L. Sarquis and E.T. Adams, The temperature-dependent self-association of ß-lactoglobulin C in glycine buffers, Arch. Biochem. Bioph., 163(1974)442-452.

[10] D.A. Albright and J.W. Williams, A study of the combined sedimentation and chemical equilibrium of ß-lactoglobulin in acid solution, Biochemistry, 7(1968) 67-78.

[11] S.N. Timasheff and R. Townend, Molecular interactions in ß-lactoglobulin. V. The association of the genetic species of ß-lactoglobulin below the iso-electric point, J. Am. Chem. Soc., 83(1961)464-476.

[12] J.J. Basch and S.N. Timasheff, Hydrogen ion equilibria of the genetic variants of bovine ß-lactoglobulin, Arch. Biochem. Bioph., 118(1967)37-47.

[13] L.J. Zeman, Adsorption effects in rejection of macromolecules by ultrafiltration membranes, J. Membrane Sci., 15(1983)213-230.

[14] S. Nakao and S. Kimura, Effect of gel layer on rejection and fractionation of different molecular-weight solutes by ultrafiltration, In: A.F. Turbak (Ed.), Synthetic membranes, Vol. II, ACS Symp. Series 154, American Chemical Society, Washington, DC, 1981, pp. 119-132.

[15] P.G. de Gennes, Scaling concepts in polymer physics, Cornell University Press, Ithaca, NY, 1979.

[16] P.J. Flory, Principles of polymer chemistry, Cornell University Press, Ithaca, NY, 1953.

[17] M.P. Tombs and A.R. Peacock, The osmotic pressure of biological macromolecules, Clarendon Press, London, 1974.

[18] V.L. Vilker, C.K. Colton and K.A. Smith, The osmotic pressure of concentrated protein solutions: effect of concentration and pH in saline solutions of Bovine Serum Albumin, J. Colloid Interface Sci., 79(1981)548-566.

[19] J.R. Barker and D. Henderson, What is liquid ? Understanding the states of matter, Rev. Modern Phys., 48(1976)587-671.

[20] J.N. de Wit, G. Klarenbeek and R. de Boer, A simple method for the clarification of whey, Proc. 20th Int. Dairy Congr., Paris 1978, pp. 919-920.

[21] R. Jenness and J. Koops, Preparation and properties of a salt solution which simulates milk ultrafiltration, Neth. Milk Dairy J., 16(1962)153.

[22] F.W. Altena, Phase separation phenomena in cellulose acetate solutions in relation to asymmetric membrane formation, Ph.D. Thesis, Twente University of Technology, Enschede, The Netherlands, 1982.

[23] International Standard FIL - IDF 20, Determination of the total nitrogen content of milk by the Kjeldahl method, Int. Dairy Federation, 1962.

[24] R. Townend and S.N. Timasheff, Molecular interactions in ß-lactoglobulin. III. Light scattering investigation of the stoichiometry of the association between pH 3.7 and 5.2, J. Am. Chem. Soc., 82(1960)3168-3174.

CHAPTER 5

MASS TRANSFER COEFFICIENTS IN CROSS-FLOW ULTRAFILTRATION.

G.B. van den Berg, I.G. Rácz and C.A. Smolders

SUMMARY

Usually in concentration polarization models the mass transfer coefficient is an unknown parameter. Also its variation with changing experimental circumstances is in quest. In literature many relations can be found to describe the mass transfer coefficient under various conditions, as well as many corrections for the deviating behaviour during ultrafiltration. To obtain reliable mass transfer coefficient relations directly from experimental data two methods were tested: a method using the osmotic pressure difference during an ultrafiltration experiment and a method based on the variation in observed retention when cross-flow velocities are changed. The osmotic pressure method appeared to be too insensitive for changing experimental circumstances (due to theoretical considerations). The velocity variation method appeared to be much more useful, although the error in the mass transfer coefficients obtained can be rather large due to experimental and fitting uncertainties. Therefore the traditional mass transfer relations used in ultrafiltration may be as reliable (and much more easy to use) as the velocity variation method. The velocity variation method probably can still be used in practice however when one or more of the parameters needed in the conventional mass transfer coefficient relations are unknown.

INTRODUCTION

Most models used in the description of concentration polarization phenomena during cross-flow membrane filtration require the knowledge of a mass transfer coefficient. Examples are the boundary layer resistance model [1], the osmotic pressure model [2] and the gel layer model [3]. Such an expression for the mass transfer coefficient should be able

to represent the effect of changing conditions in systems which are used for membrane filtration. The value of the mass transfer coefficient k can most generally be calculated from Sherwood relations which are often represented as

$$Sh = k.d_h/D = p.\ Re^q.\ Sc^r \qquad (1)$$

where d_h is the hydraulic diameter of the system, D is the diffusion coefficient, Re is the Reynolds number ($Re = \rho.v.d_h/\eta$), Sc is the Schmidt number ($Sc = \eta/[\rho.D]$) and p, q and r are adjustable parameters. Usually, the description of the mass transfer coefficient is given for laminar and turbulent conditions separately. This does not imply that there are only two relations for the mass transfer coefficient. In literature many different values for p, q and r can be found depending on the operating conditions (laminar/turbulent conditions), the value of the Reynolds and Schmidt numbers and the origin of the models.

In a recent review by Gekas et al. [4] not less than 27 different Sherwood relations were given for turbulent flow of Newtonian fluids in pipes or flat ducts. Adding the Sherwood relations for non-Newtonian fluids, as well as the relations for the laminar flow case it will be clear that choosing a relation, which describes a certain system accurately, is very difficult.

The relations mostly used in today's membrane literature are [5]:
laminar flow conditions, where the length of the entry region is $L^* = 0.029\ d_h.Re$

$L < L^*$ (Grober): $Sh = 0.664\ Re^{0.5}Sc^{0.33}(d_h/L)^{0.33}$ (2)

$L > L^*$ (Graetz-Leveque): $Sh = 1.86\ Re^{0.33}Sc^{0.33}(d_h/L)^{0.33}$ (3)

turbulent flow conditions (Re > 2000-4000)

$Sc < 1$ (Chilton-Colburn or Dittus-Boelter): $Sh = 0.023\ Re^{0.8}Sc^{0.33}$ (4)

$1 \leq Sc \leq 1000$ (Deissler): $Sh = 0.023\ Re^{0.875}Sc^{0.25}$ (5)

$Sc > 1000$ (Harriott-Hamilton): $Sh = 0.0096\ Re^{0.91}Sc^{0.35}$ (6)

Apart from the large number of different relations more fundamental problems can be expected: most relations mentioned were not developed for membrane filtration, but for mass transfer in non-porous systems, or were derived from heat transfer-mass transfer analogies.

In literature many corrections have been proposed to adapt the value of mass transfer coefficients, now used in the film model, to more realistic (ultra-)filtration circumstances, which include the presence of a layer of increased concentration due to concentration

polarization. Apart from the papers on specific aspects of the mass transfer coefficient a number of papers described the problems more in general. Hereafter an overview of these comments will be given.

- The Sherwood number is linear in f^m (f is the friction factor), $Sc^{1/3}$ (for Sc > 1000) and the Reynolds number ($Sh \sim f^m.Re.Sc^{1/3}$) [4]. The friction factor f is described usually by Blasius' formula; in case of turbulent flow conditions the friction factor is:

$$f \sim Re^{-0.25} \quad \text{for } 10^4 < Re < 10^5 \tag{7}$$

and

$$f \sim Re^{-0.20} \quad \text{for } Re > 10^5 \tag{8}$$

However, Blasius' formula is only valid for smooth non-porous surfaces, whereas membranes are porous and often rather rough on a microscopic scale. Furthermore, in literature the value for m can be found to be 0.5 (eddy diffusivity and surface renewal models) or 1.0 (e.g. in the experimental heat-mass transfer analogies). Therefore the Sherwood number can be found to depend on $Re^{0.75}$ to $Re^{0.90}$.

- The effect of variation in properties (increasing viscosity or changing diffusivity and density as a result of increasing concentrations near the membrane interface) has been used by Nakao [6] to obtain a better agreement with experimentally determined mass transfer coefficients. Gekas [4] used a correction factor $(Sc/Sc_w)^{0.11}$ based on heat transfer analogies (Sc_w is the wall Schmidt number).

- The effect of suction during filtration experiments is twofold: suction stabilizes the laminar flow pattern near the membrane interface and therefore the laminar-turbulent transition region is shifted, e.g. from Re = 2100 to Re = 4000 [7] and furthermore the mass transfer coefficient is enhanced.

The well-known Stewart correction for high mass transfer rates (= flux) [8]

$$k' / k_0 = [J_v / k_0] / [1 - \exp(-J_v / k_0)] \tag{9}$$

describes the enhanced mass transfer coefficient k', in case suction occurs, used in

$$J_v = k' * [C_m - C_b] / [C_m - C_p] \tag{10}$$

compared to the value k_0 for mass transfer without suction, used in

$$J_v = k_0 * [C_m - C_b] / [C_m - C_p] \tag{11}$$

The Stewart correction can also be derived easily from the equations 10 and 12, which have not and have been corrected for the transport towards the membrane, respectively:

$$J_v = k_0 * \ln([C_m - C_p] / [C_b - C_p]) \quad (12)$$

So as a consequence, the mass transfer coefficient relations from literature, which were derived from experiments without suction, should be used without further corrections when the usual concentration polarization equation (eq. 12) is applied.

- The use of mass transfer relations derived from reverse osmosis experiments can also be erroneous because normally there is a large difference in Schmidt numbers ($Sc = \eta/\rho.D$) [4]. For RO of salt solutions $Sc \approx 600$, while in UF of protein solutions $Sc > 10.000$. Furthermore, the effect of variation in properties due to concentration polarization can be expected to be much larger during ultrafiltration than during reverse osmosis.

- The effect of a limited effective area for filtration may be considerable in case of membranes with a low surface porosity. The surface porosity can be very low indeed for ultrafiltration membranes, values as low as 0.3 % are reported [9]. At such low porosities the build up of a concentration polarization layer will be very irregular.

- The experimental fluxes for colloidal suspensions are often up to two magnitudes higher than predicted by the film model only [10]. The dependence on the cross-flow velocity usually is stronger than $v^{0.33}$ for laminar conditions and $v^{0.8}$ for turbulent conditions. The explanation for this behaviour is an increased back-diffusion of particles due to the 'pinch effect' or radial migration. This migration occurs as a result of the non-uniform shear field near the membrane and brings the particles to an equilibrium position away from the membrane interface.

The number of different relations for the mass transfer coefficient k and the numerous corrections for non-ideal behaviour make it impossible to predict exactly which value the mass transfer coefficient will have. A precise prediction of k is necessary because of the great impact which small deviations in k will have on e.g. the concentration at the membrane interface and the osmotic pressure difference, in case the osmotic pressure model is used. The exponential and power type equations will magnify a small error in the value of k to large deviations in the osmotic pressure and flux; e.g. when the observed retention $\Re_{obs} = 1 - C_p/C_b = 1$ we have:

$$C_m = C_b . \exp(J_v/k) \quad (13)$$

$$\Pi = (RT / M) (C_m + B_2C_m^2 + B_3C_m^3 + ...) \quad (14)$$

and

$$J_v = (\Delta P - \Delta\Pi) / (\eta_0 . R_m) \quad (15)$$

We conclude that the large number of experimental variables and corrections on existing mass transfer relations are a good reason to directly determine the mass transfer coefficient experimentally.

Taking notice of the available literature the variables which will influence the value of the mass transfer coefficient can be expected to be: the applied pressure ΔP, the cross-flow velocity v, the flux J_v, the type of solute, the hydraulic dimensions of the module and the characteristics of the membrane (e.g. $\Re_{obs}$ and the hydrophilicity).

The aim of this work is to show two different methods to determine the mass transfer coefficient experimentally: the osmotic pressure model and the velocity variation method will be used. A comparison between the results of these different methods mutually and with the frequently used mass transfer relations from literature will be included. The two models which are used to calculate the value of the mass transfer coefficient from the experiments will be described in the theoretical section, as well as some results obtained by other researchers.

THEORY

Both the velocity variation method and the osmotic pressure model describe the concentration polarization phenomenon by the film theory which usually starts from the basic equation

$$\partial C/\partial t + J_v.\partial C/\partial x = \partial(D.\partial C/\partial x)/\partial x \qquad (16)$$

Using the right initial and boundary conditions it can be derived that

$$J_v = (D / \delta).\ln\{(C_m - C_p) / (C_b - C_p)\} \qquad (17)$$

where the quantity D/δ is defined as the mass transfer coefficient k. When the observed retention $\Re_{obs}$ (= $1 - C_p/C_b$) equals unity eq. 17 changes into

$$J_v = k.\ln(C_m / C_b) \qquad (18)$$

1. The osmotic pressure method

The build-up of concentration profiles and the resulting osmotic pressure differences during an ultrafiltration experiment can be expected to be as represented in figure 1. The total osmotic pressure difference across the membrane is $\Delta\Pi_{tot} = \Delta\Pi_{bl} + \Delta\Pi_b - \Delta\Pi_p$.

When the relatively small osmotic pressures of the bulk ($\Delta\Pi_b$) and the permeate ($\Delta\Pi_p$) are neglected the osmotic pressure difference can be calculated directly from the concentration at the membrane interface only, or vice versa, the concentration at the membrane interface wall C_m can be calculated from the osmotic pressure difference $\Delta\Pi$.

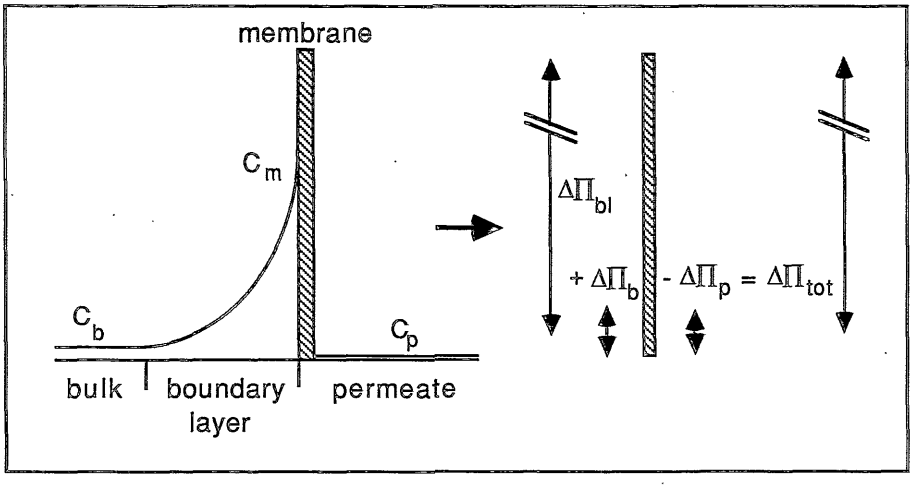

Figure 1. A schematic view of the concentration profile near the membrane interface and the resulting osmotic pressure differences, where $\Delta\Pi = \Delta\Pi_{tot} \approx \Delta\Pi(C_m)$.

From flux measurements during ultrafiltration of a certain solution, together with the data on the pure water fluxes, the mass transfer coefficient $k_{\Delta\Pi}$ can be derived as follows:
- the flux during the clean water flux-measurements is given by

$$J_w = \Delta P / (\eta_0 . R_m) \qquad (19)$$

- the flux during the experiment is given by

$$J_v = [\Delta P - \Delta\Pi] / (\eta_0 . R_m) \qquad (15)$$

so that the osmotic pressure difference $\Delta\Pi$ can be written as

$$\Delta\Pi = \Delta P \, [1 - (J_v/J_w)] \qquad (20)$$

If from independent measurements the relation between the osmotic pressure and the concentration is known, resulting in a relation described as in eq. 14, the concentration at

the membrane interface C_m can be calculated. Then using eq. 12, or eq. 18 when $\Re_{obs}= 1$, the mass transfer coefficient $k_{\Delta\Pi}$ can be derived easily.

Results obtained by other workers using the osmotic pressure method are given below. Apart from the flow conditions (laminar or turbulent etc.), the test-solute and the membrane, the magnitude of the experimental flux (or more specifically J_v/v^x) also seems to influence the comparison of experimental values of the mass transfer coefficient $k_{\Delta\Pi}$ and the various 'theoretical' values. Therefore the range of fluxes is also given when available.

i) Goldsmith [11], using several Dextrans and PEG, found good agreements for both laminar and turbulent conditions (using eqs. 2 and 6) after adapting the value of the diffusion coefficient to values of $D = 5\ 10^{-11}$ m^2/s for laminar conditions and $D = 1\text{-}2\ 10^{-11}$ m^2/s for turbulent conditions, respectively. When the normal value of the diffusion coefficient, i.e. $D \approx 6\text{-}8\ 10^{-11}$ m^2/s, would have been used the resulting experimental value for $k_{\Delta\Pi}$ would be smaller than the theoretical values resulting from the equations derived by Grober and Harriott-Hamilton respectively. The results clearly showed a dependence on the velocity, being $\sim v^{0.5}$ and $\sim v^{0.92}$ for the two different cases of flow conditions. The flux obtained was maximally $1.5\ 10^{-5}$ m/s in the turbulent case and about $1.0\ 10^{-5}$ m/s in the laminar case.

ii) Trägårdh et al. [12] also obtained a smaller experimental mass transfer coefficient $k_{\Delta\Pi}$ than the theoretical values according to the Chilton-Colburn equation (eq. 4) using Dextrans and several types of membranes, although in some cases there was a reasonable agreement. No flux data were given for the experiments.

iii) Jonsson [2], found in experiments using Dextrans and a whey protein solution that $k_{\Delta\Pi}$ is smaller (approximately 25%) than the theoretical values according to eqs. 3 and 4 for laminar and turbulent flow conditions, respectively. The tendency of the mass transfer coefficient to increase with the velocity (with an exponent 0.33 or 0.8) could be found. For the calculation of the mass transfer coefficients during these experiments identical relations were used for the osmotic pressure of Dextrans T10 and T20. The experimental fluxes J_v were $0.5 - 3\ 10^{-5}$ m/s and they increased with increasing cross-flow velocities. The ratio J_v/v was smaller than $2\ 10^{-5}$.

iv) Nakao et al. [6] showed that fluxes calculated with the osmotic pressure model and using a mass transfer coefficient according to the Leveque equation (laminar flow conditions, eq. 3) were nearly identical to experimental fluxes, while in the turbulent region (using Deissler's equation, eq. 5) the calculated fluxes were overestimated. Apparently the actual mass transfer coefficient was much smaller than given by Deissler's relation. Using a concentration dependent viscosity and diffusivity the experimental mass transfer coefficients could be estimated reasonably well.

v) Wijmans et al. [13] calculated mass transfer coefficients in the turbulent region over a

large range of fluxes and J_v/v ratios. The experiments were performed using Dextrans at various concentrations and applied pressures. The experimentally determined osmotic pressures as a function of concentration showed an almost identical dependence on the concentration for Dextrans T70 and T500. The values of the experimental mass transfer coefficients ($k_{\Delta\Pi}$) were compared to values obtained by using Deissler's equation (k_D). The ratio $k_{\Delta\Pi}/k_D$ appeared to be very dependent on the flux and especially on the J_v/v ratio: $k_{\Delta\Pi}/k_D$ increased with increasing J_v/v. Starting from $k_{\Delta\Pi}/k_D \approx 0.6$ this value increased almost linearly to 1.1; the ratio was 1 at $J_v/v \approx 2\ 10^{-5}$.

2. The velocity variation method

Using $\Re_{obs} = 1 - C_p/C_b$ for the observed retention and $\Re = 1 - C_p/C_m$ for the intrinsic (or real) retention the following relation can be derived from eq. 12:

$$\ln [(1 - \Re_{obs}) / \Re_{obs}] = \ln [(1 - \Re) / \Re] + J_v / k \qquad (21)$$

The Sherwood relations for k, as given in the introductory section, always show a certain dependence on the cross-flow velocity like $k = b.v^a$, where $\langle a \rangle \approx 0.33$ for laminar conditions and $\langle a \rangle = 0.75 - 0.91$ for turbulent conditions. Therefore the equation for the retention can be written as

$$\ln [(1 - \Re_{obs}) / \Re_{obs}] = \ln [(1 - \Re) / \Re] + J_v / (b.v^a) \qquad (22)$$

By plotting the experimental values of $\ln[(1 - \Re_{obs}) / \Re_{obs}]$ in a graph as a function of J_v/v^a, where the value of the coefficient $\langle a \rangle$ should be chosen in advance, the intrinsic retention and the constant b can be determined graphically. The relation for the mass transfer coefficient as a function of the various experimental variables can now be obtained by fitting the data found in the different experimental circumstances. A large disadvantage of this method is the necessity of an incomplete retention. While in practice for many solutes the retention preferably is complete (=1), now the retention should be rather low.

Some results obtained by other researchers are:

I) The observed retention is a function of many process-variables [11, 12, 14-18]: $\Re_{obs}$ increases with increasing molecular weight, increasing cross-flow velocity and increasing concentrations in the bulk, while $\Re_{obs}$ also increases when a solute mix is used. $\Re_{obs}$ first increases and then decreases again when the applied pressure is increased. The intrinsic retention $\Re$ increases with increasing permeate flux, increasing applied pressure and higher

molecular weights, but is constant at increasing cross-flow velocities.

II) Nakao and Kimura [18] used PEG 4000 (M_w=3000), vitamin B_{12} (M.W.=1355), raffinose (M.W.=504), sucrose (M.W.=342), glucose (M.W.=180) and glycerine (M.W.=92) during their experiments. In turbulent conditions the experimentally determined mass transfer coefficients seemed to fit excellently (graphically) with Deissler's equation (eq. 5), but appeared to deviate up to 40 % (numerically). The general tendency was that of following Deissler's equation however.

III) Jonsson and Boesen [19] calculated the mass transfer coefficient, as derived from reverse osmosis experiments with NaCl, $CaCl_2$ and $MgSO_4$, for laminar and turbulent conditions. For the turbulent case an exponent of value <a> = 0.80 was used, this resulted in k-values which were equal or only a little larger than the k-values calculated according to Chilton-Colburn's relation (eq. 4). However, when the flux increased considerably a firm deviation from the straight line could be observed (<a> smaller than 0.80). In case of laminar conditions the value of the mass transfer coefficients scattered more or less around the line for the 'theoretical' mass transfer coefficient given by the Graetz-Leveque equation (eq. 3). This depended on the Reynolds number: at low Reynolds numbers the value of the coefficient <a> was around 0.33 (up to Re≈700), but this value increased with increasing Re.

IV) Nakao et al. [20] used high flux membranes or high temperatures to study the effect of high fluxes, again using low-molecular weight solutes. When the high flux was obtained by the use of a high flux membrane the agreement between the mass transfer coefficients k_D calculated from Deissler's equation and those calculated according to the velocity variation method (k_{vv}) was very much dependent on the J_v/k_D-ratio: at low J_v/k_D-ratios (up to 0.5) the k_{vv}/k_D-ratio was approximately equal to one, while at higher J_v/k_D-ratios the k_{vv}/k_D-ratio increased. This increase appeared to fit the Stewart correction for high mass transfer very well. When the high flux was obtained by the use of high temperatures (increasing the diffusivity and decreasing the viscosity, using $\eta_0.D/T$ = constant) the k_{vv}-values matched the k_D-values excellently.

EXPERIMENTAL

Ultrafiltration experiments were performed in three different cross-flow ultrafiltration systems: system A, a membrane system with four tubular membranes in series (figure 2); system B, a system with a thin channel module in which different types of flat membranes were used (figure 3) and system C, a DDS Mini-Lab 10 system in which flat membranes were used (figure 4). The total membrane areas in the different modules were 222 10^{-4} m^2,

two membranes of about 36 10^{-4} m^2 each (variable) and 336 10^{-4} m^2, respectively. The amount of bulk solution was rather different for the three systems, being 10, 20 and 2 litres, respectively.

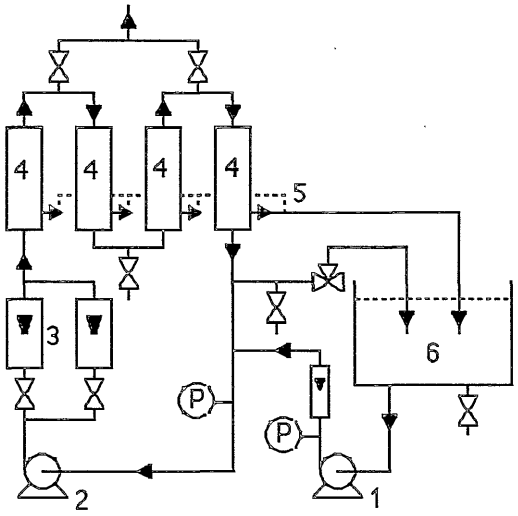

Figure 2. Schematic representation of the tubular membrane ultrafiltration equipment (system A). 1: injection pump; 2: recirculation pump; 3: flow meters; 4: membrane modules; 5: permeate drain; 6: bulk solution tank.

The solutions used were Dextrans T10, T70 and T500 (M_w = 10,500, 72,200 and 465,000 respectively) in demineralized water, which was treated by ultrafiltration and reverse osmosis before use, and solutions of the protein Bovine Serum Albumin (BSA, M.W.=69,000) in a phosphate buffer at pH = 7.4 with 0.1 N NaCl added, to give a solution with ionic strength I = 0.125 N. The concentration in the Dextran concentrate- and permeate-solutions was determined by a Beckman model 915A Total Organic Carbon analyzer. The concentration in the BSA solutions were determined using a Waters HPLC system.

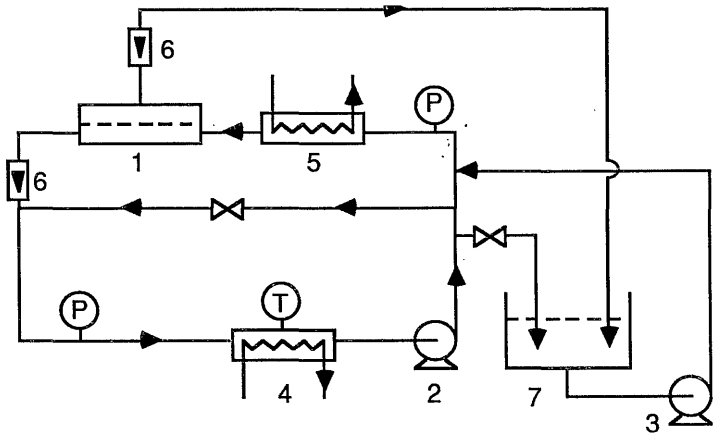

Figure 3. Schematic representation of the thin channel ultrafiltration equipment (system B). 1: membrane module; 2: recirculation pump; 3: injection pump; 4: heat exchanger with thermistor; 5: heat exchanger; 6: flowmeters; 7. bulk solution tank.

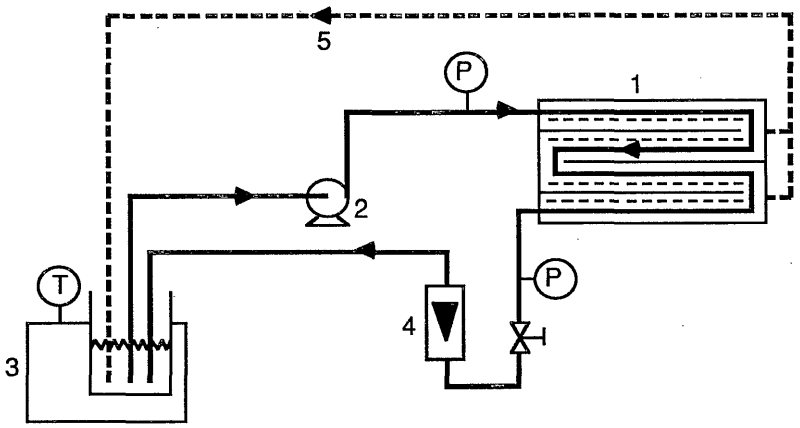

Figure 4. Schematic representation of system C with the DDS Mini-Lab 10 module. 1: membrane module; 2: recirculation pump; 3: bulk solution in thermostat bath; 4: flowmeter; 5. permeate-drain.

The equations used for the dependence of the osmotic pressure on the concentration were taken identical for the three Dextran solutions, which is correct at higher concentrations were the molecular weight is of minor importance [1,2], being:

$$\Delta\Pi_{Dextrans} = 37.5*C + 0.752*C^2 + 7.64\ 10^{-3}*C^3 \qquad (23)$$

For BSA this dependence was calculated as:

$$\Delta\Pi_{BSA} = (RT/M)* [C - 1.09\ 10^{-2} *C^2 + 1.24\ 10^{-4}*C^3 + (C^2 + 4.5761\ 10^5)^{0.5} - 1.38\ 10^4] \qquad (24)$$

The latter equation was developed according to Vilker et al., taking into account the excluded volume (first term) and the Donnan effects (second term) [21]. The values of the parameters needed for this calculation can be found in this latter reference (see also [22]).

The tubular membranes (obtained from Wafilin B.V., Hardenberg, the Netherlands) used in system A were WFS-5010 and WFS-6010 (polysulfone), WFE-X005 and WFE-X006 (polyethersulfone) and WFA-3010 and WFA-4010 (polyacrylonitrile) all having a 99+% observed retention for the solutes studied (Dextran T70 and BSA). The membranes used in system B were Kalle Nadir 47, Nadir 66 and P.S. 50 (polysulfone) having a 99+%, 90+% and 65+% observed retention, respectively, for Dextran T70 and 99+% for BSA. The membranes used in the DDS Mini-Lab 10 (system C) were CA600PP (cellulose-acetate) having a 99+% observed retention for Dextran T70 and T500 and for BSA, for Dextran T10 the observed retention was smaller and varied with the experimental conditions.

The flow conditions were different for the various systems. They were considered to be for system A: turbulent (Re = 14,400*v, varying from 14,400 to 43,200 depending on v); for system B: turbulent (Re = 10,900*v, minimally 3,270 to 15,260) and for system C: laminar (Re = 1,500*v, which is Re =765 to 2820 maximally). Although the lower limit of the Reynolds numbers in system B and the upper limit in system C can be expected to fall in the transition region of the laminar and turbulent flow regime, for reasons of convenience they will be treated as being turbulent and laminar, respectively. The comparison of the influence of the flow conditions in one system will then be more realistic as well.

The temperature was 25 °C during the experiments performed in systems B and C, whi the temperature of the bulk solution varied when system A was used. In the latter case the appropriate correction for the varying viscosity was applied.

When using various solutes and membranes flux reduction as a result of adsorption and pore-blocking is very common, especially when proteins and hydrophobic membranes are

involved. For that reason the flux decline due to concentration polarization of protein solutions filtered through a hydrophobic membrane was calculated from the actual flux and the clean water flux measured after the experiments were performed. In the cases that Dextrans were involved, or when cellulose-acetate membranes were used, the flux decline was very small usually and no significant difference in results was found whether the clean water flux before or after the ultrafiltration experiment was used.

RESULTS

In this section first the results of the method using the osmotic pressure difference will be given. General tendencies will be shown, as well as the influence of the various experimental circumstances on the calculated mass transfer coefficient. Then the results of the velocity variation method will be presented, after which these two methods will be compared mutually. The plots given in this section will represent typical results taken from many ultrafiltration experiments with Dextrans or BSA in the three different systems.

A typical result of a set of ultrafiltration experiments, with Dextran T70 as the solute, is given in figure 5.

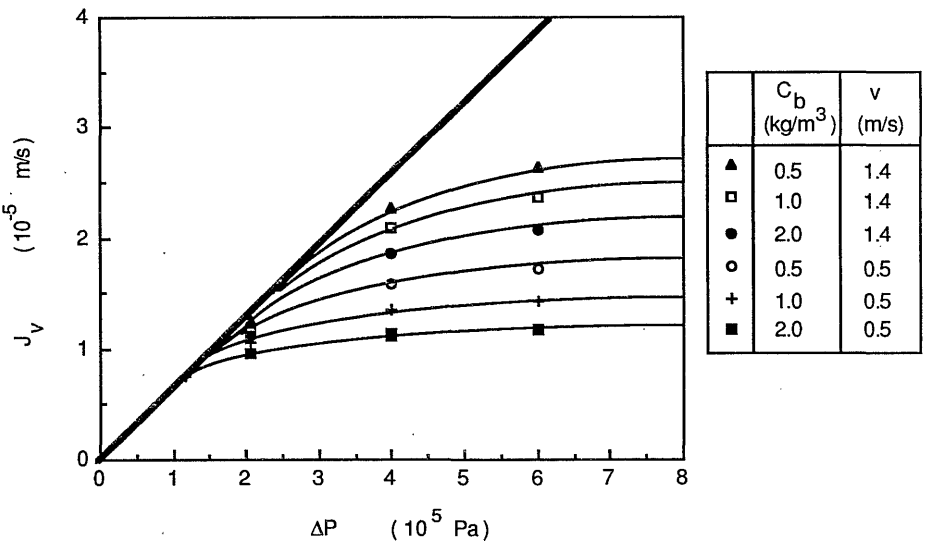

Figure 5. The permeate flux as a function of the bulk concentration and the cross-flow velocity. The straight line represents the clean water flux. Experiments performed in ultrafiltration system B, with Dextran T70 as the solute.

The permeate flux J_v increases with increasing pressure, though not linearly. Beyond a certain applied pressure and depending on the concentration in the bulk solution and the cross-flow velocity, the flux will even reach the so called limiting flux region,, where an increase of the applied pressure will not lead to a further increase of the permeate flux. In figure 5 it can be seen that the flux decreases with increasing concentration in the bulk and with decreasing cross-flow velocity. The limiting flux region is nearly reached in the case of $C_b = 2.0$ kg/m^3 and $v = 0.5$ m/s beyond $\Delta P = 4.0\ 10^5$ Pa.

A. The osmotic pressure method

When the fluxes during ultrafiltration of a solution are known they can be compared to the 'clean water flux' at equal applied pressures, and by using eq. 20 the osmotic pressure difference across the membrane can be calculated. With the help of the relations for the osmotic pressure as a function of the concentration the concentration at the membrane wall is obtained. Then, using the value of the concentration in the bulk, the mass transfer coefficient $k_{\Delta\Pi}$ can be calculated (equation 18).

Although in literature the values of the (experimental) mass transfer coefficients are mostly compared to coefficients calculated from Deissler's equation (k_D, eq. 5), for solutes like BSA and Dextrans (Sc ≈ 13,000 - 22,000) mass transfer coefficients calculated from the Sherwood relation by Harriott and Hamilton (k_{HH}, eq. 6) should be used. In figures 6 to 9, and in the figures 11 and 12, the calculated experimental coefficients $k_{\Delta\Pi}$ will be compared to k_{HH}, studying the influence of the different process parameters. The varying experimental parameter will be the frequently used J_v/v-ratio.

In figure 6 the $k_{\Delta\Pi}/k_{HH}$-ratio is given for three different bulk concentrations C_b, 0.1, 0.5 and 1.0 kg/m^3, resulting in a different dependence on the J_v/v-ratio. The k-ratio dependence on J_v/v seems to be almost linear, where the slope of the line for $C_b = 0.1$ kg/m^3 is clearly smaller than the slopes of the lines for $C_b = 0.5$ and 1.0 kg/m^3. The difference between 0.5 and 1.0 kg/m^3 is much smaller. Although there is a trend for the $k_{\Delta\Pi}/k_{HH}$-ratio being larger for $C_b = 1.0$ kg/m^3 than for 0.5 kg/m^3 this is perhaps not significant, due to the experimental error (ca. 10%) and the resulting error in the k-ratio. Because of this dependence on the concentration the other parameters will be studied using concentrations of 0.5, 1.0 and 2.0 only. In figure 6 the $k_{\Delta\Pi}/k_D$-ratio is also given for comparison. This ratio is about 1.5 times larger than the $k_{\Delta\Pi}/k_{HH}$-ratio, which is caused for the major part by the smaller exponent of the Schmidt number in Deissler's equation. In figures 7 and 8 the influence of the cross-flow velocity is represented.

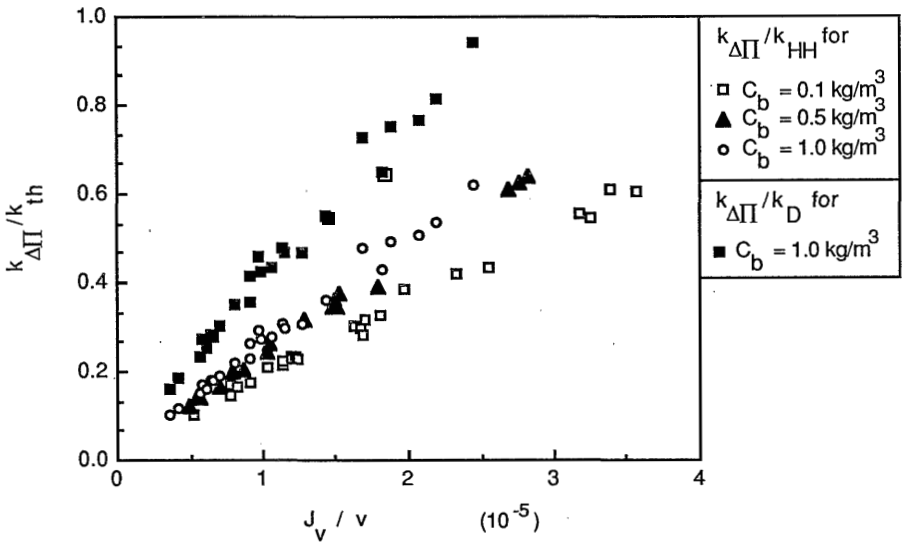

Figure 6. Comparison of the mass transfer coefficient $k_{\Delta\Pi}$ obtained from experiments with the mass transfer coefficient according to Harriott-Hamilton k_{HH}, for three different bulk concentrations and one comparison with the mass transfer coefficient according to Deissler k_D. Experiments were performed with BSA at pH = 7.4 in ultrafiltration system A.

In figure 7 the $k_{\Delta\Pi}/k_{HH}$-ratio is plotted as a function of the J_v/v-ratio for experiments performed with Dextran T70 in system A, while in figure 8 the results of experiments with BSA in system B are represented. From both the data in figure 7 and in figure 8 it can be concluded that there is no difference in results when the velocity is varied. For all velocities equal trends can be observed: the $k_{\Delta\Pi}/k_{HH}$-ratio increases with increasing J_v/v-ratio. All data together show that the increase is almost linear.

When two different solutes are studied in the same ultrafiltration system there are two essentially different physico-chemical parameters: the osmotic pressure as a function of concentration and the (bulk-)diffusion coefficient. In figure 9 the results of ultrafiltration experiments in system A with BSA and Dextran T70 are given.

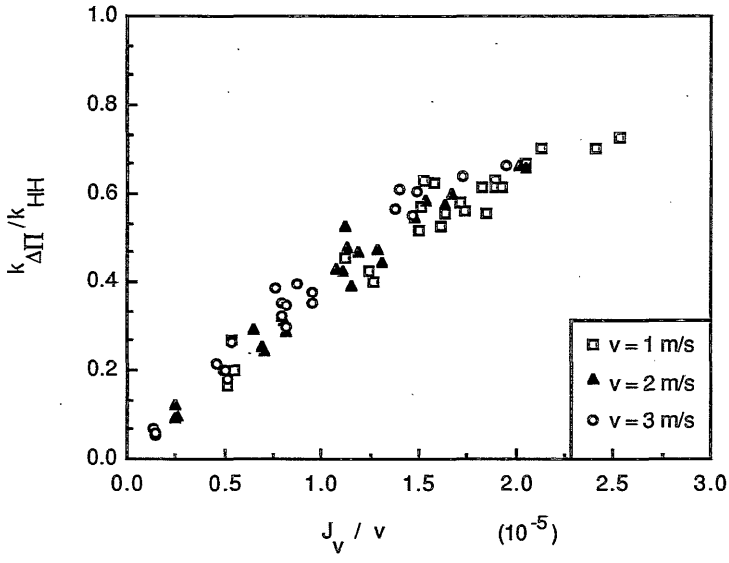

Figure 7. The $k_{\Delta\Pi}/k_{HH}$-ratio as a function of the J_v/v-ratio, at three different cross-flow velocities. Experiments performed with Dextran T70 in ultrafiltration system A.

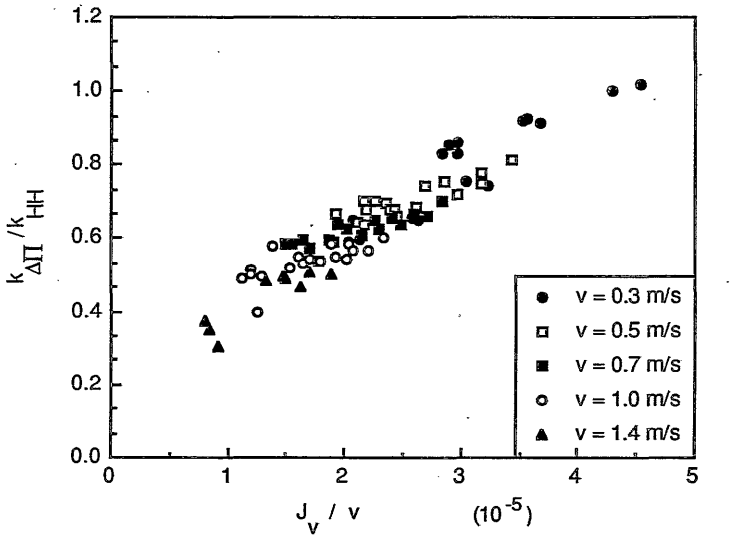

Figure 8. The $k_{\Delta\Pi}/k_{HH}$-ratio as a function of the J_v/v-ratio, at five different cross-flow velocities. Experiments performed with Dextran T70 in ultrafiltration system B.

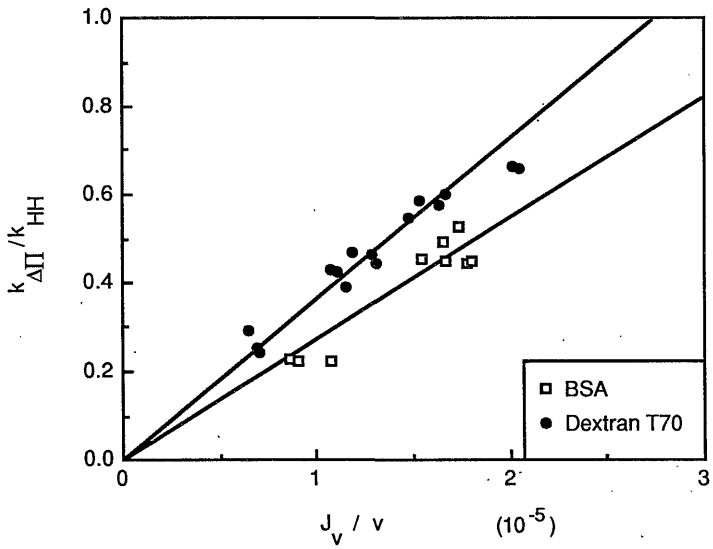

Figure 9. The $k_{\Delta\Pi}/k_{HH}$-ratio as a function of the J_v/v-ratio, for different solutes. The experiments were performed with BSA and Dextran T70 in ultrafiltration system A, at v = 2 m/s (turbulent conditions) and C_b = 1 kg/m^3.

Despite the not too many data points and the scatter in the data the results show that there is a difference between the two solutes when filtered at the same bulk concentration in the same system. The mass transfer coefficient ratio $k_{\Delta\Pi}/k_{HH}$ for BSA is some 20 % smaller than for Dextran T70. This same conclusion can be drawn when other concentrations and velocities are studied.

In figure 10 this comparison is made for BSA versus three different Dextrans, but in a totally different ultrafiltration system (system C) and at laminar flow conditions. The $k_{\Delta\Pi}/k_{GL}$-ratio seems to be smaller again for BSA than for the Dextrans, although the difference is not as large as in the case of turbulent flow conditions.

In figure 11 the results of experiments performed at different applied pressures, with one solute (Dextran T70) in one ultrafiltration system (B), are compared.

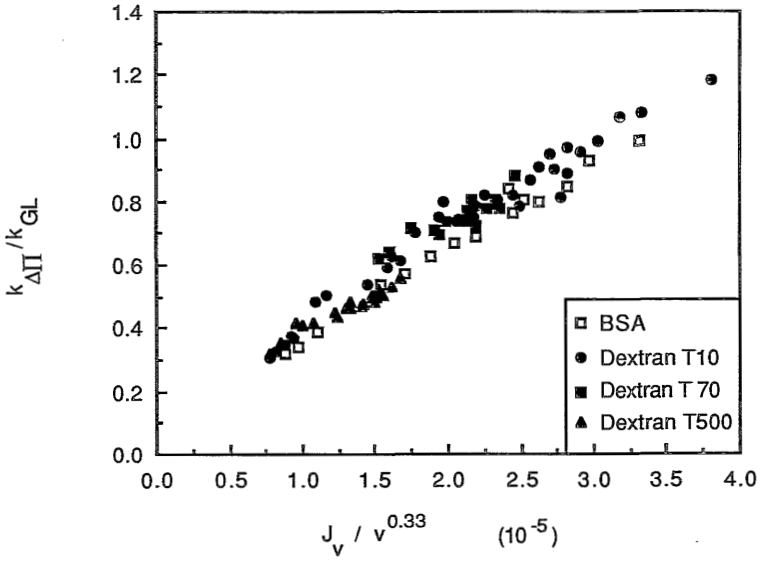

Figure 10. The $k_{\Delta\Pi}/k_{GL}$-ratio as a function of the $J_v/v^{0.33}$-ratio, for different solutes. The experiments were performed with BSA and Dextran T10, T70 and T500 in ultrafiltration system C, at various cross-flow velocities and C_b = 1 kg/m^3.

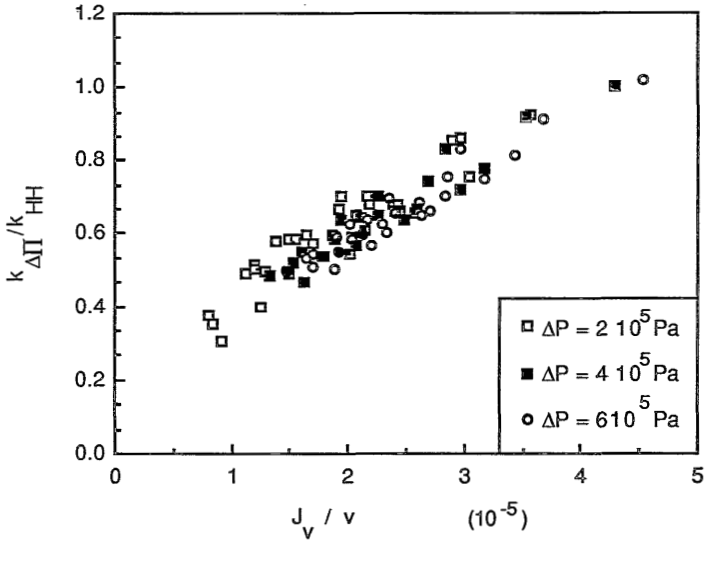

Figure 11. The $k_{\Delta\Pi}/k_{HH}$-ratio as a function of the J_v/v-ratio, at three different applied pressures. Experiments performed with Dextran T70 in ultrafiltration system B.

No systematic difference can be observed between the data points of $\Delta P = 4.0\ 10^5$ Pa and $\Delta P = 6.0\ 10^5$ Pa, while for the data obtained at $\Delta P = 2.0\ 10^5$ Pa the $k_{\Delta\Pi}/k_{HH}$-ratio is slightly larger, at equal J_v/v-ratios.

An other important variable is the hydraulic diameter d_h of the membrane filtration system. Although the dependence of the mass transfer coefficient on d_h is only $(d_h)^{0.09}$ in Harriott-Hamilton's Sherwood relation, d_h determines the Reynolds number (for one solute, together with the cross-flow velocity) and so the laminar-turbulent transition region. In figure 12 a comparison is made between the ultrafiltration systems A and B with hydraulic diameters of $1.45\ 10^{-3}$ m and $1.09\ 10^{-2}$ m, respectively.

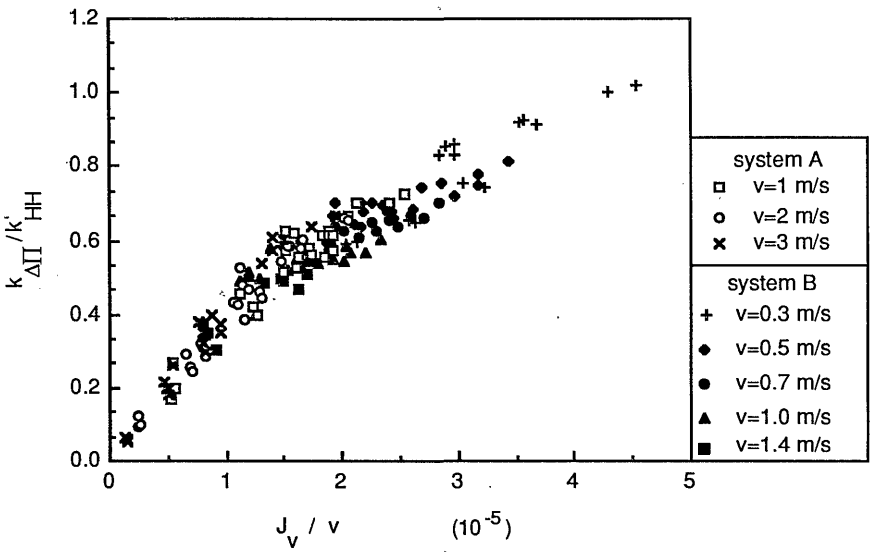

Figure 12. The $k_{\Delta\Pi}/k_{HH}$-ratio as a function of the J_v/v-ratio at different cross-flow velocities in two ultrafiltration systems: system A with $d_h = 1.45\ 10^{-3}$ m and system B with $d_h = 1.09\ 10^{-2}$ m. The experiments were performed with Dextran T70 at $C_b = 1.0$ kg/m^3.

From the data points in figure 12, which overlap closely for the two systems, it can be concluded that the mass transfer coefficient ratio is not significantly dependent on the system or its difference in hydraulic diameter.

Further remarks on the experimental results can be found in the discussion section.

B. The velocity variation method.

As shown in the theoretical section, the experimental data needed for a typical plot in the velocity variation method are the observed retention $\Re_{obs}$, the flux J_v and the cross-flow velocity v. After choosing the exponent <a> of the cross-flow velocity (in $k = b.v^a$, which depends on laminar or turbulent conditions) the main variable for a certain combination of solute and membrane appears to be the applied pressure. In figure 13 a typical example is given.

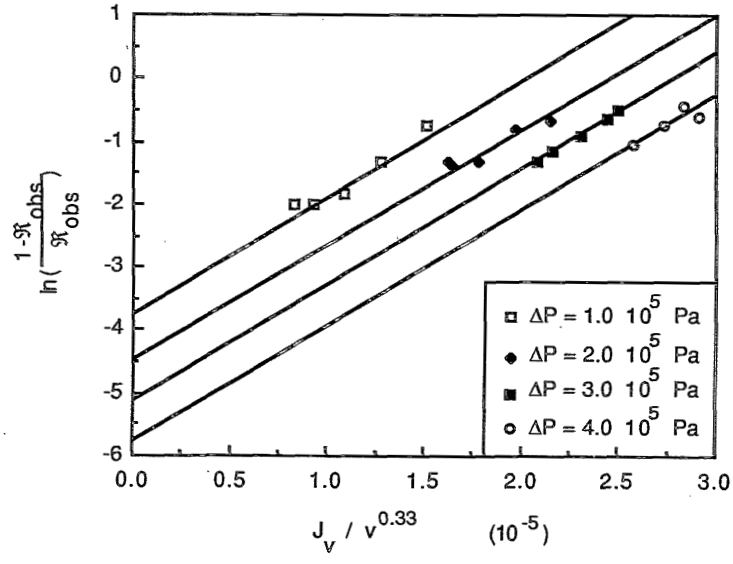

Figure 13. The typical 'velocity variation plot' for laminar conditions, ln[(1 - $\Re_{obs}$) / $\Re_{obs}$] as a function of $J_v/v^{0.33}$. Dextran T10 was used in ultrafiltration system C using a CA600PP membrane, C_b = 1.0 kg/m^3.

The lines fitting the data points all show the same slope, which is 1/b in $k = b.v^a$. This was imposed because equal slopes are expected when the applied pressure is the only variable and more important: when a fit is made at each pressure separately the difference in slopes can be very large (in this case up to 35%); then the extrapolation to $J_v/v^{0.33} = 0$, to obtain the values of the intrinsic retention at the various pressures, would give nearly random values. Now the intrinsic retentions vary from $\Re = 0.975$ at $\Delta P = 1.0\ 10^5$ Pa, via $\Re = 0.989$ and $\Re = 0.994$, to $\Re = 0.997$ at $\Delta P = 4.0\ 10^5$ Pa.

Improvement of these results is hard to achieve as a certain combination of solute and membrane only gives a limited range of fluxes and observed retentions. Duplicate measurements, given in figure 14, show the same trends, although for some data points a deviation can be observed (the two lowest velocities at each pressure).

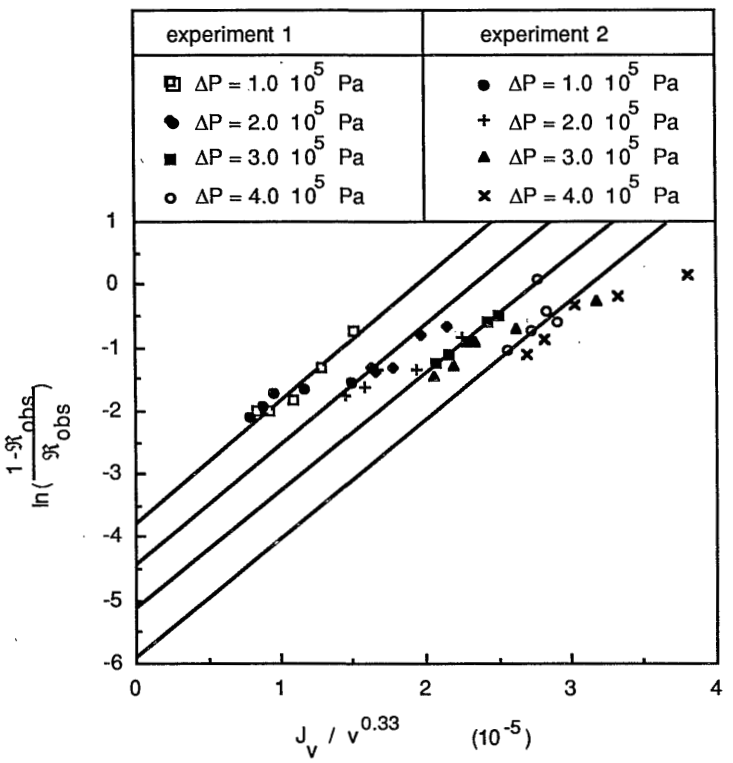

Figure 14. A 'velocity variation plot' for laminar conditions. A duplicate measurement in which Dextran T10 was used in ultrafiltration system C using a CA600PP membrane, C_b = 1.0 kg/m^3.

It will be clear that the derived mass transfer coefficient k_{vv} (for one solute) will have the same dependence on the velocity as the theoretical relations, because all slopes in the $\ln[(1-\Re_{obs}) / \Re_{obs}]$ versus $J_v/v^{0.33}$ plot are equal. When the ratio k_{vv}/k(theoretical), where the relation of Graetz-Leveque is used ($\sim v^{0.33}$), is calculated this results in a constant ratio k_{vv}/k_{GL}.

The range for choosing the exponent <a> for the cross-flow velocity is not very small , as can be seen in figure 15, in which $v^{0.50}$ is used instead of $v^{0.33}$. This is a realistic exponent as well, as it can be found in Grober's Sherwood relation (eq. 2).

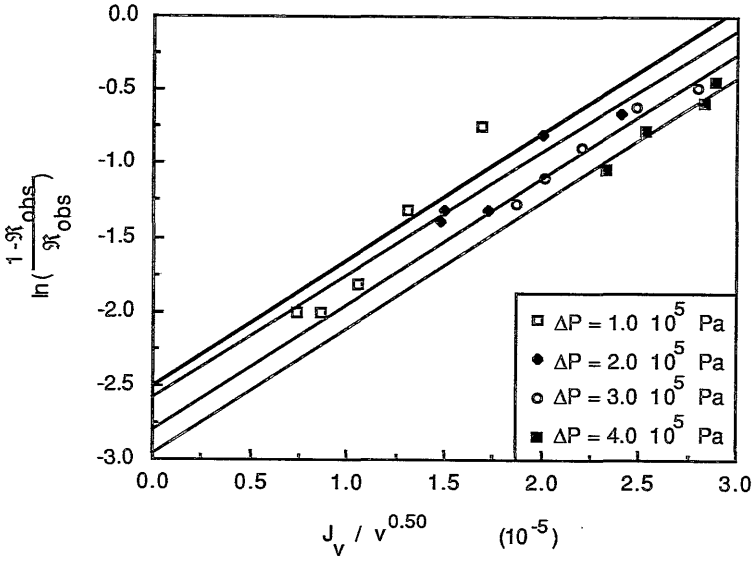

Figure 15. The 'velocity variation plot' for laminar conditions, now plotted as $ln[(1 - \Re_{obs}) / \Re_{obs}]$ vs. $J_v/v^{0.50}$. Dextran T10 was used in ultrafiltration system C using a CA600PP membrane.

When these scattering data are compared to the more linear fits for data in figure 13 it must be concluded that the exponent <a> should be 0.33 instead of 0.50. The difference in scattering is not very large however when the data from figure 15 are compared to the combined sets of data represented in fig. 14 (duplicate measurements). The problem of choosing the right exponent <a> still does exist.

As described above, the curves of these experimentally determined mass transfer coefficients k_{vv} or their ratio to k_{GL} (the Graetz-Leveque relation for laminar flow conditions) as a function of $J_v/v^{0.33}$ will show a completely different picture from the $k_{\Delta\Pi}/k_{GL}$-ratio. In figure 16 the k_{vv}/k_{GL} and k_{vv}/k_{Gr}-ratios are given for the duplicate measurements mentioned above. Both the mass transfer coefficient according to the velocity variation method (using $v^{0.50}$ as well) and the osmotic pressure method are

calculated and compared to the mass transfer coefficient according to Graetz-Leveque (~ $v^{0.33}$, eq. 3) and Grober (~ $v^{0.50}$, eq. 2).

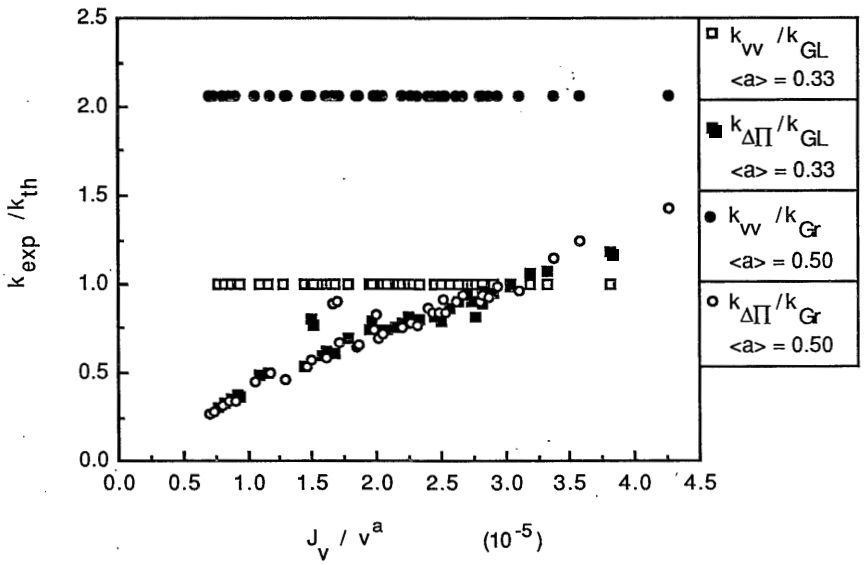

Figure 16. Comparison of experimentally determined mass transfer coefficients according to the velocity variation method (using $v^{0.33}$ and $v^{0.50}$) and the osmotic pressure method, with mass transfer coefficients calculated from the Graetz-Leveque equation and Grober's equation, respectively. Dextran T10 was used in ultrafiltration system C using CA600PP membranes, C_b = 1.0 kg/m^3.

The large difference between the two sets of results will be clear: while the osmotic pressure method results in mass transfer coefficient ratios which are more or less linear to the variable $J_v/v^{0.33}$ the velocity variation method shows a constant ratio. When the k_{vv}/k_{GL}-ratio is compared for $v^{0.33}$ and $v^{0.50}$ a large difference can be found: the ratio is about 1.0 when v^a is taken as $v^{0.33}$ and about 2.1 for $v^{0.50}$.

When the velocity variation method is used for turbulent flow conditions the plots obtained can show the same trends: in figure 17 the experimental results for ultrafiltration of Dextran T70, using two different membranes at two applied pressures are represented. Since the experimental conditions were turbulent the exponent <a> in J_v/v^a can be expected to be 0.91, according to the Harriott-Hamilton relation (eq. 6).

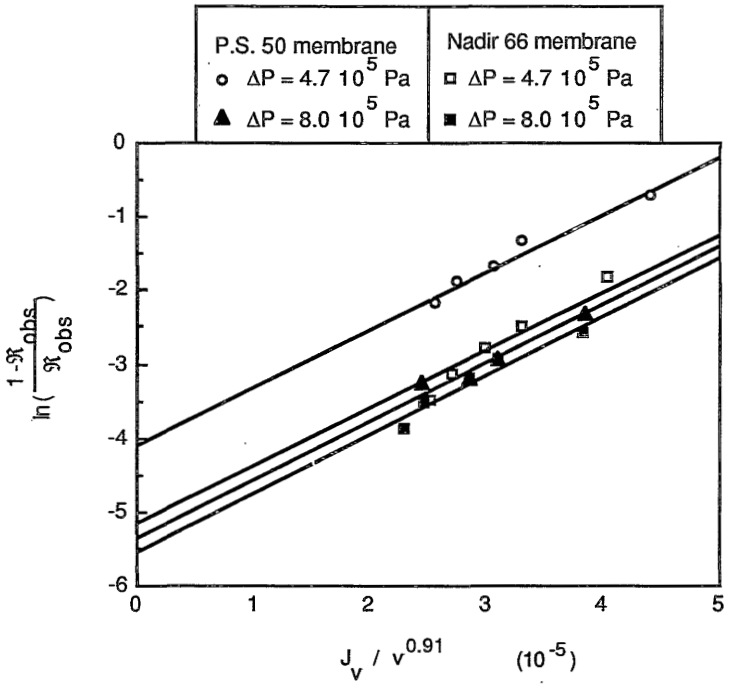

Figure 17. The velocity variation plot for turbulent conditions. Dextran T70 was used in ultrafiltration system B with Nadir 66 and P.S. 50 membranes, C_b = 0.5 kg/m^3. ΔP was 4.7 or 8.0 10^5 Pa.

Again distinct sets of data can be found for each applied pressure and each membrane, indicating that the velocity variation method is much more responsive to experimental differences than the osmotic pressure method. Although the data given here show a rather linear and consistent behaviour with changing experimental circumstances, in practice a deviating behaviour can be observed sometimes, which will force one to extend the series of experiments.

DISCUSSION

Osmotic pressure method

The results of the osmotic pressure method to determine mass transfer coefficients show rather scattering data in general. For some experimental circumstances clear changes in the value of the mass transfer coefficient ratio can be observed, e.g. when the concentration in

the bulk solution is very low (fig. 6) or when the applied pressure is rather low (fig. 11). In the latter case it can be concluded that the mass transfer coefficient ratio appears to be relatively large when the flux reduction due to concentration polarization is not very large, i.e. when the limiting flux region is not reached at all. The influence of the other process variables (the cross-flow velocity and the hydraulic diameter) is found to be not significantly different from the $1/v^a$ dependence. Furthermore, the results seem to be dependent on the type of solute used, which probably is a result of the values of the physico-chemical parameters used in the calculations. E.g., for the diffusion coefficient of BSA a value of 6.9 10^{-11} m^2/s was used, while in literature also many other values can be found (for a review see [23]), varying from 6 to 9 10^{-11} m^2/s. For the diffusion coefficient of Dextrans the value of 6.0 10^{-11} m^2/s was used, which is the intermediate value of the coefficient at low concentrations (ca. 4 10^{-11} m^2/s) and the coefficient at high concentrations (ca. 8 10^{-11} m^2/s) [1]. Adaptation of the calculated mass transfer coefficient ratios $k_{\Delta\Pi}/k_{HH}$ and $k_{\Delta\Pi}/k_{GL}$ e.g. using a value of 8.0 10^{-11} m^2/s would result in a close overlap of the two sets of data.

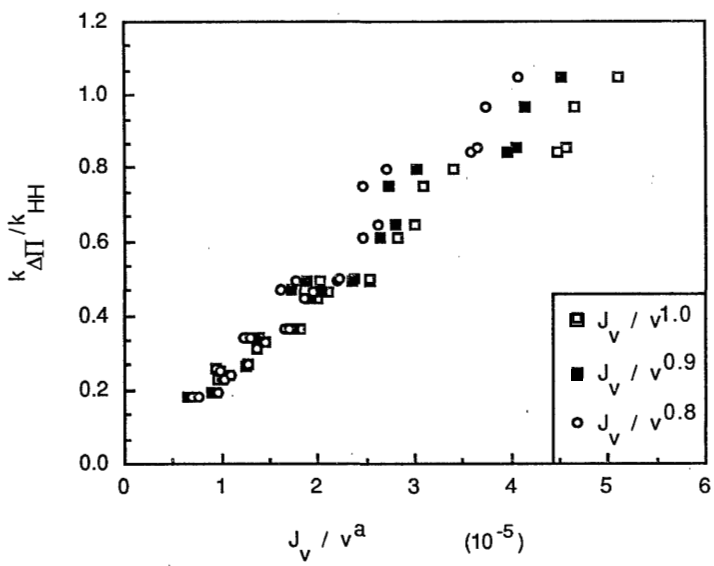

Figure 18. Comparison of the $k_{\Delta\Pi}/k_{HH}$-ratio as a function of the J_v/v^a-ratio, in which the exponent <a> varied from 0.8, via 0.9 to 1.0. The experiments were performed with BSA at pH = 7.4 in ultrafiltration system B, C_b = 1.0 kg/m^3.

The fact that the cross-flow velocity seems to have no influence on the general course of the $k_{\Delta\Pi}/k_{HH}$ or $k_{\Delta\Pi}/k_{GL}$ versus J/v^a dependence (fig. 7 and 8) implies that the correct exponent <a> of the cross-flow velocity is used. However, when for instance in case of turbulent conditions an exponent 0.8 or 0.9 is used hardly any difference can be observed. In figure 18 this is illustrated using <a> = 0.8, 0.9 or 1.0. Except for a somewhat steeper increase of the ratio $k_{\Delta\Pi}/k_{HH}$ when $J_v/v^{0.8}$ is used as the variable on the abscissa, compared to J_v/v, the same dependence is found using different exponents <a>.

Comparison of our results with results obtained by others is possible, e.g. when the dependence of $k_{\Delta\Pi}/k_D$ on the J_v/v-ratio in figure 6 is envisaged. Wijmans [13] found very similar results for Dextran T70 in the range $J_v/v = 1 - 2.5\ 10^{-5}$ m/s, while the work done by other researchers, as mentioned in the theoretical section, usually showed an experimental mass transfer coefficient which was smaller than the 'theoretical' one k_{HH}, k_D, k_{Gr} or k_{GL}. A more specific dependence of the mass transfer coefficient ratio on other parameters was not given and therefore can not be compared to our results.

When the plots of $k_{\Delta\Pi}/k_{th}$ as a function of J_v/v are looked at in another way the results do not seem to be very consistent anymore: e.g. the influence of the cross-flow velocity can be regarded as almost random when the range of mass transfer coefficient ratios are given as a function of the cross-flow velocity (see fig. 7 and 8). In fig. 7 the $k_{\Delta\Pi}/k_{HH}$-ratio varies from 0.2 to 0.7 for v = 1 m/s and for v = 3 m/s these figures are $k_{\Delta\Pi}/k_{HH}$ = 0.07 to 0.7. A slightly more specific range for each velocity can be given when the most extreme data points are left out. Then the ranges are 0.4 - 0.7, 0.3 - 0.6 and 0.2 - 0.6 for cross-flow velocities of 1, 2 and 3 m/s, respectively. *Obviously there is no narrow range for the mass transfer coefficients when described as a function of the cross-flow velocity*. This same conclusion can be drawn when the other process variables are studied. The use of a certain mass transfer coefficient ratio at a certain J_v/v ratio to predict fluxes therefore seems to be impossible because of the large spreading in the experimental results.

The origin of this failure to describe the influences on the mass transfer coefficient correctly may be found in the way we calculate and represent the data. This can be made clear as follows:
the experimental mass transfer coefficient is calculated via

$$k_{\Delta\Pi} = J_v / \ln(C_m/C_b) \qquad (25)$$

while the theoretical mass transfer coefficient can be represented as

$$k_{th} = \beta.v^a \qquad (26)$$

When now a plot is made of e.g. $k_{\Delta\Pi}/k_{HH}$ as a function of J_v/v^a we find that the data in the

plots can be described generally by a linear relationship

$$k_{\Delta\Pi}/k_{HH} = \gamma.J_v/v^a \qquad (27)$$

So we find

$$[J_v / \ln(C_m/C_b)] / \beta.v^a = \gamma.J_v/v^a \qquad (28)$$

or

$$\ln(C_m/C_b) = 1/(\beta.\gamma) \qquad (29)$$

Realizing that γ is a constant for one combination of solute and ultrafiltration system and that β should be practically constant (dependent on D, η and ρ only), the quantity $\ln(C_m/C_b)$ then has to be almost constant, which is not very realistic at first sight, since during an ultrafiltration experiment the applied pressures were varied from 2 to 6 10^5 Pa. However, when the logarithmic concentrations at the membrane wall are considered it appears to be possible: when C_m=500 kg/m^3 the value of $\ln(C_m/C_b)$ is only 9 % higher than in the case of C_m=300 kg/m^3, while a considerable difference in $\Delta\Pi$ (11.6 10^5 Pa and 2.86 10^5 Pa respectively for Dextran T70) and actual flux does exist. The conformity of the quantities plotted, as well as this very small dependence of the $\ln(C_m/C_b)$-value on the calculated concentration C_m, probably is the origin of the bad agreement with our expectations. Since the main reason for our problem must be found in the equation $k_{\Delta\Pi} = J_v / \ln(C_m/C_b)$, which is characteristic for the film-model in general, no better solution can be expected for this theoretical inconvenience.

Velocity variation method

The results obtained using the velocity variation method must be evaluated rather differently: the slopes 1/b in $k = b.v^a$ in the $\ln[(1 - \Re_{obs}) / \Re_{obs}]$ versus J_v/v^a plot are made equal for equal circumstances. Doing so this results in a relationship for the experimental mass transfer coefficient k_{vv} which is proportional to b and to the (chosen) quantity v^a. So in fact, the two main parameters from which the mass transfer coefficient is composed are chosen within reasonable limits. The results for the velocity variation method using $v^{0.33}$ in the laminar case are encouraging (figure 13) and the comparison with the Graetz-Leveque equation also: $k_{vv}/k_{GL} \approx 1.0$, indicating that the values are in the right order of magnitude. When $v^{0.50}$ is used the data show a less satifying linear behaviour (figure 15), while the agreement with Grober's relation is also worse (figure 16). The results obtained for turbulent conditions show that the velocity variation method is applicable in this range

as well. The use of Dextran T10 and T70 as solute in the systems mentioned above has one disadvantage: Dextrans have a broad molecular weight distribution (M_w = 10,500 and 72,200, while M_n = 5,100 and 38,400, respectively). The measured retentions will therefore be average retentions, which will make the evaluation less precise.

From the results given above, it will be obvious that quite a number of accurate data are needed to determine the mass transfer coefficient using the velocity variation method: a rather large range of observed retentions and fluxes is necessary to obtain a reliable slope in the $\ln[(1 - \Re_{obs}) / \Re_{obs}]$ versus J_v/v^a plot. The disadvantage of the necessity to employ incompletely rejecting membranes may be overcome by a better description of the mass transfer coefficient.

When both the experimental and the mathematical errors (choosing an exponent a and calculating the slope 1/b) are taken into account the uncertainty in the magnitude of the mass transfer coefficient k_{vv} is rather large. Therefore in many cases the mass transfer coefficient may as well be described by the known, rather simple, mass transfer coefficient relations instead of employing the elaborate velocity variation method. These expressions will always be better than results obtained from the osmotic pressure method, which can hardly reflect the influence of changing experimental circumstances. The velocity variation method can still be very useful in cases which are hard to be described using the usual expressions, e.g. when the magnitude of one of the parameters (hydraulic diameter or diffusion coefficient etc.) cannot be estimated appropriately.

CONCLUSIONS

The determination of mass transfer coefficients from experiments is a rather complicated matter. When the osmotic pressure difference during an ultrafiltration experiment is used to determine the mass transfer coefficient ($k_{\Delta\Pi}$), via the concentration at the membrane interface, an almost linear dependence of the $k_{\Delta\Pi}$/k(theoretical)-ratio on the flux/cross-flow velocity ratio (J_v/v) is found. The dependence on the various process parameters (solute type, C_b, v, ΔP and d_h) is not very distinct, which must be a result of the theoretical conformity of the various equations used in the model. Therefore, it is impossible to obtain mass transfer coefficients when employing the osmotic pressure method for the evaluation of the flux equation.

The velocity variation method results in mass transfer coefficients, which are constant over the entire J_v/v^a range but with a substantial uncertainty. The exponent <a> in $k_{vv} = b.v^a$ has to be chosen in advance, while the value of 1/b is calculated from the slopes in a $\ln[(1 - \Re_{obs}) / \Re_{obs}]$ versus J_v/v^a plot) and is a result of combining data at various

pressures. Doing so a rather large uncertainty in the value of the mass transfer coefficient can be introduced.

Neither one of the methods mentioned is a very reliable method for determining the mass transfer coefficient since the osmotic pressure method is very insensitive to changing parameters and the velocity variation method is rather sensitive to the chosen values of experimental parameters. The best experimental method for determining the mass transfer coefficient still is that of evaluation of the observed retention at varying velocities. Due to all the problems mentioned the use of normal mass transfer relations can be as reliable (and much more easy) as the velocity variation method. The velocity variation method probably can still be used in practice when one or more of the parameters needed in the conventional mass transfer coefficient relations are unknown.

ACKNOWLEDGEMENTS

The authors gratefully acknowledge the experimental assistance of Ms. A. Gonlag, Mr. H.J.G. Haarman, Mr. R. Huwaë, Mr. P.J. Roeleveld and dr. S. Stevanovic. We also thank Mr. M.J. van der Waal for using some of his data and Wafilin B.V., Hardenberg, the Netherlands, for supplying us with the tubular membranes.

LIST OF SYMBOLS

<a>	exponent in $k = b.v^a$	(-)
b	constant in $k = b.v^a$	(-)
B_n	n^{th} virial coefficient	$(m^{3(n-1)}.kg^{-n+1})$
C_b	concentration in the bulk	(kg/m^3)
C_m	concentration at the membrane interface	(kg/m^3)
C_p	concentration in the permeate	(kg/m^3)
D	diffusion coefficient	(m^2/s)
d_h	hydraulic diameter	(m)
f	friction coefficient	(-)
I	ionic strength	(N)
J_v	flux	(m^3/m^2s)
J_w	pure water flux	(m^3/m^2s)
k	mass transfer coefficient	(m/s)
k_D	mass transfer coefficient according to Deissler	(m/s)

k_{GL}	mass transfer coefficient according to Graetz-Leveque	(m/s)
k_{Gr}	mass transfer coefficient according to Grober	(m/s)
k_{HH}	mass transfer coefficient according to Harriott-Hamilton	(m/s)
$k_{\Delta\Pi}$	experimental mass transfer coefficient calculated according the osmotic pressure method	(m/s)
k_{vv}	experimental mass transfer coefficient calculated according to the velocity variation method	(m/s)
L	length of a membrane module	(m)
L^*	length of the entry region in a membrane module	(m)
M	molecular weight	(kg/kmol)
M.W.	molecular weight	(kg/kmol)
M_n	number averaged molecular weight	(kg/kmol)
M_w	weight averaged molecular weight	(kg/kmol)
R	gas constant	(J/mol.K)
$\Re$	intrinsic retention coefficient	(-)
R_m	hydraulic resistance of the membrane	(m^{-1})
$\Re_{obs}$	observed retention coefficient	(-)
T	temperature	(K)
v	cross-flow velocity	(m/s)
δ	thickness of the concentrated boundary layer	(m)
ΔP	applied pressure	(Pa)
η_0	viscosity of the solvent	(Pa.s)
ρ	density	($kg.m^{-3}$)
Π	osmotic pressure	(Pa)

REFERENCES

[1] J.G. Wijmans, S. Nakao, J.W.A. van den Berg, F.R. Troelstra and C.A. Smolders, Hydrodynamic resistance of concentration polarization boundary layers in ultrafiltration, J. Membrane Sci., 22(1985)117-135.

[2] G. Jonsson, Boundary layer phenomena during ultrafiltration of dextran and whey protein solutions, Desalination, 51(1984)61-77.

[3] W.F. Blatt, A. Dravid, A.S. Michaels and L. Nelsen, Solute polarization and cake formation in membrane ultrafiltration: causes, consequences, and control techniques, in: J.E. Flinn (Ed.), Membrane Science and Technology, Plenum Press, 1970, pp. 47-97.

[4] V. Gekas and B. Hallström, Mass transfer in the membrane concentration polarization layer under turbulent cross flow. I. Critical literature review and adaption of existing Sherwood correlations to membrane operations. J. Membrane Sci., 30(1987)153-170.

[5] D.E. Wiley, C.J.D. Fell and A.G. Fane, Optimisation of membrane module design for brackish water desalination, Desalination, 52(1985)249-265.

[6] S. Nakao, T. Tanabe and S. Kimura, Mass transfer coefficient in ultrafiltration of macromolecular solutions, poster presented at the 5th International symposium on Synthetic Membranes in Science and Industry, Tübingen, FRG, September 2-5, 1986.

[7]] G. Belfort and N. Nagata, Fluid mechanics and cross-flow filtration: some thoughts, Desalination, 53(1985)57-79.

[8] R.B. Bird, W.E. Stewart and E.N. Lightfoot, Transport Phenomena, J. Wiley and sons, New York, 1960.

[9] A.G. Fane, C.J.D. Fell and A.G. Waters, The relationship between membrane surface pore characteristics and flux for ultrafiltration membranes, J. Membrane Sci., 9(1981)245-262.

[10] A.G. Fane, C.J.D. Fell, D. Wiley and R. McDonogh, Concentration polarization, mass transfer and fluid dynamics in membrane systems, Summer School on Engineering Aspects of Membrane Processes, Aarhus, Denmark, 1986.

[11] R.L. Goldsmith, Macromolecular ultrafiltration with microporous membranes, Ind. Eng. Chem. Fundam., 10(1971)113-120.

[12] G. Trägårdh and K. Ölund, A method for characterization of ultrafiltration membranes, Desalination, 58(1986)187-198.

[13] J.G. Wijmans, The mass transfer coefficient in ultrafiltration, in: Ph.D. Thesis, Twente University of Technology, Enschede, the Netherlands (1984).

[14] G. Schock, A. Miquel and R. Birkenberger, Characterization of ultrafiltration membranes: cut-off distribution measurements by gelpermeation chromatography, poster presented at the 1987 International Congress on Membranes and Membrane processes, Tokyo, June 8-12, 1987.

[15] E. Klein, P. Feldhoff and T. Turnham, Molecular weight spectra of ultrafilter rejection. II. Measurements on highly rejecting filters, J. Membrane Sci., 15(1983)245-257.

[16] J. Kassotis, J. Shmidt, L.T. Hodgins and H.P. Gregor, Modelling of the pore size distribution of ultrafiltration membranes, J. Membrane Sci., 22(1985)61-76.

[17] S. Nakao, S. Yumoto and S. Kimura, Analysis of rejection characteristics of macromolecular gel layer for low molecular weight solutes in ultrafiltration, J. Chem. Eng. Japan, 15(6)(1982)463-468.

[18] S. Nakao and S. Kimura, Analysis of solutes rejection in ultrafiltration, J. Chem. Eng. Japan, 14(1)(1981)32-37.

[19] G. Jonsson and C.E. Boesen, Concentration polarization in a reverse osmosis test cell, Desalination, 21(1977)1-10.

[20] S. Nakao, T. Nomura, H. Ohya and S. Kimura, Preprints 'Workshop on concentration polarization and membrane fouling', held at the University of Twente, Enschede, the Netherlands, May 18-19, 1987.

[21] V.L. Vilker, C.K. Colton and K.A. Smith, Concentration polarization in protein ultrafiltration. Part II: Theoretical and experimental study of albumin ultrafiltered in an unstirred cell, AIChE Journal, 27(4)(1981)637-645.

[22] G.B. van den Berg, J.H. Hanemaaijer and C.A. Smolders, Ultrafiltration of protein solutions; the role of protein association in rejection and osmotic pressure, J. Membrane Sci., 31(1987)307-320, Chapter 4 of this thesis.

[23] G.B. van den Berg and C.A. Smolders, The boundary layer resistance model for unstirred ultrafiltration. A new approach, accepted for publication in J. Membrane Sci., Chapter 2 of this thesis.

SUMMARY

When a membrane filtration process such as ultrafiltration is used in one of the many industrial applications a flux- and yield-decline can be observed. The causes are i) concentration polarization (i.e. accumulation of retained solutes) and ii) fouling phenomena such as adsorption, pore-blocking and deposition of solidified solutes. Concentration polarization can be considered to be reversible and immediately occuring during every filtration process, while fouling is a long-term, and more or less irreversible process. The result of both these phenomena are a decreasing driving force for the filtration or an increasing resistance against transport of the permeating solvent during the filtration.

The degree of flux decline depends on many variables, both solution and equipment related. In the former case a dependence can be expected on e.g. concentration, pH and ionic strength, while in the latter case a considerable influence can be expected whether the solution is pumped to flow tangentially over the membrane during the filtration (cross-flow filtration) or the solution does not move at all while under pressure (unstirred dead-end filtration).

In this thesis the occurrence of concentration polarization, its description and its consequences, is brought in close relation to various experimental parameters. The increasing resistance is described in Chapters 2 and 3, the origin of a diminished driving force in Chapter 4, while in Chapter 5 the mass transfer coefficient in cross-flow ultrafiltration is discussed. Special attention is paid to the solute in Chapters 2, 3 and 4.

In Chapter 2 a new approach of the boundary layer resistance model for unstirred dead-end ultrafiltration is described. In the newly developed model the unsteady state equation for solute mass transport is used instead of a cake-filtration type of description (Nakao's model), which makes computer simulations of the filtration process possible. These simulations agree very well with the experimental data, which are obtained from ultrafiltration experiments with the protein BSA at pH = 7.4, at various concentrations and applied pressures. Many agreements with analyses according to Nakao's model are found and furthermore some new data on the concentration polarization phenomenon are obtained.

In Chapter 3 the flux decline behaviour of binary mixtures of equally and unequally charged proteins (α-lactalbumin, BSA and lysozyme) is studied, as well as the behaviour of the proteins separately. Of special interest are the proteins lysozyme and α-lactalbumin because these proteins are physico-chemically practically identical, except for the sign of their charge, which is expressed in identical flux declining characteristics. In case the mixture consists of oppositely charged proteins sometimes a considerable increase of the resistance of the concentrated layer near the membrane interface can be observed, which

depends on the mixing ratio of the proteins. When equally charged proteins are filtered the resistance decreases a little sometimes, again depending on the mixing ratio. Classical filtration laws are applied as well on the concentrated layer, which is developed during the filtration of mixtures, where the effect of denser packing as a result of unequal dimensions is included. It is shown that the charge of the proteins, especially opposite charges, influences the flux behaviour much more than the slightly denser packing will allow for.

In Chapter 4 the monomer-dimer equilibrium of the protein ß-lactoglobulin is investigated. The formation of the larger dimers appears to influence the retention during ultrafiltration. The osmotic pressure, which reduces the driving force during filtration, turns out to be very dependent on the protein concentration. Comparison with experimental data shows that the osmotic pressure can be described very well theoretically, taking into account the state of association, the excluded volume and the Donnan effects. The effect of pH on the osmotic pressure appears to be considerable: a minimum is found at pH = 4.5, where maximum protein-protein interaction occurs.

In Chapter 5 the mass transfer coefficient in cross-flow ultrafiltration is examined. In literature a large number of relations to calculate the mass transfer coefficient can be found, as well as many corrections in case filtration is under discussion. Two methods to obtain the mass transfer coefficient experimentally are tested: the osmotic pressure method and the velocity variation method. The osmotic pressure method appears to be too insensitive to changing experimental circumstances to obtain reliable mass transfer coefficients, due to theoretical relations. The velocity variation method is more useful despite a considerable error in the results, which is caused by experimental and fitting uncertainties. Because of these results the use of the traditional mass transfer relations may be as reliable, and they are much more easy to handle as well. The velocity variation method can still be useful in practice however when one or more of the parameters needed in the conventional mass transfer coefficient relations are unknown.

SAMENVATTING

Wanneer een membraanfiltratie proces als ultrafiltratie in de industrie in een van de vele toepassingen gebruikt wordt treedt er altijd een bepaalde flux- en rendementsafname op. De redenen hiervoor zijn: i) concentratie polarisatie (ophoping van tegengehouden deeltjes bij het membraan) en ii) vervuilings-verschijnselen zoals adsorptie, porieverstopping en het neerslaan van aanvankelijk opgeloste stoffen. Concentratie polarisatie kan worden beschouwd als een reversibel en altijd direkt optredend verschijnsel tijdens filtratie, terwijl vervuiling een min of meer irreversibel proces is dat in de loop van de tijd steeds toeneemt. Het gevolg van deze verschijnselen uit zich in een afname van de drijvende kracht voor de filtratie of in een toename van de weerstand tegen het permeëren van het oplosmiddel tijdens het filtreren.

De mate van flux afname hangt van een groot aantal variabelen af die zowel verband kunnen houden met de oplossing die gefiltreerd wordt als met de apparatuur die gebruikt wordt. In het eerste geval kan een invloed verwacht worden van bijv. de concentratie, de pH of de ionsterkte, terwijl het in het tweede geval veel zal uitmaken of de te filtreren oplossing tangentiaal langs het membraan gepompt wordt (cross-flow filtratie) of dat de oplossing, onder druk, stil staat boven het membraan (niet-geroerde dead-end filtratie).

In dit proefschrift is het optreden van concentratie polarisatie, het beschrijven van dit verschijnsel en de gevolgen ervan, nauw gekoppeld aan talrijke experimentele grootheden. Zo wordt in de Hoofdstukken 2 en 3 de toename van de weerstand beschreven, in Hoofdstuk 4 de oorzaak voor een afname van de drijvende kracht bestudeerd en in Hoofdstuk 5 de stofoverdrachtscoëfficiënt tijdens cross-flow ultrafiltratie nader bekeken, veelal als funktie van een groot aantal variabelen. In de Hoofdstukken 2, 3 en 4 is daarbij veel aandacht geschonken aan de opgeloste stoffen in de filtratievloeistof.

In Hoofdstuk 2 wordt een nieuwe aanpak van het grenslaag weerstand model voor niet-geroerde dead-end ultrafiltratie beschreven. In dit nieuwe model wordt de niet-evenwichtsvergelijking voor het transport van de opgeloste stof gebruikt i.p.v. een beschrijving volgens de koek-filtratie theorie, zoals in Nakao's model. Zo is het simuleren van het ultrafiltratie proces m.b.v. de computer mogelijk gemaakt. Deze simulaties komen erg goed overeen met experimentele gegevens die verkregen zijn door het uitvoeren van experimenten met het eiwit BSA, bij pH = 7,4, bij verscheidene concentraties en opgelegde drukken. Er is een groot aantal overeenkomsten gevonden met analyses die m.b.v. Nakao's model uitgevoerd zijn en daarnaast is nog een aantal nieuwe gegevens over het verschijnsel concentratie polarisatie verkregen.

In Hoofdstuk 3 wordt het vervuilingsgedrag van zowel binaire mengsels van gelijk of ongelijk geladen eiwitten bestudeerd (α-lactalbumine, BSA en lysozym), als van deze

eiwitten afzonderlijk. De eiwitten α-lactalbumine en lysozym krijgen hierbij speciale aandacht omdat deze eiwitten fysisch-chemisch identiek zijn, op het teken van de lading na. Dit blijkt ook uit de gelijke vervuilings-karakteristieken. Wanneer een mengsel uit tegengesteld geladen eiwitten bestaat kan de weerstand van de geconcentreerde laag bij het membraan soms behoorlijk toenemen. De mate hiervan hangt af van de mengverhouding van de eiwitten. De weerstand van een mengsel van gelijk geladen eiwitten blijkt daarentegen tijdens filtratie soms te kunnen afnemen, ook dit hangt weer af van de mengverhouding. De klassieke filtratie wetten worden toegepast op de geconcentreerde laag die tijdens de filtratie van mengsels eiwitten ontstaat, waarbij ook rekening wordt gehouden met het effekt van een iets dichtere pakking t.g.v. het stapelen van ongelijk grote deeltjes. De lading van de eiwitten beïnvloedt het flux-gedrag meer dan de dichtere pakking; dit geldt speciaal voor tegengesteld geladen ladingen.

In Hoofdstuk 4 wordt het monomeer-dimeer evenwicht van het eiwit ß-lactoglobuline onderzocht in relatie met de ultrafiltratie beïnvloedende grootheden retentie en osmotische druk. De vorming van de grotere dimeren blijkt de retentie tijdens ultrafiltratie behoorlijk te beïnvloeden. De osmotische druk, die de drijvende kracht doet afnemen, is erg afhankelijk van de eiwitconcentratie. Uit vergelijking met experimentele gegevens blijkt dat de osmotische druk theoretisch zeer goed beschreven kan worden wanneer rekening wordt gehouden met de associatietoestand, het uitgesloten volume en de Donnan effekten. Het effekt van een variërende pH op de osmotische druk is aanzienlijk; een minimum wordt gevonden bij pH = 4,5, waar ook maximale eiwit-eiwit interakties optreden.

In Hoofdstuk 5 wordt de stofoverdrachtscoëfficiënt tijdens cross-flow ultrafiltratie nader bekeken. In de literatuur is een groot aantal relaties gevonden waarmee een stofoverdrachtscoëfficiënt berekend kan worden, maar ook vele korrekties daarop omdat het nu speciaal over filtratie gaat. Om de stofoverdrachtscoëfficiënt experimenteel te bepalen zijn twee methoden getest: de osmotische druk methode en de snelheids-variatie methode. De osmotische druk methode blijkt te ongevoelig voor veranderende omstandigheden om stofoverdrachtscoëfficiënten betrouwbaar weer te kunnen geven; dit is een gevolg van een aantal theoretische betrekkingen. De snelheids-variatie methode is bruikbaarder ondanks een aanzienlijk grote fout in de uiteindelijke resultaten. Deze fout is een gevolg van zowel experimentele als wiskundige onzekerheden. In de praktijk zal daarom het gebruik van de traditionele stofoverdrachts relaties even betrouwbaar zijn als de hier genoemde, terwijl deze ook nog veel gemakkelijker te gebruiken zijn. De snelheids-variatie methode kan echter wel gebruikt worden bij het ontbreken van gegevens over één of meer van de parameters die nodig zijn voor de beschrijving m.b.v. de conventionele stofoverdrachtscoëfficiënt.

LEVENSLOOP

Gert van den Berg werd op 7 mei 1960 geboren te Amersfoort.

In 1978 behaalde hij het VWO-diploma aan het Chr. College Nassau-Veluwe te Harderwijk en begon in datzelfde jaar met de studie Chemische Technologie aan de Technische Hogeschool Twente, nu Universiteit Twente, te Enschede. Hij behaalde in 1983 het baccalaureaatsdiploma (vakgroep Proceskunde en Industriële Processen) en in 1985 het ingenieursdiploma (vakgroep Makromoleculaire Chemie en Materiaalkunde).

Op 1 juli 1985 trad hij in dienst van de T.H. Twente als wetenschappelijk assistent in de onderzoeksgroep 'Membraanfiltratie' van de vakgroep Makromoleculaire Chemie en Materiaalkunde om het beschreven promotie-onderzoek uit te voeren.